A microplate co-culture assay comprising patient-derived 3D microtumors

Dissertation

der Mathematisch-Naturwissenschaftlichen Fakultät

der Eberhard Karls Universität Tübingen

zur Erlangung des Grades eines

Doktors der Naturwissenschaften

(Dr. rer. nat.)

vorgelegt von

Mona Bodenhöfer

aus Esslingen am Neckar

Tübingen

2021

Gedruckt mit Genehmigung der Mathematisch-Naturwissenschaftlichen Fakultät der Eberhard Karls Universität Tübingen.

Tag der mündlichen Qualifikation:	18.10.2021
Dekan:	Prof. Dr. Thilo Stehle
1. Berichterstatter/-in:	Prof. Dr. Ulrich Rothbauer
2. Berichterstatter/-in:	Prof. Dr. Michael Schwarz

Ich habe keine besondere Begabung, sondern bin nur leidenschaftlich neugierig.

Albert Einstein

1. Table of Contents

2. Abbreviations

°C	Degrees Celsius
µl	Microliter
µM	Micromolar
2D	Two-dimensional
3D	Three-dimensional
ACT	Adoptive cellular transfer
aCTLA-4	Anti- cytotoxic T-lymphocyte-associated protein 4
Akt	Protein Kinase B
ALDH1A1	Aldehyde dehydrogenase 1 family, member A1
APC	Antigen-presenting cell
aPD-1	Anti-programmed cell death protein 1
ATP	Adenosine triphosphate
BCG	Bacille Calmette-Guérin
BKM-120	Buparlisib
BMI1	Polycomb complex protein
BRAF	Kinase in MAPK Signalling
Calcein-AM	Calcein-acetoxymethyl ester
CAR	Chimeric antigen receptor
CD	Cluster of differention
CSC	Cancer stem cell
Cy5	Cyanine 5
DMSO	Dimethylsulfoxid
DNA	Deoxyribonucleic acid
DTU	Technical University of Denmark
E:T	Effector to target cell ratio
EMT	Epithelial–mesenchymal transition
ERK	Extracellular signal-regulated kinases
FACS	Fluorescence-activated cell sorting
FCS	Fetal calf serum
FDA	U.S. Food and Drug Administration
g	G force
G2/M	G2/M checkpoint in cell cycle
GLV	Giardia virus
h	hour
H&E	Hematoxylin and eosin
HBSS	Hank's Balanced Salt Solution
HCC	Hepatocellular carcinoma
HLA	Human leukocyte antigen
IKP	Institut für Klinische Pharmakologie
IL	Interleukin
ITH	Intratumor heterogeneity
MACS	Magnetic cell separation system
MAP	Mitogen-activated protein
MAPK	Mitogen-activated protein kinase

MART1	Melanoma-associated antigen recognized by T cells
MDR	Multidrug-Resistance-Protein
MEK	Ras-Raf-MEK-ERK pathway
Mel	Melanoma
MEV	Mink enteritis virus
MHCI	Major histocompatibility complex I
min	Minute
ml	Milliliter
mM	Millimolar
MOI	Multiplicity of infection
mTor	Mechanistic target of Rapamycin
NCI-60	Group of 60 human cancer cell lines by the National Cancer Institute
nM	Nanomolar
nm	Nanometer
nmol	Nanomol
NSCLC	Non-small cell lung cancer
p38	P38 mitogen-activated protein kinas
p53	Tumor suppressor
PBMC	Peripheral blood mononuclear cell
PBS	Phosphate-buffered saline
PCR	Polymerase chain reaction
PD-L1	Programmed cell death 1 ligand 1
PDM	Patient-derived microtumor
PDX	Patient-derived xenografts
PE	Phycoerythrin
PI3K	Phosphatidylinositol-4,5-bisphosphate 3-kinase
PTT	Patient tumor tissue
qPCR	Real-time quantitative PCR
Ras/Raf	Ras/Raf signaling
Rb	Retinoblastoma protein
RCC	Renal cell carcinoma
REP	Rapid expansion protocol
RFP	Red fluorescent protein
RNA	Ribonucleic acid
RNAseq	RNA sequencing
RPPA	Reverse phase protein array
s	Second
SHP2	Src homology-2 protein
SOC	Standard of care
TAA	Tumor associated antigen
TCR	T cell receptor
TIL	Tumor-infiltrated lymphocytes
TK	Tyrosine kinase
TM	Trademark
TMC	Tumor stromal matrix proteins
TNM	TNM Classification (tumor, lymph node, metastasis)
T-Vec	Talimogene laherparepvec

UKT	Universitätsklinik Tübingen
US	United States
UV	Ultraviolet
VEGF	Vascular endothelial growth factor
VIM	Vimentin
Wnt	WNT signaling pathway

3. Introduction

The nature of cancer is now better understood than in the time of the ancient Greeks. Hippocrates is credited to be the one coining the term 'cancer' and described it as a disease of black bile and constitutional melancholy [1, 2]. There has been significant progression in research in the field of cancer therapy, such as preventive vaccines, high-resolution imaging diagnostics or targeted cancer therapy, and major funding agencies, governments as well as international agencies invest in the goal of curing cancer. Nevertheless, it is still a massive burden to our society with no direct answer to control it [1, 3]. The cost of cancer treatment in the European Union rose from € 35.7 billion in 1995 to € 83.2 in 2014. The cost of cancer drugs themselves rose from € 7.6 billion in 1995 to € 19.1 billion in 2014 [4]. Furthermore, between 2007 and 2013 the European Union funded cancer research with € 1.5 billion and continued this funding with the Horizon 2020 project comprising over € 30 billion for three years (2018-2020) [5, 6].

3.1 Development of cancer

As explained in more detail in the following chapters, albeit, there are some specific cancer types, which develop in early childhood [7], cancer is a disease of old age due to the accumulation of different mutations in the genome. Tumorigenesis can start as early as the age of 20, but the detection of a grown tumor usually is at the age of 50. In most cancer types, 300-500 genes are modified to result in the cancer phenotype. The estimated factor of genetic predisposition is a low 5-10%, whereas the remaining cases of cancer development are due to the life style choices of the individual [8]. Thus, the low percentage of predispositions make a cancer specific treatment difficult and led to the idea of personalized medicine for each patient (see 3.5 Personalized cancer therapy).

3.1.1 Cancer development through mutation

The classical view of cancer development is a model with two general steps: initiation followed by the promotion of tumor growth. First, a normal tissue cell needs to get initiated by a transforming agent, like UV light, cigarette smoke or viruses [9-11]. Second, the cell must be exposed to a promoting agent for neoplastic promotion to be induced (Figure 1).

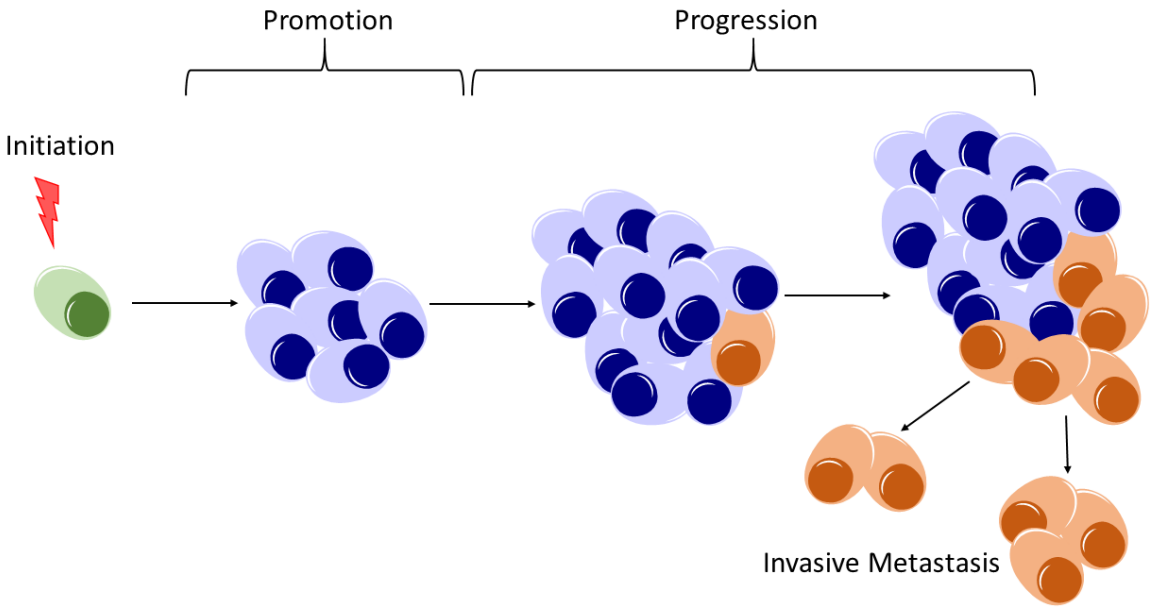

Figure 1: Cancer development after initial mutation of a healthy cell followed by the promotion and tumor progression phase. Adapted from Scott, Wille [12].

The sequential steps are essential for the development of a malignant transformation [13]. The initiation is defined as a process that causes an irreversible change in the DNA [14]. The promotion is caused by agents, which by themselves are not mutagenic. They can, however, stimulate the growth of a tumor [15].

It holds true that cancer is an accumulation of mutations in cells and so far, roughly 350 genes have been found to be involved in cancer development, and it is still unknown which is the ‘true' number of cancer genes [16]. After the first initiating mutation, the secondary mutations can be classified into driver and passenger mutations. Driver mutations are mutations needed by the cancer cells to survive under selective pressure during tumorigenesis, whereas passenger mutations are accumulated ‘on the way’ but do not contribute to cancer cell survival [17]. Driver mutations are often found to encode kinase proteins, such as the constitutive active mutation variant of the BRAF kinase, BRAF V600E, in malignant melanoma. These mutated or false-regulated kinases also prove to be promising drug targets in some cases [18].

Another well-known driver mutation is the proto-oncogene p53. In a healthy cell, damaging the DNA leads to the activation of the DNA damage pathway and thereby induces the p53-dependent cell cycle arrest, which leads to senescence or even apoptosis [19]. In precancerous lesions, this senescence and apoptosis can still be observed; however, both get down-regulated upon tumor progression [20]. The loss of p53 is a common way of tumors to evade that pathway since a single amino acid change is enough to inactivate the protein due to a lowered melting temperature [19]. Thus, the protein cannot fold into its active form and instead is actively degraded by the cell.

Additionally, the loss of p53 does not compromise the G2/M-phase of the DNA damage checkpoint, which is necessary for the DNA repair and thus has a survival benefit [21, 22].

Evasion of cell death by tumor cells leads to a constant change in favorable driver mutations and thereby to an evolutionary accumulation of mutations in the tumor. The carcinogenesis model of initiation and promotion of tumor growth is consistent with a linear evolution of the tumor in which each new driver mutation eliminates the previous one [23]. Yet, it has been known since the late 1800s [24] that tumors not only consist of one single cell type, but display an intratumoral heterogeneity (ITH). It is believed that tumor evolution does not follow a single evolutionary theory, but a mixture. Linear evolution is not supported in advanced carcinomas, but found in early stages of the disease and mutations then shift to a branched evolution [25].

This simple model on cancer development held true till the late 1940s [26]. However, further dissection on how cancerous disease developed proved that a more complex model for cancer development is needed [12, 27, 28].

3.1.2 Cancer development from cancer stem cells

The first theory about the existence of cancer stem cells (CSC) was made in 1875 by Conheim, who proposed the existence of self-renewing cells with pluripotent properties in malignant tissue [29].

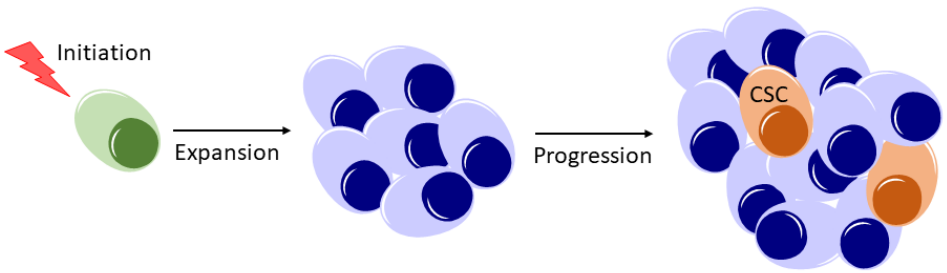

Figure 2: After initial cell growth a percentage of cells regain stem cell-like properties. These cancer stem cells (CSC) are slow-dividing, chemo- and radiotherapy resistant cells, which have the ability to regrow the tumor. Adapted from Visvader [30].

The hypothesis is that a tumor not only consists of the fast-dividing tumor cells, which are susceptible to chemotherapy, but also of a slow-dividing cell population, which exhibits stem cell-like characteristics (Figure 2) [31, 32]. This stem cell-like character is in line with the clinical observation of the almost inevitable relapse of the disease after initial response to chemotherapy or radiation [33]. A multitude of CSC markers have been identified for solid tumors, like CD133, CD44 and CD24 [32]. Additionally, CSC can express common stem cell markers. Indeed, CSC and normal adult stem cells share common characteristics like self-renewal, rely on the same signaling

pathways (e.g. Wnt, Hedgehog or Nanog), show high expression of ABC transporters as well as DNA repair proteins, display a quiescent state and exhibit a long life span [34, 35].

These findings lead to the hypothesis that eliminating the CSC is a crucial step in curing cancer.

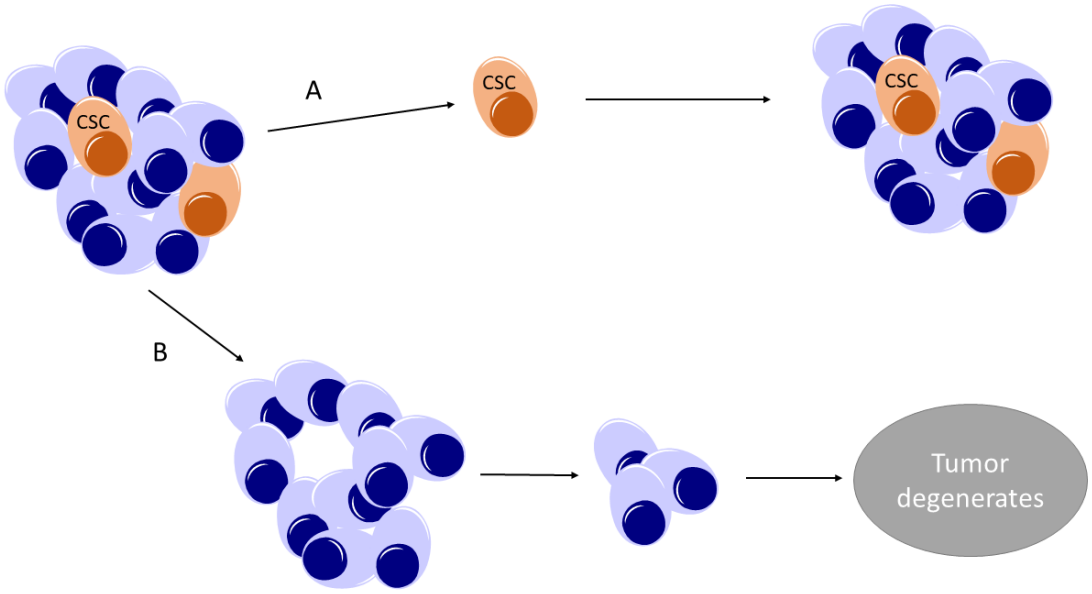

Figure 3: **A** Classical cancer therapy targeting fast-dividing tumor cells allows the regrowth of the tumor due to the remaining CSC. **B** Targeting the CSC followed by classical chemotherapy would lead to tumor degradation due to the limited life span of the fast-dividing tumor cells. Adapted from Reya, Morrison [35].

Since the occurrence of CSC is extremely low (less than 0.04 % of tumor cells [36]) they have so far been largely overseen in cancer therapy. Most of the classical chemotherapeutics are incapable of targeting the low-cycling CSCs, which explains the cases in which the tumor relapsed after an initial reduction of tumor mass (Figure 3A). Hence, the goal now is to find a therapy to target the CSCs specifically so that subsequently, the remaining tumor starts to dissociate due to the limited lifetime of the differentiated (i.e. non-CSC) tumor cells (Figure 3B). However, in the field of cancer research the existence of CSC is still under debate. Nevertheless, leaders in the field are urging to move on in this debate and rather consider the consequence in cancer therapy [37, 38]. Even tough, if CSCs mimic the properties of normal stem cells and the eradication of the CSCs would lead to the remission of the cancer, it is not clear yet if this normal cell cycle, and thus, cell death, is preserved in cancer. Thus, the eradication of the CSC could potentially not be sufficient to treat cancer [38]. Furthermore, CSC-specific treatment is not approved for cancer treatment yet. However, several approaches to target the CSCs are in clinical trials [32, 33].

Another research effort is to not target the CSCs but the stem cell niche that provides them with the needed signals for their stem cell-like phenotype. It is assumed that an intact cancer stem cell niche can reform CSCs after the CSCs being targeted with chemotherapeutics. Destroying the

cancer stem cell niche, however, would deprive them of the needed survival signals and the CSC would exhaust [33].

3.1.3 Hallmarks of Cancer

Based on previously described ways for cancer development, Hanahan and Weinberg [39] defined the six hallmarks of cancer, which healthy cells acquire during malignant transformation (Figure 4) [40].

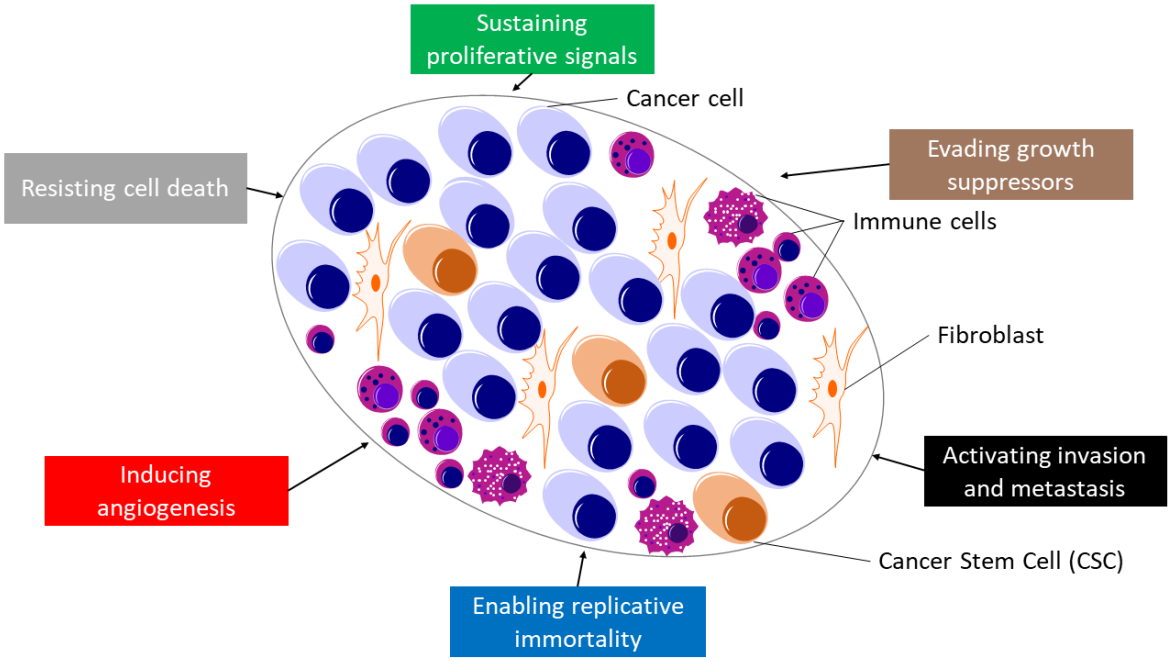

Figure 4: The six hallmarks of cancer. Cancer cells gain these six functions to develop an unlimited growth potential and the potential for metastasize. Adapted from Hanahan and Weinberg [39].

Firstly, one of the most important traits of tumor cells is their ability of indefinite proliferation. As a result of deregulation or acquiring independence of growth factors the cells proliferate in an unregulated fashion. There are different ways for cells to achieve this: Cancer cells can express the growth signal autonomously, or the surrounding tumor microenvironment can provide it for the tumor cells [41]. Alternatively, the cancer cells can upregulate the expression of respective growth factor receptors, thereby becoming more susceptible to growth signals, or the cancer cells can become independent of the growth signal altogether by constitutive activation of downstream signaling pathways.

Secondly, tumor cells circumvent the suppression of cell growth. Two major tumor suppressors are the aforementioned p53 as well as the Rb (Retinoblastoma-associated) proteins. These proteins are major players in the decision of cell fate. The Rb protein governs cell fate depending on extracellular signals, whereas the p53 protein reacts to stress or DNA damage signals from inside the cell.

Another important property of p53 is that it can trigger apoptosis. By mutating these tumor suppressors, cancer cells escape the natural control of cell growth [42, 43].

Thirdly, cancer cells gain the ability to grow in an invasive form and metastasize. Before invading a new tissue, the tumor cells undergo epithelial-to-mesenchymal transition (EMT). The mesenchymal form allows tumor cells to enter blood vessels or the lymphatic system. In order to achieve mesenchymal characteristics, cell-cell contacts need to be lost. Therefore, the expression of cell adherence proteins, like E-cadherin, or adherence junctions is downregulated, and the expression of mesenchymal markers, like Vimentin, is increased [44]. This is facilitated by the transcription factors Snail, Slug, Twist and Zeb1/2, which can directly influence the expression of E-cadherin. Upon losing the cell-cell contacts, the morphology of the cell changes to a more spindly/fibroblastic shape [39]. The expression of the EMT regulators is traced back to cancer-associated fibroblasts (CAFs), which interact with the neighboring cancer cells and thus induce the transition [45, 46].

This process is followed by the escape from the respective vessels into distant tissue, where metastases can form, which is called the mesenchymal-to-epithelial transition (MET) [39, 40, 47]. It is suggested that the absence of the EMT-initiating factors at the metastasis site enables the cells to retransform into an epithelial state by re-inducing E-cadherin expression [47]. For this process, the presence of the appropriate microenvironment to initiate tumor growth is necessary [48].

Fourthly, normal cells have a limited lifespan, after which they enter senescence. Tumor cells, however, overcome this limitation to form a macroscopic tumor. This is achieved by the presence of cancer stem cells (also see 3.1.2 Cancer development from cancer stem cells). Three hypotheses try to explain the origin of the CSCs. The first hypothesis is that cancer cells arise form stem cells. Thus, the cancer cells could use the inherent ability of self-renewal. The second hypothesis is that cancer arises from progenitor cells. These cells are more abundant than stem cells in an adult tissue and still contain a limited ability of self-renewal. The third hypothesis is the origin of cancer stem cells from differentiated adult cells. Here, the adult cells de-differentiate and, by means of genetic mutation, acquire the ability of self-renewal. Even though, no specific model has been suggested yet, the laws of probability state that in a large enough number of differentiated cells, a small fraction could undergo the change necessary for de-differentiation [49].

Fifthly, tumor tissue requires supply of the necessary nutrients and oxygen and metabolic waste and carbon dioxide need to be removed. Like in normal cells, these functions are carried out by blood vessels in the tumor. In healthy individuals, *de novo* vascularization is mostly nonexistent, whereas during tumor progression, angiogenesis is almost always active. This abnormal angiogenesis is predominantly driven by the vascular endothelial growth factor (VEGF), which can

be upregulated by hypoxia and oncogenic signaling [50]. The blood vessels produced in the tumor are typically aberrant. They display precocious sprouting, convoluted and excessive vessel branching, distorted and enlarged vessels as well as an abnormal level of endothelial cell proliferation and apoptosis [51].

Sixthly, another hallmark of cancer is the resistance towards programmed cell death by apoptosis, which is a natural barrier against the development of cancer. Hence, tumor cells need to find a way to circumvent that barrier. One of the most common ways is the loss of the tumor suppressor p53, which is a major regulator of apoptosis. Tumors may also evade apoptosis by increasing the expression of antiapoptotic factors like Bcl-2 or Bcl-x_L or downregulating pro-apoptotic factors like Bax, Bim or Puma [21, 52].

3.2 Cancer types in focus

The focus of this thesis is on renal cell carcinoma and malignant melanoma. These two tumorous diseases accounted for over 48,000 new cancer cases in 2020 in Germany alone [53].

3.2.1 Renal Cell Carcinoma

3-4% of all malignant tumors in adults are renal tumors, 80%-90% of which are renal cell carcinomas (RCC). In 2014, roughly 15,000 patients were diagnosed with RCC in Germany, with men being affected almost twice as often as women. Smoking, obesity as well as high blood pressure are important risk factors for the disease. A familiar predisposition is only observed for the Hippel-Lindau syndrome where the disease is often multifocal and bilateral in younger patients [54, 55].

RCCs can be divided in several histological subgroups. Both clear cell RCC as well as papillary RCC originate from the epithelium of the proximal tube, whereas chromophobe and collecting duct RCC originate in the distal nephron. The most common form of RCC is the clear cell RCC, which represents 75-80% of RCCs, followed by papillary RCC (10-15%) and chromophobe RCC (5%). RCCs are classified using the TNM-status, with T for extension of primary tumor, N for lymph node involvement and M for presence of distant metastases. T1 tumors have a size below 7 cm and should be treated with a kidney-preserving surgery. Tumors staged T2 are larger than 7 cm but confined to within the kidney and are usually treated with a nephrectomy. T3 and T4 tumors have invaded the surrounding tissue and mostly have lymph node involvement. In addition to surgery, targeted therapy using small molecules can be used for low risk as well as high risk patients (Table 1) [55, 56].

Table 1: Targeted drugs for the use in treating advanced RCC according to risk-profile and line of treatment. Adopted from Doehn, Grunwald [55] and the ‚S3-Leitlinie Diagnostik, Therapie und Nachsorge des Nierenzellkarzinoms Kurzversion_1.1' from February 2017, valid until 01.09.2019 [57].

Line of treatment	Risk profile	Standard	Alternative	Target
First-line	Low/moderate	Pazopanib Sunitinib	Bevacizumab + INF	Tyrosine kinase (TK) / VEGF + Immune system
	High	Temsirolimus	Pazopanib Sunitinib	mTor / TK
Line of treatment	**Prior treatment**	**Standard**	**Alternative**	**Target**
Second-line	VEGF based therapy	Nivolumab	Cabozantinib	PD1/PDL1 Interaction / TK
	VEGF-Inhibitor Failure	Lenvantinib + Everolimus		TK+mTor
	Sunitinib	Axitinib		TK
	Cytokines	Axitinib	Pazopanib Sorafenib	TK
In general, if treatment with mTOR-Inhibitors fails, treatment with tyrosine kinase inhibitors can be initiated.				

3.2.2 Malignant melanoma

In 2014, 21,000 men and women were diagnosed with malignant melanoma of the skin in Germany. The most common type of melanoma is the spreading melanoma, which has a good prognosis, whereas the rare nodular or amelanotic melanomas have an unfavorable prognosis. Still, the relative 5-year survival in Germany is 94 % for women and 91 % for men [54].

The main endogenous risk factors are the number of freckles and the fairness of the skin. The main exogenous risk factor is UV-light exposure. Thereto, not only direct sun exposure, but there is also a clear correlation between the risk for malignant melanoma and indoor tanning.

Around 90 % of melanomas are found on the skin of regularly UV-exposed sites like the trunk and the extremities. The acronym ABCDE was introduced in 2004 to help with the diagnosis of melanoma, which often presents with some or all of the ABCDE features, A asymmetry, B border irregularities, C color variation, D diameter over 6 mm and E evolution or change [58]. After a biopsy of the suspected melanoma confirms the diagnosis, a histological staging is done. For melanomas

stage I-IIIB, surgery is the primary treatment. Adjuvant treatment is often recommended to improve survival chances. There are multiple treatment options approved by the FDA. In Germany, the guidance for treatment of metastatic melanomas recently added checkpoint inhibitors to the first line treatment of melanomas without BRAFV600E, MEK or c-Kit mutations. It also recommends the combination of the targeted therapy with immune checkpoint inhibitors if possible. In case a treatment with checkpoint inhibitors is not possible, the first-line response is the treatment with Dacarbazine [59].

For melanomas, it is standard to screen for known mutations in the cancer cells, since there are targeted therapy options available. A common mutation in melanomas is the BRAFV600E mutation, which leads to a constitutively active RAS/RAF pathway. Vemurafenib is selective for the mutated BRAF and is approved for treatment of unresectable and metastatic melanomas harboring the mutation. Trametinib is another targeted treatment option in metastatic or unrespectable melanomas. Trametinib acts downstream of the RAS/RAF signaling pathway and inhibits the MEK kinase, thereby inhibiting cell proliferation. It is frequently observed in melanomas that the disease shows regression before expanding and forming metastases. This is due to the involvement of tumor infiltrating lymphocytes (TILs), which is later antagonized by the tumor. There are multiple FDA-approved treatments for melanomas that activate the immune system. The most common ones are Ipilimumab, an aCTLA-4 antibody, and Nivolumab, an aPD-1 antibody. Both antibodies inhibit the downregulation of cytotoxic T cells activity by the tumor [60].

3.3 The immune system in cancer

The immune system plays an important role in cancer development. More than 135 years ago, the German physicians Busch and Fehleisen noticed regression in cancer patients after infections by erysipelas. Later, Busch intentionally infected cancer patients with erysipelas and noticed the malignancy shrinking. Subsequently, Fehleisen identified *Streptococcus pyogenes* to cause the disease. [61-63]. The first treatment utilizing the activating effect of infections on the immune system to treat cancer was approved in 1976 by the FDA with the use of Bacillus Calmette-Guérin (BCG) in bladder cancer [64]. The discovery of immunomodulating treatment for cancer is a result of basic research in many fields, which could have never been realized without the interplay of molecular biology, virology, structural biology, immunology and cell biology.

3.3.1 Reaction of the immune system to cancer

The immune system is classically divided into two parts, the innate immune system, and the adaptive immune system. The innate immune system, comprising natural killer cells and macrophages, does not need a stimulus from antigens prior to its immune response. The adaptive

immune system, such as $CD8^+$ cytotoxic T cells, $CD4^+$ T helper cells and B lymphocytes, on the other hand requires an antigen presented by antigen-presenting cell (APCs) for activation.

It is estimated that a tumor can have up to 11,000 mutations, which can give rise to cancer-specific tumor-associated antigens (TAAs). This can include neoantigens, mutated proto-oncogenes, tumor suppressors, over- or aberrant expression of proteins, altered glycoproteins or cell type-specific differentiation antigens [65]. The concept of cancer immunosurveillance was first proposed by Burnet and Thomas and is now considered a part of cancer immunoediting. The process of immunoediting can be divided into three parts: elimination, equilibrium and escape. Firstly, the elimination phase is the initial damage to and possible destruction of tumor cells by the innate immune system and the following presentation of TAAs by APCs to the adaptive immune system in order to activate tumor specific $CD8^+$ and $CD4^+$ T cells. These T cells can destroy the remaining cancer cells in case of complete elimination. Secondly, the equilibrium phase is the time any remaining cancer cells cannot be eliminated by the immune system, but the cancer also does not progress. Lastly, in the escape phase, the remaining tumor cells break the equilibrium with the immune system and progress into a solid tumor and form metastases. The escape can have multiple reasons, the most common are loss of antigen expression and even loss of MHC class I expression [66-68]. The tumor microenvironment plays another important role in the escape, as it can shield the tumor from the immune cells by producing various cytokines or building a barrier of cancer-associated fibroblasts (CAFs) around the tumor. A growing and progressing tumor forms an immunosuppressive microenvironment to avoid detection by the immune system by recruiting regulatory immune cells, such as T_{reg}, T_{H17} helper cells or tumor-associated macrophages (TAMs) [69-71]. In more detail, TAMs are recruited to the tumor through the production of various cytokines and chemokines, like colony stimulating factor 1 (CSF1) or vascular endothelial growth factor A (VEGFA). These TAMs can suppress cytotoxic $CD8^+$ T cells either by expressing inhibitory ligands like the programmed cell death 1 ligand 1 (PD-L1) or by recruiting T_{reg} cells trough the expression of CCL22.

Another group of myeloid cells in the vicinity of a tumor are the myeloid-derived suppressor cells (MDSCs). These cells can suppress the proliferation and cytokine production of T cells. However, so far this has only been shown in in vitro or animal models and their role in the immune evasion of tumors *in vivo* has to be more precisely studied [72].

T_{reg} cells depend on the recruitment to the tumor by CCL22 or CCL5. T_{reg} cells can be identified for example via their expression of CD25 and of transcription factor forkhead box P3 (FOXP3). It has been shown that the absence of T_{reg} cells lead to a reduced metastatic activity of the tumor, suggesting its importance in tumor metastasis [73]. Furthermore, it has been shown that the recruitment of T_{reg} cells to the tumor enhances $CD8^+$ T cell apoptosis [74].

By the secretion of IL-6, IL-23 and TGFβ by MDSCs the accumulation of T_{H17} helper cells at the tumor site is promoted. The presence of T_{H17} cells in turn promotes further recruitment of MDSCs and the expression of immunosuppressive genes in these cells. Furthermore, T_{H17} cells promote cancer-associated fibroblasts to secrete the granulocyte colony-stimulating factor (G-CSF). This factor promotes the immunosuppressive function of myeloid cells [69, 75, 76].

In recent years, multiple ways to circumvent the downregulation of the immune system have been found.

3.3.2 Counteracting the downregulation of the immune system by cancer

The journal 'Science' called the year 2013 the year of the breakthrough of immune therapy [77]. One of the reasons for this headline was the successful use of antibodies, so called 'checkpoint inhibitors' to block the tumor-induced inhibition of immune system activation via checkpoint receptors. One of these checkpoints is the cytotoxic T lymphocyte-associated protein 4 (CTLA-4), which was discovered by James Allison and Jeffrey Bluestone. CTLA-4 translocates to the cell membrane of cytotoxic T cells after T cell receptor engagement and competes with the costimulatory factor CD28 for the binding to CD80 or CD86, which are expressed on tumor cells (Figure 5). After binding, CTLA-4 mediates an inhibitory signal to the T cell nucleus which leads to an arrest of proliferation and activation [78, 79]. The first antibodies (Ipilimumab and Tremelimumab) to block the interactions of CTLA-4 with CD80/CD86 entered clinical trials in 2000. The clinical activity of aCTLA-4 treatment was most successful in patients with metastatic melanomas [80] and was FDA-approved in the USA for metastatic melanoma in 2011 [77].

The other major player in the downregulation of cytotoxic T cell activation in cancer is the programmed cell death 1 (PD-1) receptor, which downregulates the effector function of the cytotoxic T cell when binding to its ligand, programmed cell death ligand 1 (PD-L1), which is expressed on the tumor cells (Figure 5). This downregulation is mediated by tyrosine phosphatase SHP-2, which dephosphorylates signaling molecules downstream of the T cell receptor (TCR) [81]. Expression of PD-L1 is upregulated in inflamed tumor microenvironments leading to an exhausted T cell phenotype and inhibition of respective antitumor response.

The blockade of the PD-1/PD-L1 interaction has a more direct effect on the antitumor activity of T cells than aCTLA-4 treatment: the interaction between CTLA4 and CD80/CD86 blocks T cell activation during the maturation of T cells and the PD-1/PD-L1 interaction leads to a downregulation of already matured and activated T cells. The first antibodies targeting PD-1, Nivolumab and Pembrolizumab, were approved for the treatment of refractory malignant melanoma by the European Commission in 2018 and early 2019, respectively [82, 83]. Additionally, both these agents were the first to be approved by the FDA for cancer treatment not based on the

tissue of origin but for the treatment of tumors with genomic microsatellite instability in general [77].

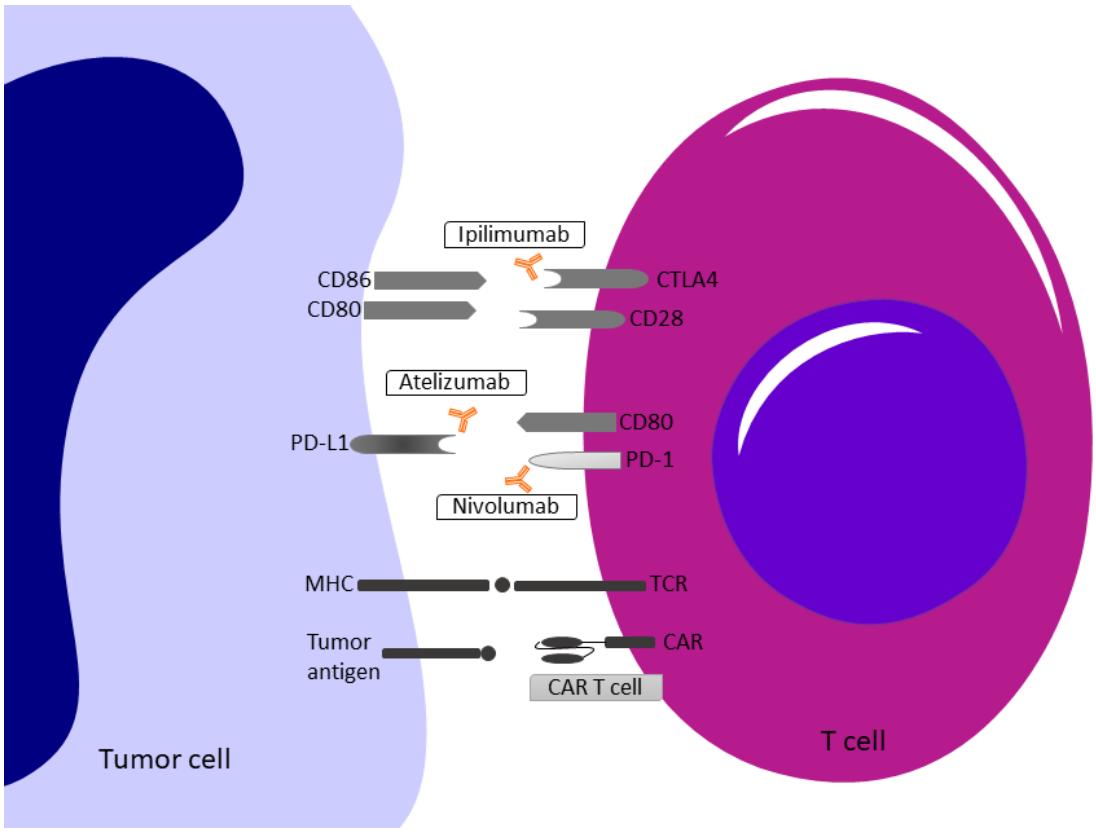

Figure 5: Interactions between TILs and the tumor, which downregulates the immune response and the respective ways to overcome this downregulation using immunotherapy. Adapted from Domingues, Lopes [60].

Another way to harness the anti-tumor capabilities of the immune system is adoptive cell transfer (ACT) using mostly cytotoxic T cells. Three different forms of ACT with T cells have been used so far [84]. First, using TILs from tumor biopsy samples, second, expanding antigen-specific T cells from peripheral blood and third, using genetically modified T cells expressing the desired, tumor specific TCR or a chimeric antigen receptor (CAR) (Figure 5). Here, only the ACT with a TIL population isolated from a tumor biopsy will be described in more detail. TILs are mostly cytotoxic T cells that have infiltrated tumor tissue due to the recognition of a MHC class I-presented TAA [85]. The TILs are then expanded *in vitro* commonly using high-dose IL-2 to a cell number as high as 10^{11}. Next, they are again selected for specificity and then reinfused into the patient. This ACT has been primarily used in metastatic melanoma patients until now, as spontaneous regression due to immune cell activity is a known phenomenon in this type of cancer [84, 86, 87].

3.4 Anti-cancer drug development

Drug discovery is an interplay between many disciplines, including high-throughput genomics to identify the target and biomarkers, biochemical and cell-based assays to determine the effectiveness of a discovered drug, structural biology to determine the binding and inhibition mode of action, bioinformatics for the analysis of the data and *in silico* chemistry for optimizing the chemical lead. The preclinical development of small molecules is classically depicted as a linear process moving from molecular target identification through early chemical hit and lead discovery, optimized lead compound selection, to preclinical development, and finally to a drug candidate entering clinical trials. In this classical approach, potential anti-cancer drugs are first evaluated using a panel of malignant cell lines, like the National Cancer Institute 60 (NCI-60) panel. If an activity is observed in a potential hit, the compound is also tested in animal disease models, and the mode of action is determined. Another strategy is to search for specific compounds, which inhibit known cancer development pathways. Agents identified in the aforementioned investigations are then tested for their pharmacokinetic profile and advanced into clinical testing [88].

By using this approach, merely around 5 % of anti-cancer drugs enter the clinic after phase III studies. For comparison, the clinical success rate in cardiovascular disease drugs is 20 % [89]. It is hypothesized that this is, among other reasons, due to the application of inadequate preclinical models with low predictive value as well as insufficient translational research. A lot of effort is currently invested in changing this high failure rate, such as developing more representative cancer cell lines for distinct cancer subtypes and resistances, optimizing mouse models by using patient-derived xenografts (PDX) or genetically modified mouse models with germline mutations of known oncogenes. This should enable the preclinical models to better validate the drug target and identify the mode of action [88].

3.5 Personalized cancer therapy

The basis of personalized cancer therapy is the assumption that each patient's cancer is different and more similar to another patient's cancer by mutational profile and not tissue of origin. Therefore, biomarkers to identify good treatment targets are an essential tool. Using the available panomics technologies and network analysis, driver networks can be identified from resected tumor or biopsy material. After identifying targets in these driver networks, *in vitro*, *in vivo* and *in silico* methods are used to identify the best treatment option for the patient. Subsequently, the success of treatment must be monitored by biomarkers in liquid biopsies or by imaging methods. Upon relapse of the tumor, new biopsy material can be analyzed in the same way and treatment can be adjusted to new driver networks [90-92].

3.5.1 Personalized test systems

The best way to validate a potential personalized treatment option for a cancer patient is to assess its advantageous effects using patient-derived test systems. There are multiple patient-derived test systems in use, each with their own advantages and disadvantages.

3.5.1.1 2D primary cell lines

One way to test chemotherapeutics on patient material is to generate 2D primary cell lines from biopsy material. Classical primary cell culture has the disadvantage that a large proportion of such primary 2D cell lines become senescent after a few passages and thus cannot be used in a high-throughput assay system or for long-term studies. Using the 'conditional reprogramming' proposed by Schlegel and colleagues [93, 94], primary tumor cells can be immortalized and then be used in a high-throughput setting. This allows to directly impact treatment decisions of patients by providing information on treatment response of the primary cell lines of needle biopsies as early as two weeks after the biopsy [95]. Still, this technique also has its limitations. The artificial immortalization of the cell lines can change the response to drug treatment and thus, falsify the results.

In 2D cell culture the 3D architecture of the original tumor as well as its microenvironment consisting of fibroblasts, including CAFs, innate immune cells, T cells, stromal cells, blood vessels and extracellular matrix is lost [96, 97]. Due to the cells growing on a flat surface, tissue specific properties like the topology, cell-cell contacts and differentiation cannot be fully reproduced. The missing extracellular matrix changes the cells behavior towards signals for growth, migration, inflation, and differentiation. Furthermore, drug effects can be more variable when treating 2D cultures compared to 3D tissue-like cultures [98].

Additionally, finding the correct culturing conditions for each tumor type and patient can prove challenging [98, 99]. However, this limitation is not inherent to the 2D culturing of primary tumor cell but is also faced when culturing primary cells in a 3D setting.

3.5.1.2 Patient-derived Xenografts

For the generation of patient-derived xenograft (PDX) mouse models, biopsy material is implanted or dissociated and injected into immunodeficient mice. Usually the PDX model is heterotopic, meaning that the tumor material is implanted subcutaneously making tumor growth and treatment response easier to monitor. In order to get a more realistic setting for the PDX model, the tumor material can also be implanted orthotopically, meaning that it is implanted into the organ of origin with the same external milieu. Using these disease models, the response of the tumor to treatment can be assessed and the treatment of the patient planned accordingly. Since normally mice for PDX models are immunodeficient, cancer immunotherapy, e.g., the checkpoint inhibitors, cannot be

tested in this type of animal model. Hence, a novel approach for testing immunotherapeutic approaches for cancer treatment in PDX models as well is to use humanized mice with a human-like immune system, which at least in part simulates the human immune system. To do so, the mice can either be injected with TILs of the patient, leading to severe graft versus host disease in the mice, or be injected with hematopoietic stem cells, resulting in an almost complete hematopoietic reconstitution in the mice [100]. The main drawbacks of PDX models are that they are rather cost-intensive, especially when using humanized models. Moreover, PDX cannot be generated from all tumor biopsies as some specimen do not engraft in the mouse [100, 101]. Finally, the generation of functional PDX models is time-consuming and takes too long to impact treatment decisions for the patient.

3.5.1.3 *Ex vivo* tissue slices

Even though the PDX models resemble the original tumor closer than 2D primary cell culture, they still lack crucial parts of the tumor. More specifically, the tumor microenvironment and structural architecture of the tumor, as most of the PDX models, are heterotopically grown. *Ex vivo* tissue slices, on the other hand, retain the structure and microenvironment of the tumor *in vivo* without extensive manipulation or artificial matrices. The disadvantage of tissue slices is their limited survival in culture. Cultivation longer than a few hours after surgery requires extensive optimization of the culturing conditions. Additionally, the culture media is often supplemented with various growth hormones that can alter the behavior of the tumor towards certain chemotherapeutics [102]. A way to overcome the limitations of *ex vivo* tissue slices requiring artificial growth hormones was proposed by Majumder & Baraneedharan [103] with the development of the CANScript technology. Here, the tissue slices are cultured in a culture dish coated with tumor-stromal matrix proteins (TMCs) that are cancer type and grade-matched as well as with media, which is supplemented with 2% autologous patient serum. This culture method enhances tumor slice viability significantly and can even lead to tumor growth. In their publication, Majumder & Baraneedharan [103] also propose that the CANScript technology can be used to predict patient outcome by matching their data with PDX as well as clinical data.

One major drawback of *ex vivo* tissue slices can still not be overcome by the CANScript model. The tissue has to be used directly after surgery and cannot be cryo-conserved for later testing of additional treatment options. Furthermore, throughput of compound and drug testing is limited due to the comparably low amount of tissue slices that can be generated from one single biopsy.

3.5.1.4 3D Tumor organoids

Tumor organoids develop when a mixture of single tumor cells is embedded into a 3D matrix to mimic the extracellular matrix. In order to do this mostly the Matrigel™ matrix by Corning is used. This matrix was developed 30 years ago to mimic the extracellular matrix (ECM) needed to grow mouse sarcoma cells. The ECM proteins are isolated from Engelbreth-Holm-Swarm (EHS) mouse sarcoma. The main components of Matrigel™ are laminin, collagen IV, heparan sulfate proteoglycans, entactin/nidogen, and various growth factors. Still, the Matrigel™ on the market is derived from mice [104]. Even though Matrigel™ is one of the most commonly used matrices for cell culture, the undefined source for the ECM proteins leads to disadvantages of the system. The natural origin of the soluble factors, like growth factors, varies from batch to batch and is poorly defined. This can lead to difficulties in obtaining reproducible results. Additionally, these natural biomaterials have low tensile strength; thus, the biodegradation can be rapid, hindering the use in drug screening purposes. Developing synthetic alternatives could overcome the limitations of the natural ECM source. The mostly described synthetic polymers in 3D culturing are polycaprolactone, polyglycolide and polylactide. Even though these synthetic polymers overcome the low tensile strength of the natural matrix these components lack the natural adhesion sites as well as growth factors, hormones and other biologically active molecules. In order to mimic the natural cell niche, these components have to be added to the artificial matrix in the right composition [105].

Organoid cultures can be established and expanded from *ex vivo* samples as small as patient tumor biopsies. In case of a fully resected tumor, multiple sites of the tumor can be used to generate organoids to represent the heterogeneity of the original tumor even after several passages [106]. Organoid models have recently shown promising potential in drug discovery. Even though the use of organoids in cancer drug development is still in its infancy, a proof-of-concept study has been made with organoids from metastatic colorectal cancer patients. It could be correctly predicted, that 80 % of the patients would benefit from irinotecan-based therapies without misclassification of patients. However, a prediction for the benefit of 5-flourouracil in combination with oxaliplatin could not be made successfully [107].

Using 3D models, like organoids, in drug testing and discovery, the drug mode of action and individual response can be modeled. Additionally, long-term progression as well as long-term drug use can be modeled [108]. Furthermore, organoids are discussed as possible testing opportunity for personalized cancer treatment. For example, organoids could be used for gene-drug correlation studies and then testing the response of the identified drug in the organoids. A study screening 160 FDA-approved chemotherapeutics found a high correlation between drug response in organoids and the respective PDX model [109, 110].

The main advantage for the use in personalized medicine is that tumor organoids can be grown from small sample sizes, such as from a fine-needle biopsy [109]. Another major advantage over *ex vivo* tissue slice cultures is that tumor organoids can be cryo-conserved and therefore be used to generate biobanks of several tumor samples. In a recent study, tumor organoids from metastatic gastro-intestinal cancers were used to determine the predictability of personalized medicine. When tested against a compound library of drugs from clinical trials, the authors could show a positive predictive value in 88 % and a negative predictive value in 100 % of the cases. These findings suggest that tumor organoids simulates the response in clinical trials and thus present an excellent model for personalized medicine [111]. However, in most of the cases the follow-up clinical data was already available; thus, the desired result was already known. Furthermore, the study using metastatic colorectal cancer PDOs shows, that not all treatment options allow for a response prediction.

The dependency on extracellular matrices like Matrigel, which is poorly defined and suffers from high batch-to-batch variation in composition, can influence the outcome of an experiment. Furthermore, inhibitors are added already at the beginning of organoid cultures to ensure that tumor cells cannot be overgrown by epithelial cells. These inhibitors or pathway activators, like A83-1, SB202190, Noggin or R-spondin, remain in the media while culturing [112]. This, however, could prime the organoids into a dependency on specific signaling pathways and is a major drawback of this technology. Hence, the response to certain drugs could be correlated to the dependency on these pathways rather than a tumor-specific response in the patient [113].

Additionally, for a long time, the lack of stromal components of the tumor as well as blood vessels and immune cells counted as major limitations of the organoid technology. This limits the spectrum of drugs and investigational compounds that can be tested in this model system. However, Neal *et al*. recently published an article on organoid modeling containing the immune microenvironment [114]. It describes the generation of patient-derived organoids (PDOs), which retain the stromal component of the tumor as well as immune cells. It has been shown that the PDOs retained $CD8^+$ and $CD4^+$ T cells as well as B cells and NK cells with PD -1 expression of the $CD3^+$ T cells. Next, it has been shown that the TCR expression profile of the T cells found in the PDOs matched the TCR in the original patient tumor. Testing a clinically relevant time frame of 7 days it has been shown that the addition of aPD-1 antibody could enhance T cell activity. Using this model, an induction of $CD3^+$ T cells in 6/20 PDOs when treated with aPD-1 was observed, correlating with clinical data in the respective tumor type. No correlation between tumor expression of PD-L1 and the response to aPD-1 treatment was found. Thus, this model represents a way to test the patient's response towards aPD-1 treatment in a clinically relevant timeframe. However, this model still exhibits the

limitations of the organoid culturing system. Even though the organoids are grown in an air-liquid interface, they are still embedded in Matrigel which remains poorly defined. Furthermore, for the optimal growth of the PDOs the media is supplemented with the afore mentioned inhibitors and pathway activators.

Additionally, the assay testing the effects of aPD-1 treatment shows the increase in $CD3^+$ T cells, it fails to although recapitulate the cytotoxic effect on the PDOs by these T cells.

3.5.2 Linking multiple readouts leads to treatment decisions

In personalized medicine, it is not only important to choose the right test system before finding a treatment for the patient, but also to get as much information about the tumor as possible. The cancer field has learned early on, that the tissue of origin is not the only important factor for treatment decisions even though it remains one of the most important determinants in the clinic. As a result of gaining more knowledge about the underlying genetic alterations in cancer, more targeted therapies entered the market. Yet, this still does not cover the entirety of the tumor. Thus, the next step must be to integrate as much data as possible on the tumor before making the treatment decision. Therefore, the tumor's entire 'Omics', like genomics but also proteomics and metabolomics, should be investigated and analyzed and combined with clinical data to find the best-fitting treatment option which can, after being validated using patient-derived functional tumor models *in vitro*, be used to help the patient [92].

4. Objectives

The main disadvantages of the aforementioned test systems are that they either rely on cancer cell lines, which do not reflect patients' tumors, PDX models, which are time and cost-intensive, or organoids, relying on the use of undefined external matrices and signaling pathway inhibitors to grow, and thus possibly priming the organoids in another direction than the original tumor.

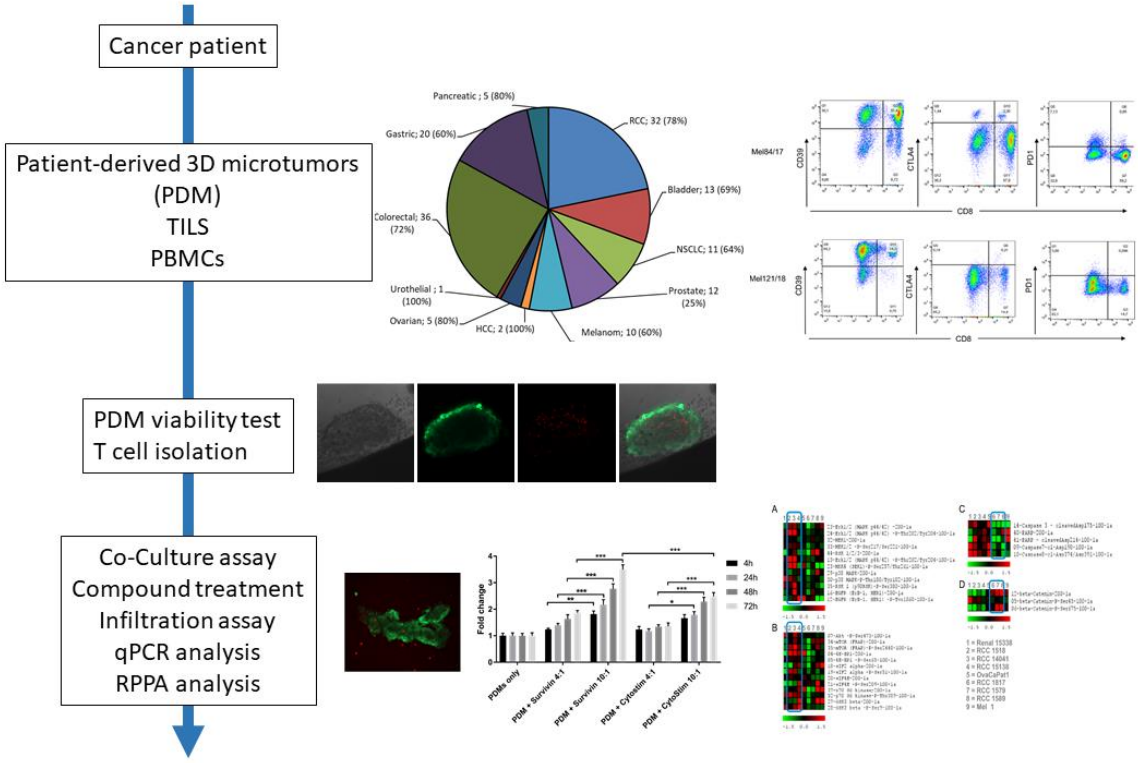

Figure 6: Work-flow from the PDM isolation to the different assays and read-outs that can be generated.

Focusing on renal cell carcinoma and malignant melanoma the aim of this thesis was to develop and validate an assay system together with readout-technologies that circumvents these disadvantages (Figure 6). It is based on 3D patient-derived microtumors (PDM) which are viable in a matrix- and inhibitor-free media. Using autologous immune cells isolated from the tumor tissue or the peripheral blood of a patient the possibility to test immune modulatory drugs in co-cultures of PDMs with such immune cells should be assessed. Moreover, the PDM culture model should be linked with multiple read-outs including the quantification of the direct response to treatment with standard-of-care (SOC) and/or immune modulatory drugs, as well as RNA and protein expression profiling to assess pathway alterations or the presence of cancer stem cells.

5. Results

5.1 Cultivation of the patient-derived 3D microtumors

The aim of this PhD thesis was to establish and characterize a 3D platform with patient-derived microtumors (PDMs) of different tumor types for late pre-clinical phase drug development and mode-of-action analyses. From a long-term perspective, this platform would facilitate the validation of a drug candidate under close-to-*in-vivo* conditions reflecting a patient's tumor before moving on to clinical trials. Furthermore, the aim was to create a system that could support approaches of personalized medicine to tailor cancer treatments to individual patients in the future. Therefore, a rapid isolation of PDMs as well as immune cells from patients and closely reflecting the cancer situation in the patient (e.g. not using extracellular matrix components from mice like in Matrigel™) is crucial. Towards this aim, the first step was to establish a robust protocol (see method section 12.1.1) for isolation and culturing of PDMs *ex vivo*. Kondo *et al.* have previously provided a methodology for isolation and cultivation of 3D-cancer-tissue-originated spheroids from colorectal cancer [115]. In this thesis, based on this methodology, a protocol for isolation of microtumors from a variety of tumor entities (Figure 7) was developed with the main focus on renal cell carcinoma (RCC) and melanoma PDMs for compound efficacy testing and mode-of-action analyses.

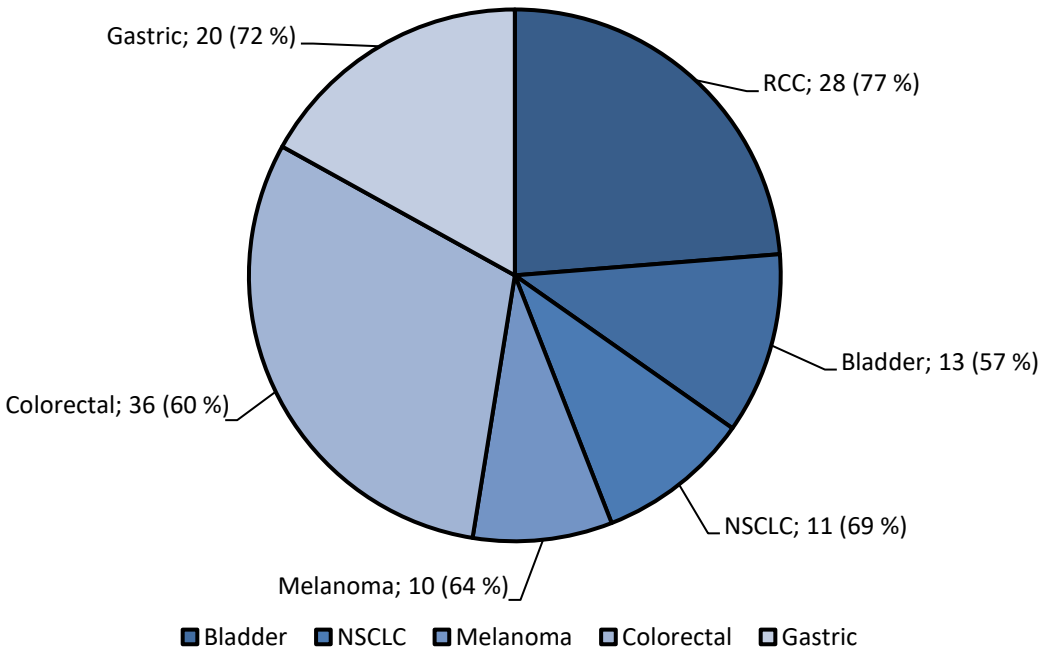

Figure 7: Pie chart of the tumor entities used for PDM isolation. The number stated after the tumor entities describes the number of samples received and the percentage given in brackets shows the success rate of isolating viable PDMs in a quantity sufficient for testing at least 10 different assay conditions (see method section 12.5).

The PDMs were cultured in a basal stem cell medium (see material section 11.4) to maintain their spherical structure without attaching to the culture dish and their cellular heterogeneity. Importantly, no serum is needed while culturing. This reduces the variability of the media due to the poorly defined serum and reduces influencing the growth and expression of cancer specific cellular markers in the PDMs due to growth factors contained in the serum. However, the media may be adjusted depending on cell type, for instance, by adding hormones in hormone-dependent tumor types. Furthermore, if heparinized peripheral whole blood from the same patient is available, autologous serum can be used to enhance the viability of the PDMs.

A successful isolation of PDMs from tumor tissue of different origin was achieved (percentage stated in brackets for each tumor type tested; see Figure 7), when the viability of the PDMs was generally above 70% shown by Calcein-AM live cell staining (5.2.2) and the amount of PDMs was sufficient (at least 1000 PDMs) for testing at least 3 compounds at each 5 conditions in triplicate using the CellTox™ Green Cytotoxicity Assay (either SOC treatment or coculturing with T cells) (see method section 12.5).

5.2 Characterization of the PDMs

The use of PDMs grants access to a novel patient-derived disease model to assess the efficacy of different approaches in cancer therapy and must therefore be carefully characterized and validated. In order to show that this rapidly available disease model is suitable to mimic the disease and the response of the tumor to either SOC treatment or co-culturing with immune cells, it is important to have a reliable response to the PDMs to the treatment as well as a reliable assay system to measure the response. Furthermore, in order to understand the response of the PDMs to treatment, it is important to characterize the different PDM models regarding the cellular composition as well as their expression profile of different tumor as well as cancer stem cell markers.

Accordingly, different aspects of the PDMs; (including cellular viability, expression of cancer stem cell markers on RNA as well as protein level, histological characterization by immunohistochemical staining of tumor markers in PDMs side-by-side with corresponding primary patient tissue, qRT-PCR based gene expression analysis, protein expression analysis as well as TIL characterization using flow cytometry) were investigated.

5.2.1 Patient information and tumor entities

Medical record numbers and patient identifiers from the Universitätsklinik Tübingen were converted to a pseudonym for all PDM models prior to shipment. For all samples an appropriate ethics vote was available. The corresponding study plans for the respective projects had been submitted to the ethics committee for consultation. Furthermore, all patients whose material was used during this thesis have been informed about the project from the medical side and have agreed to the corresponding use of residual tumor tissue. In Table 2, the clinical data for renal cell carcinoma as well as for malignant melanoma PDM models is given. This entails patient gender, age and TNM status.

Table 2: Clinical data for tumor tissue samples used for successfully isolated renal cell carcinoma PDMs. For these samples, their pseudonym, gender, age and most importantly TNM status, as it reflects the clinical status of the tumor tissue, are given.

ENTITY	PATIENT-ID	GENDER	AGE	TNM STATUS	HISTOLOGY
RCC	RCC15-138	Female	68	T4N2M1	Clear cell
	RCC1435	Male	59	T1an0m0	Papillary
	RCC1436	Female	69	T1aN0M0	Papillary
	RCC1438	Male	77	T3aN0M0	Clear cell
	RCC1447	Male	72	rT1anN0M0	Clear cell
	RCC1518	Male	61	T1aN0M0	Clear cell
	RCC1519	Female	65	T3cN0M0c	Clear cell
	RCC1575	Female	71	T3bN0M0	Clear cell
	RCC1579	Male	63	T3aN0M0	Chromophobe
	RCC1589	Male	84	T3aN0M0	Papillary
	RCC1577	Male	54	T1bN0M0	Chromophobe
	RCC17-014	Female	43	T2aN0M0	Clear cell
	RCC16-433	Male	84	T3aN0M0	Clear cell
	RCC14-041	Male	60	T1N1M2	Clear cell
	RCC17-025	Male	55	T3bN0M0	Clear cell
	RCC17-108	Male	54	T1bN0M1	Papillary
	RCC17-139	Male	65	T3aN0M0	Clear cell
	RCC1753	Female	57	T3aN0M1	Clear cell
	RCC1755	Female	61	T1bN0M0	Clear cell
	RCC17-098	Male	66	T1aN0M0	Chromophobe
	RCC17-119	Male	88	T1bN0M0	Clear cell
	RCC17-142	Male	74	T1aN0M0	Clear cell

	RCC1764	Male	63	T1aN0M0	Clear cell
	RCC1773	Female	65	T2aN0M0	Clear cell
	RCC17-109	Female	83	T3aN0M0	Clear cell
	RCC1817	Male	53	T1bN0M0	Chromophobe

RCCs can be divided into several histological subgroups. Both clear cell RCCs as well as papillary RCCs originate from the epithelium of the proximal tube, whereas the chromophobe RCCs originate in the distal nephron. The most common form of RCC, is the clear cell RCC which represents 75-80 % of RCCs, followed by papillary RCCs (10-15 %) and chromophobe RCCs (5 %) [56].

The PDM models generated from RCC tumor tissue closely reflect the situation in the clinic. 69% (18 samples) of the samples originated from a clear cell RCC, whereas 15% (4 samples each) originated from either papillary or chromophobe RCC samples. The remaining 1% was later found not to be tumor tissue. The untypically high percentage of chromophobe RCC compared to papillary RCC could be due to the low sample size in general.

Looking at the success rates for PDM generation, it can be said that from roughly 50% of the clear cell RCC tumor samples the generation was successful. 89% of the successfully generated PDMs from clear cell RCC had a tumor status of 2a or higher. The same observation could not be made for papillary or chromophobe RCC, which could again be due to the small sample size. In general, no link between sex and age of the patient to the success rate of PDM generation could be found.

Table 3: Clinical data for tumor tissue samples used for successfully isolated malignant melanoma PDMs. For these samples, their pseudonym, gender, age and most importantly TNM status, as it reflects the clinical status of the tumor tissue, are given.

ENTITY	PATIENT-ID	GENDER	AGE	TNM STATUS	MUTATIONS
MALIGNANT MELANOMA	Mel 84/17	Female	39	T4bN2M0	Braf WT, NRas WT, cKit WT
	Mel100/17	Male	73	-	Braf WT, NRas WT, cKit WT
	Mel102/17	Female	59	pT4aN3cM1a	Braf V600E, NRas WT, cKit WT
	Mel122/18	Female	64	pT4bN3M1c	Braf V600E, NRas WT, cKit WT
	Mel124/18	Male	66	-	Braf WT, NRas Q61R, cKit WT
	Mel10030K18	Female	54	pT3bN1aM0	Braf WT, NRas mut Exon 2, cKit WT

Looking at the melanoma samples, no similar link between the TNM status or the mutation profile and the success rate for PDM generation could be found. However, when isolating TILs for a subsequent CellTox™ Green Cytotoxicity Assay it could be observed that the amount and viability of the T cells was higher in WT melanoma samples.

This thesis is focused on the characterization of RCC and malignant melanoma PDM models. For the following experiments, six RCC PDM models (RCC1589, RCC1518, RCC1575, RCC1579, RCC15-138 and RCC1817) were chosen as they reflect the three different RCC subgroups. In the following experiments using malignant melanoma PDMs, the models Mel84/17 and Mel100/17 were chosen, as they are Braf, NRas and cKit WT, and thus, a high viability and amount of TILs could be isolated for subsequent experiments in these samples.

5.2.2 Viability of isolated PDMs in culture

It was crucial to ensure working with a highly viable PDM culture before running any assays, as a reliable result is only achieved with a viable cell population. Otherwise, the measured cell death could also be the result of an inherent problem of the PDM culture, meaning that the low viability diminishes the stability of the PDM culture and therefore, the significance of any subsequent performed assay. As such, fluorescent Live/Dead cell staining was performed with Calcein-AM and SytoxOrange. Calcein-AM, which is used to stain viable cells, can enter the live cells by diffusion and is then processed by esterases in the cytoplasm to green fluorescent Calcein [116]. Furthermore, without the ester group the Calcein can no longer pass through the cell membrane and is thus confined to the cell. Sytox Orange is a cell membrane-impermeable dye that is used to stain dead cells. It emits red fluorescence upon binding to DNA and can only enter cells with a compromised plasma membrane (i.e. dead or late apoptotic / dying cells) [117]. After isolation, the PDMs were cultivated for two passages (one passage for the PDMs is defined here as a complete media exchange through centrifugation performed every two to three days) to allow the formation of a spherical and smooth microtumor structure. Then, the PDMs were stained with Calcein-AM and SytoxOrange, and phase contrast as well as fluorescent microscopic images in green (Calcein) and red (SytoxOrange) channels were taken (see method section 12.1.4).

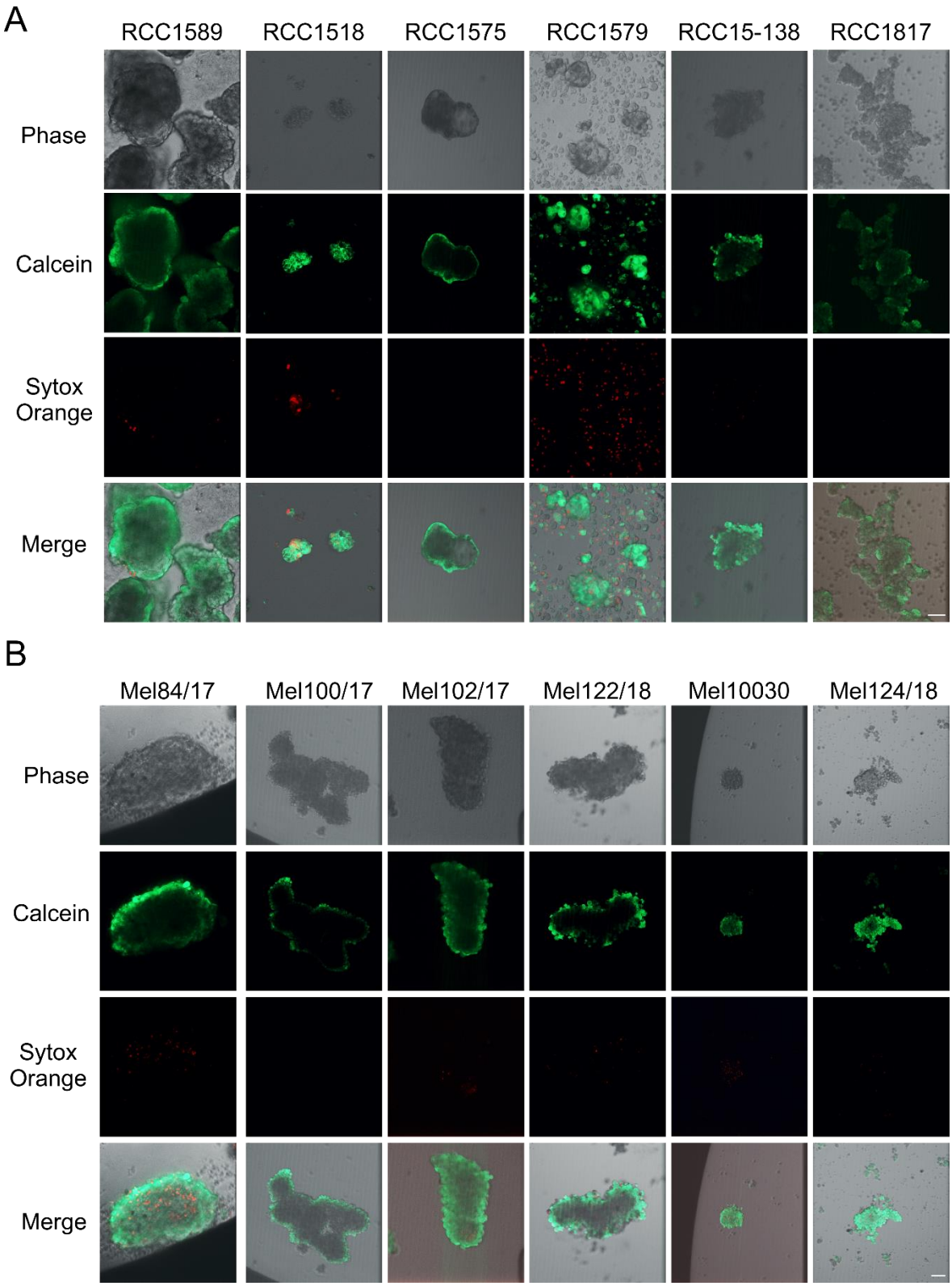

Figure 8: Live/Dead assay of PDMs isolated from respective RCC (**A**) and malignant melanoma (**B**) tissue specimen. After isolation and cultivation for two passages (one passage for the PDMs is defined here as the complete media exchange through centrifugation performed every two to three days), the PDMs were stained with Calcein-AM and SYTOX Orange to determine the viability of the PDMs. **A** Live/Dead assay of the RCC PDMs used in the following experiments **B** Live/Dead assay of the melanoma PDMs used in the following experiments. Please note visual evaluation by human eye of pictures in panels above is less sensitive than software measurements of raw data. Scale bar: 100 µm.

In Figure 8 A the Live/Dead assay of PDMs derived from primary RCC tissue specimen is shown. The diameter of the PDMs differed between models derived from different tumor tissue specimen. In the RCC PDM samples, the PDM diameter was roughly 100 µm except for the RCC1589 PDMs, which here roughly 300 to 400 µm in diameter. The overall viability of the RCC PDM samples was between 84.1 % (RCC1518) and 99.3 % (RCC1817). Thus, the PDMs all displayed a viability above 80% and were therefore suited for cytotoxicity assays (Table 4, for determination of viability and diameter see method section 12.1.4). With a viability of 80% or higher, it could be ensured that the measured cell death in the subsequently performed assays is not due to the low stability and viability of the PDM culture.

Individual microtumors in PDM models obtained from the malignant melanoma tissue samples (Figure 8 B) had generally larger diameters than the RCC samples. Except for the PDMs samples Mel10030 and Mel124/18, which were roughly 150 µm in diameter, the malignant melanoma PDM samples were around 400 to 500 µm. The overall viability of the malignant melanoma PDMs was between 76.7 % (Mel102/17) and 99.9 % (Mel100/17). With a viability below 80 %, Mel102/17 and Mel10030/17 PDMs were not suitable for further cytotoxicity assays. However, most of the malignant melanoma PDM samples displayed a viability above 80 % and could therefore be used in the subsequent experiments.

It could be observed that the green fluorescence focuses on the outer cell layers of the PDM, especially in larger PDMs (e.g. RCC1589, Mel 84/17 or Mel 122/18). This effect has also been described by others when working with 3D spheroid models derived from immortalized cancer cell lines [118]. One explanation for this phenomenon could be that Calcein-AM is already processed to Calcein in a high extent by the outer layer cells of the PDM, preventing its diffusion between the neighboring cells, and thus to inner cells of the PDMs. However, no literature was found on that topic to prove this hypothesis. As no difficulties of the SYTOX orange agent to defuse into the center of the PDMs were observed, it was likely that the cells in the center are alive cells.

Table 4: Percentage of live and dead cells in the respective PDM model. Only PDM models with a viability higher than 80% are used for subsequent assays.

PDM model ID	Measured fluorescence green	Measured fluorescence red	Percentage live cells [%]	Percentage dead cells [%]
RCC				
15-138	7.674	0.215	97.2	2.8
1518	9.175	1.46	84.1	15.9
1575	5.769	0.345	94.0	6.0
1579	7.631	0.963	87.4	12.6
1589	12.893	0.377	97.1	2.9
1817	5.775	0.04	99.3	0.7
Malignant melanoma				
84/17	24.669	2.741	88.9	11.1
100/17	1.739	0.001	99.9	0.1
102/17	13.752	3.208	76.7	23.3
122/18	6.129	0.191	96.9	3.1
124/18	10.21	0.087	99.1	0.9
10030/17	14.545	3.193	78.0	22.0

5.2.3 Comparison of PDMs to the original tumor tissue

The PDMs are supposed to serve as a model system for a patient's tumor, to test different treatment options and respective individual responses. In order to be able to use the PDMs as such, it needs to be confirmed that they maintain the features of the original tumor tissue. Therefore, the PDMs were thoroughly characterized at the molecular level and compared to corresponding primary tissue of the original patient tumor.

5.2.3.1 Immunohistochemical staining of tumor markers

Immunohistochemical staining of FFPE (formalin-fixed paraffin-embedded) sections of the PDMs is used to determine the overall structure (Hematoxylin & Eosin (H&E) staining) of the microtumors as well as for tumor markers (for method see 12.1.5 Immunohistochemical staining of the microtumors and parental tissue).

For the fixation of the PDMs, FFPE is used, because patient tissue is generally also FFPE fixed in the clinic and can therefore be used to compare PDM sections with the original tumor tissue.

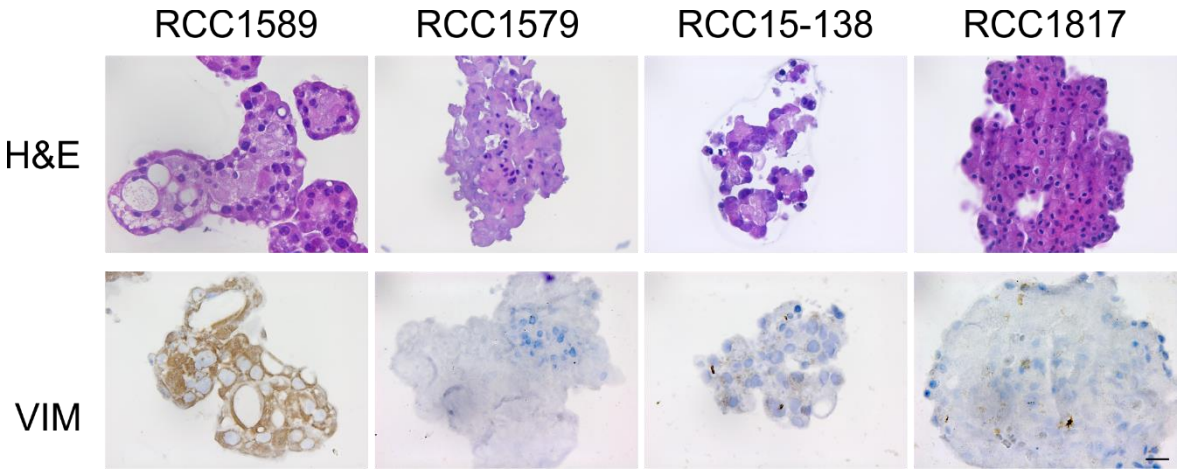

Figure 9: RCC models are stained with Hematoxylin & Eosin (H&E) to visualize the overall structure of the PDMs. The RCC PDMs were stained for Vimentin (VIM), a known clear cell RCC marker. Scale bar: 20µm. Pictures were provided by Jennifer Schieber.

In four of the RCC PDMs the cytoplasm and the nuclei were stained using H&E. This revealed clear differences in the cellular structure of the PDMs from different patients, which nicely corresponds to the histology of the clinical data (Table 3). The following description and assessment was not performed by a pathologist but only compared with available sources.

The papillary RCC PDMs of RCC 1589 display slightly enlarged and irregular nuclei in the H&E staining, which reflects the Fuhrman grade 2 also found in the clinical data of the tumor [119, 120]. Furthermore, the PDMs show a strong signal for the EMT marker Vimentin. The expression of Vimentin in RCC tumors is associated with clear cell and papillary RCC. In around 87 % to 100 % of these tumors, an expression of Vimentin can be observed [121]. This shows that the expression of Vimentin is sustained from the papillary tumor to the respective PDMs.

RCC15-138 PDMs, which originate from a clear cell RCC, displayed large nuclei and a comparatively small cytoplasm (Figure 9 upper panel). This correlates to the clinical Fuhrman grade 3 of the parental tumor [122]. As expected for clear cell RCC, the staining for Vimentin shows a slight expression of the EMT marker in RCC15-138 PDMs. However, the staining is not as strong as in RCC1589 PDMs.

RCC1579 and RCC1817 are both chromophobe RCCs and in both PDMs the nuclei are small and stained intensely purple, which could explain the absence of Fuhrman grading in the parental tissue of these patients. As described in literature for chromophobe RCC no expression of Vimentin could be detected in the PDMs of RCC1579 [123]. For RCC1817, a single Vimentin-positive cell can be observed in the staining. This could be due to the EMT marker also being expressed in healthy renal tubular cells, which could be incorporated in the PDMs [124].

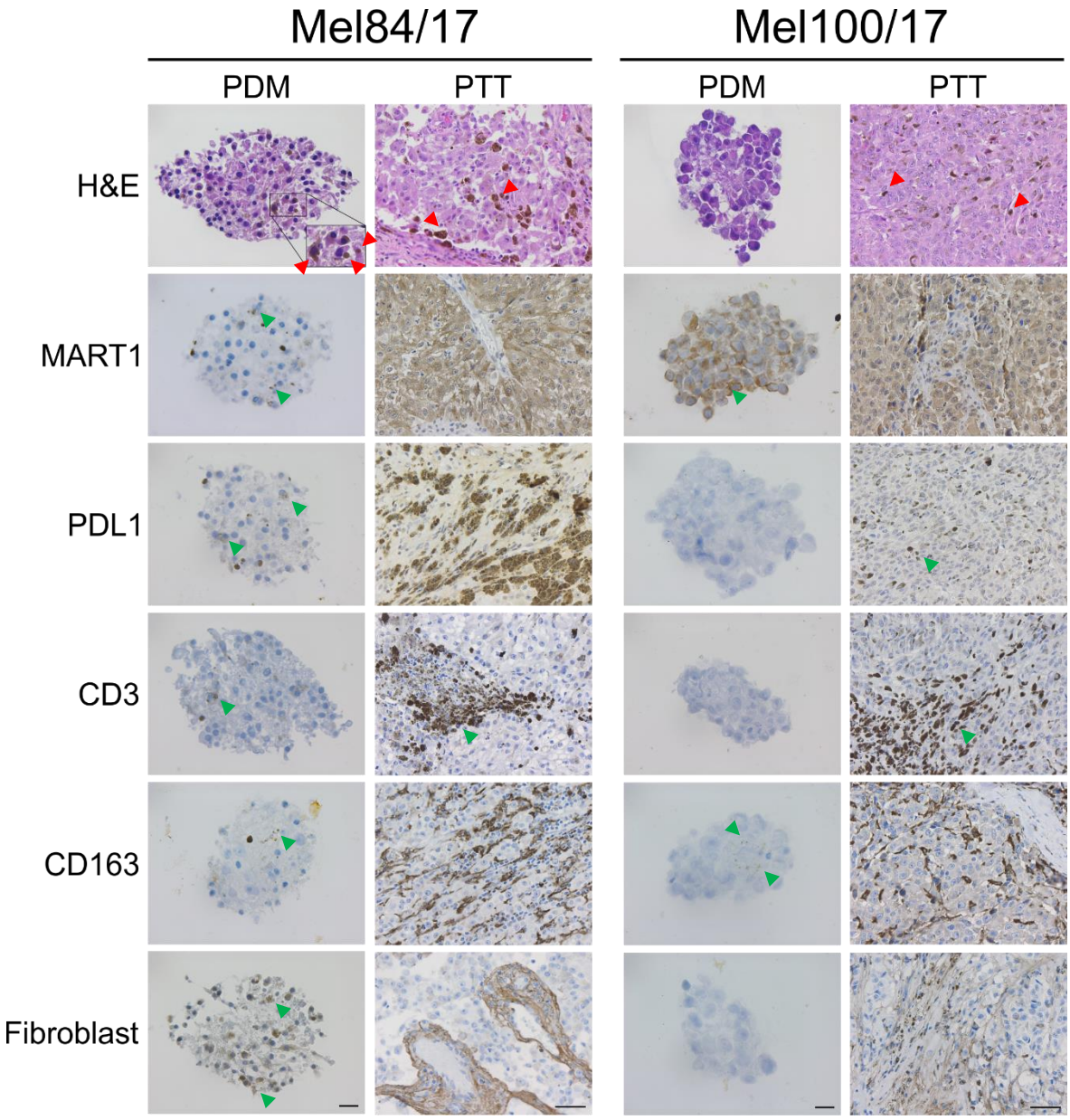

Figure 10: Melanoma PDMs and the corresponding patient tumor tissue (PTT) are stained with H&E as well as for the melanoma antigen MART1, the presence of PDL1, CD3 for the presence of T cells in the PDMs, CD163 for the presence of macrophages and for the presence of fibroblasts in the PDMs. The fibroblast antibodies were generated by inoculation with whole human thymic stoma cells; therefore, no specific antigen is known [125].Scale bars are 20 µm in the PDMs and 50 µm in the PTT; red arrows mark melanocytes; green arrows mark the positive staining. Pictures were provided by Jennifer Schieber.

Melanoma PDMs were stained with H&E to visualize the overall structure. It could be observed that the PDMs of Mel84/17 retained melanocytes which are visible as brown spots in the PDM (see Figure 10 enlargement and red arrows). In the staining of the PTT, the melanocytes are clearly visible (red arrows). For Mel100/17, on the other hand, only a few melanocytes were visible in the PTT and none in the PDMs (Figure 10).

The PDMs were stained for the melanoma antigen MART1, the presence of PDL1 the ligand of the checkpoint protein receptor PD1 expressed on T cells, CD3 as a marker of T cells in the PDMs [126], CD163 as a marker of macrophages [127] and for the presence of fibroblasts.

Staining for MART-1 is used to establish the diagnosis of metastatic melanoma in patients [128]. Staining for MART-1 in the parental tissue of both, Mel100/17 and Mel84/17 resulted in a strong signal. For Mel100/17, this strong MART-1-positive phenotype is retained in the corresponding PDMs. For Mel 84/17, the MART-1 staining is almost completely lost. However, when taking a closer look at the parental tissue of Mel84/17, areas with lower MART-1 expression are visible, suggesting the stained PDMs resulted from an area with weaker MART-1 expression.

Staining for PDL1, the ligand of the checkpoint protein receptor PD1 expressed on T cells, in Mel84/17, a signal could be observed in the parental tissue as well as in the PDMs suggesting a susceptibility of the tumor for aPD-1 treatment [129, 130]. In Mel100/17, on the other hand, even though a faint signal for PDL1 could be observed in the parental tissue, the PDMs showed no signal after staining for PDL1.

Staining for CD3 shows the infiltration of the tumor tissue by T cells and the retention of T cells in the PDM. In both parental tissue stainings, infiltrated T cells could be observed. In contrast, in the PMDs only for Mel84/17 a signal for CD3 can be observed, suggesting that T cells are partly retained in the PDMs of this model.

Staining for CD163 reflects the M2 macrophages infiltrated in the tumor tissue [131]. For both parental tissues, a CD163 signal can be observed. For both PDM models, Mel 84/17 as well as Mel100/17, a staining signal for CD163 can be observed as well. Thus, macrophages from the parental tumor are retained in the PDMs.

In both parental tissues, the presence of fibroblasts can be observed. However, only in Mel84/17 PDMs these fibroblasts are retained. The presence or absence of fibroblasts in the tumor can be important, since cancer-associated fibroblasts (CAF) are crucial in the formation of tumor niches and modulate the tumors response to therapeutics [132].

In summary, the PDM models analyzed here partly retain the histological properties of the corresponding parental tumor. However, not all properties are reflected with the same intensity as in the parental tumor. Especially the localization of T cell and macrophages in the tumor tissue is less prominent in the PDM models, which could either reflect that the immune cells are washed out during the preparation of the PDM models or that the cultivation conditions are not optimal for immune cells. In case the immune cells are washed out during the preparation, it is important to

collect the flowthrough and thus, the immune cells therein. In case the cultivation conditions are optimized to prolong the viability of the immune cells retained in the PDMs, the viability of the PDM models has to be carefully checked as well.

Taken together, it is important to characterize the PDMs of each patient to better understand the subsequent assay results.

5.2.3.2 Identification of cancer stem cells in PDM models

An emerging field in cancer therapy is the treatment of cancer stem cells, which were first described in 1875 by Conheim, who proposed the existence of self-renewing cells with pluripotent properties in malignant tissue [29]. The hypothesis is that a tumor not only consists of the fast-dividing tumor cells, which are susceptible to chemotherapy, but also of a slow-dividing cell population, which exhibits stem cell-like characteristics [31, 32].

In order to evaluate whether PDMs are a valid model to test compounds targeting cancer stem cells, qPCR as well as protein profiling using Reverse Phase Protein Microarrays (RPPA) for the presence of cancer stem cell markers was performed (see method section 12.1.3 and 12.7). Due to the fact that no parental tissue was available for this analysis, a comparison of the expression profiles of the PDM models and the respective parental tissue was not possible.

For the analysis, the following CSC as well as stem cell markers were chosen:

- Gli1 and 2, which are downstream proteins of the Hedgehog signaling pathway an important CSC regulator [133, 134].
- Prom1/CD133, which is widely used as a marker the detection and isolation of CSC. Even though its physiological function remains elusive, its localization in the membrane of microvilli suggests an involvement in the organization of the membrane [135].
- BMI1, which plays an important role in the self-renewal of normal stem cells, is also frequently upregulated in CSCs. However, the expression of BMI1 alone does not mark a CSC. It is mostly co-expressed with other CSC markers like CD133 and CD44 [136].
- CD44, which can bind to several heparan sulfate-binding growth factors like the fibroblast growth factor or the epidermal growth factor thereby leading to a survival advantage. CD44 alone or in combination with other markers (e.g. CD24 or CD133) is identified as a typical CSC marker [137].
- CD24 functions in cell-cell and cell-matrix interactions in healthy cells. Together with CD44 and CD133 it is one of the most commonly used CSC markers. Furthermore, its association with metastasis makes it an important prognostic factor [138].

- ALDH1A1 is one of the aldehyde dehydrogenases, which are critical for the detoxification of aldehyde substrates. The subgroups ALDH1A1, ALDH1A2 and ALDH1A3 are associated with CSCs as well as normal stem cells and are involved in self-renewal, differentiation and self-protection [139].

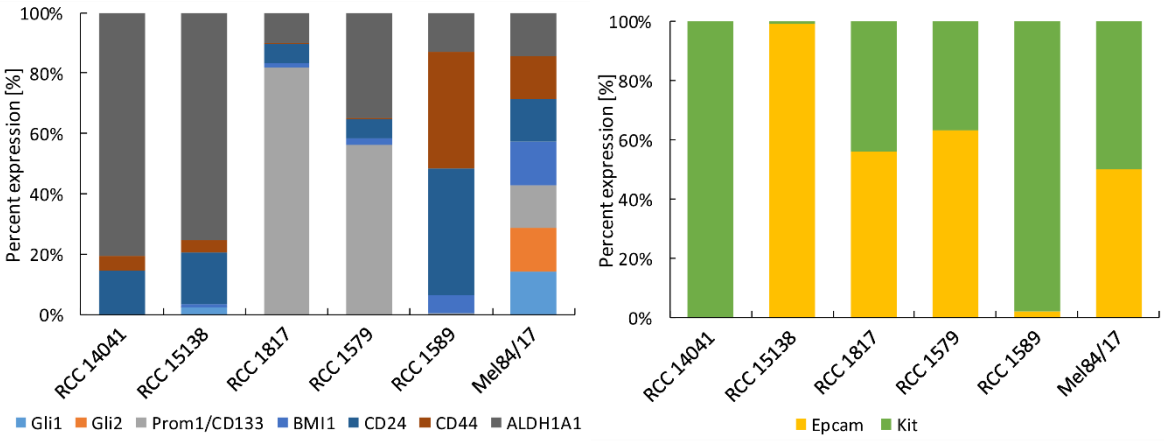

Figure 11: qPCR for the expression of cancer stem cell markers. The expression of the cancer stem cell markers was analyzed in the PDMs and normalized to the expression in Mel84/17.

qPCR analysis (Figure 11) showed that the gene expression of selected cancer stem cell markers could be detected in all RCC PDM models tested as well as the Mel84/17 PDM model derived from malignant melanoma. The Mel84/17 model was used to normalize target gene expression in the analyzed samples, since all tested markers were expressed in this model. For the RCC PDM models, it was observed that each model expresses a different set of stem cell markers and the intensity of expression differs between the models. For instance, RCC1817 showed no expression of Gli1&2, a low expression of BMI1, CD24, CD44 and ALDH1A1 and a high expression of Prom1/CD133, whereas RCC1589 showed no expression of Prom1/CD133, a low expression of BMI1 and ALDH1A1 and a high expression of CD24 and CD44.

This implies that each RCC PDM model has a unique subset of CSCs expressing an also unique combination of cancer stem cell proteins. This suggests that the PDM models are suited for the testing of CSC targeting therapeutics. However, it should be considered to determine the stem cell protein subset of each cancer patient to ensure targeting the right CSC protein.

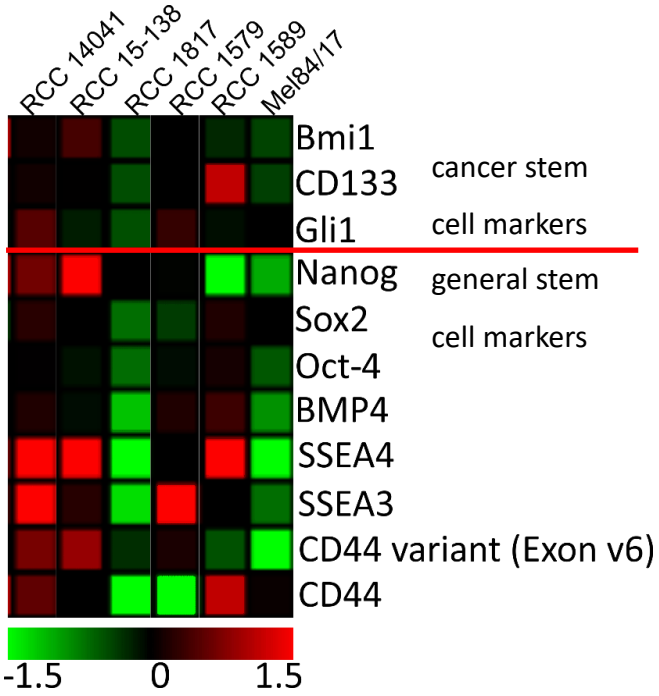

Figure 12: Protein analysis for the expression of cancer stem cell markers. Cancer stem cells can also be detected using RPPA protein profiling. The heat map shows a downregulation of the marker expression in green and an upregulation in red. Colors reflect the $\log^2$ transformed median centered normalized fluorescence units which have been normalized to the protein amount used for the assays.

Furthermore, the presence of cancer stem cell markers in the PDMs could be shown on the protein level using RPPA analysis (Figure 12). Here, additionally to the above-described CSC and stem cell markers BMI1, CD133, Gli1 and CD44, the general stem cell markers Nanog, Sox2, Oct-4, BMP4, SSEA4 and SSEA3 were analyzed. Nanog and Oct-2 are described as key stem cell factors in RCC and a co-expression of both factors predicts a poor prognosis [140]. The Oct-2/Nanog downstream protein SOX2 is a general embryonic stem cell (ESC) marker, which is also described in CSCs of RCCs and breast cancer. The pathway is important as it is described to be involved in tumorigenesis and self-renewal [140, 141]. The bone morphogenic protein 4 (BMP4) plays an important role in embryonic development and the maintenance of the hematopoietic stem cell niche [142]. The stage-specific embryonic antigens 3 and 4 are a key marker in identifying ESC. SSEA3 is found in adult human mesenchymal stem cells, whereas SSEA4 is expressed in mesenchymal and cardiac stem cells. Both have been described to be expressed in breast cancer cells and CSCs [143].

As observed in the qPCR analysis, the protein level of different markers varies between different models. One striking observation was that there were two distinguishable groups of RCC PDMs, which cluster regarding the protein profile: group 1 with RCC14-041 and RCC15-138 on one hand and group 2 with RCC1817, RCC1579 and RCC1589 on the other.

Comparing the protein data to the qPCR data, it can be observed that the correlation between RNA and protein data is not given for all markers, which indicates that a strong transcription of CSC markers does not necessarily reflect a high expression of the respective proteins. However, the presence of CSCs in the PDM models could be shown on the RNA as well as the protein level. Thus, the PDM models do reflect the *in vivo* situation for the presence of CSCs and can be used to test the effects of CSC-specific therapeutics in a close to *in vivo* situation.

5.3 Protein array analysis of cancer-related signaling pathways

It has become evident in recent years that the genome-based approach of characterizing tumors and identifying respective treatment strategies is challenging due to the rapid genomic and cellular evolution of tumors. Tumors are accumulating mutations, and these are rarely shared between individual cancer patients with the same malignancy. Therefore, a more relevant and robust way to analyze each patient's tumor on pathway aberrations is needed. One way to do so is RPPA protein profiling (see method section 12.7). Using this method, up- and downregulation of cancer related protein signaling pathways can be analyzed, as not only the total protein but also the phosphorylated and i.e., activated protein can be measured. Furthermore, it is important to base therapeutic testing and subsequently decisions on the protein levels as most therapeutics target proteins.

Using RPPA protein profiling, not only the presence of cancer stem cell markers was tested (5.2.3.2 Identification of cancer stem cells in PDM), but also cancer related pathways were investigated with regard to their activation status as well as up- or downregulation of key players of these pathways.

A total of 109 proteins phosphorylated or unphosphorylated were analyzed (see appendix Figure 34). Two different signaling pathways were investigated in more detail: the MAP kinase pathway and the Akt/mTOR pathway. The MAP kinase pathway is a highly complex signaling pathway, which is often involved in oncogenesis, tumor progression and drug resistance. Even though members of the MAP kinase pathway have been targeted by specific therapeutics, resistance to these inhibitors, often by downstream mutations, is a current problem [144]. The Akt/mTor pathway plays an important role through combining a variety of extracellular stimuli to regulate growth and development. However, the pathway has also been described as one of the most deregulated pathways in the pathogenesis of various human cancers. The central role of this pathway led to a large effort to develop pharmaceutical agents targeting this pathway [145].

This quantitative analysis of the phospho-protein signature of the different PDM samples allows for a discrimination of tumor groups with higher or lower functional pathway activities.

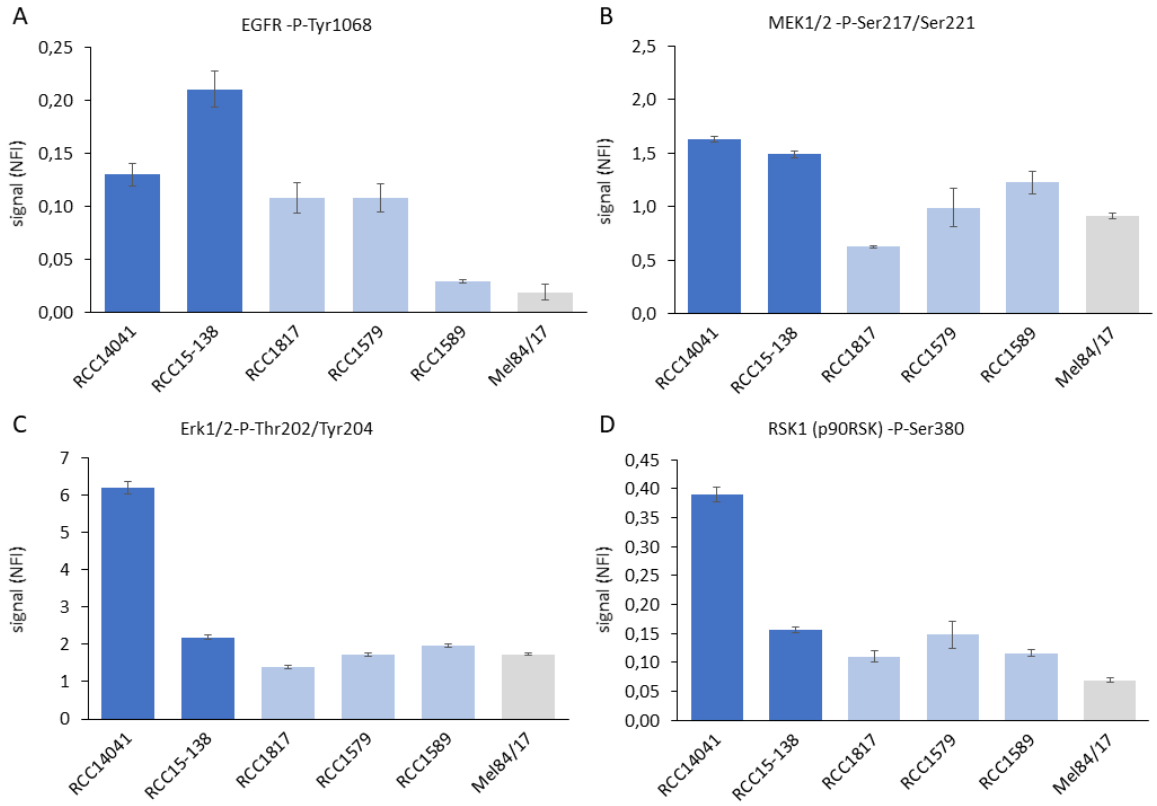

Figure 13: RPPA analysis key markers of the MAP Kinase pathway. **A** Analysis of the presence of phosphorylated epidermal growth factor receptor (EGFR). **B** Analysis of the presence of phosphorylated MEK1/2 **C** Analysis of the presence of phosphorylated Erk1/2 **D** Analysis of the presence of phosphorylated RSK1.
The dark blue bars reflect the expression cluster group 1; the light blue bars reflect the expression cluster group 2; the grey bar reflects the malignant melanoma PDM Mel84/17. (NFI = normalized fluorescence units; normalized on protein amount used for the assay).

In Figure 13, the presence of phosphorylated, thus activated, MAP kinase pathway proteins, EGFR, MEK1/2, Erk1/2 and RSK1, is visualized using bar graphs. EGFR is the receptor for the epidermal growth factor activating the MAP kinase pathway [146]. An activating mutation of this receptor can lead to a constantly active signaling cascade [147]. MEK1/2 is located upstream of Erk1/2 in the MAP kinase signaling cascade. The mutational activation of MEK1/2 can lead to a constantly phosphorylated state of Erk1/2, leading to an abnormal activation of the signaling cascade [148]. Phosphorylated or mutationally activated Erk1/2 can activate the downstream p90 ribosomal S6 kinase (RSK) by phosphorylation [149].

The grouping of the PDM samples observed during the CSC analysis (5.2.3.2 Identification of cancer stem cells in PDM) can also be observed in the activated MAP kinase pathway profile. The PDMs of group 1 (RCC14041 and RCC15-138 (dark blue)) show an upregulation of phosphorylated MAP kinase pathway proteins. In Figure 13A, the quantitative analysis of EGF receptor phosphorylated at Tyrosine 1068 is shown. This specific phosphorylation of the receptor, EGFR-P-Tyr1068, is associated with the activation of GAB1 or GRB2 signaling cascade and a sensitivity against erlotinib

[150, 151]. It is visible that in the group 1 RCCs, especially in RCC15-138, the EGF receptor is strongly phosphorylated, leading to an activated MAP kinase pathway. This is also reflected by the presence of phosphorylated MEK in this RCC sample (Figure 13B). In the group 1 RCC RCC14041, on the other hand, neither EGFR nor MEK are highly phosphorylated but their downstream proteins ERK and RSK1 display an activating phosphorylation (Figure 13C&D). This suggests a downstream mutation in this sample, leading to an EGF receptor-independent activation of the pathway. Group 2 PDM samples show a slightly elevated presence of phosphorylated EGFR and MEK, however comparable to RCC14041 without the striking upregulation of phosphorylated downstream pathway proteins.

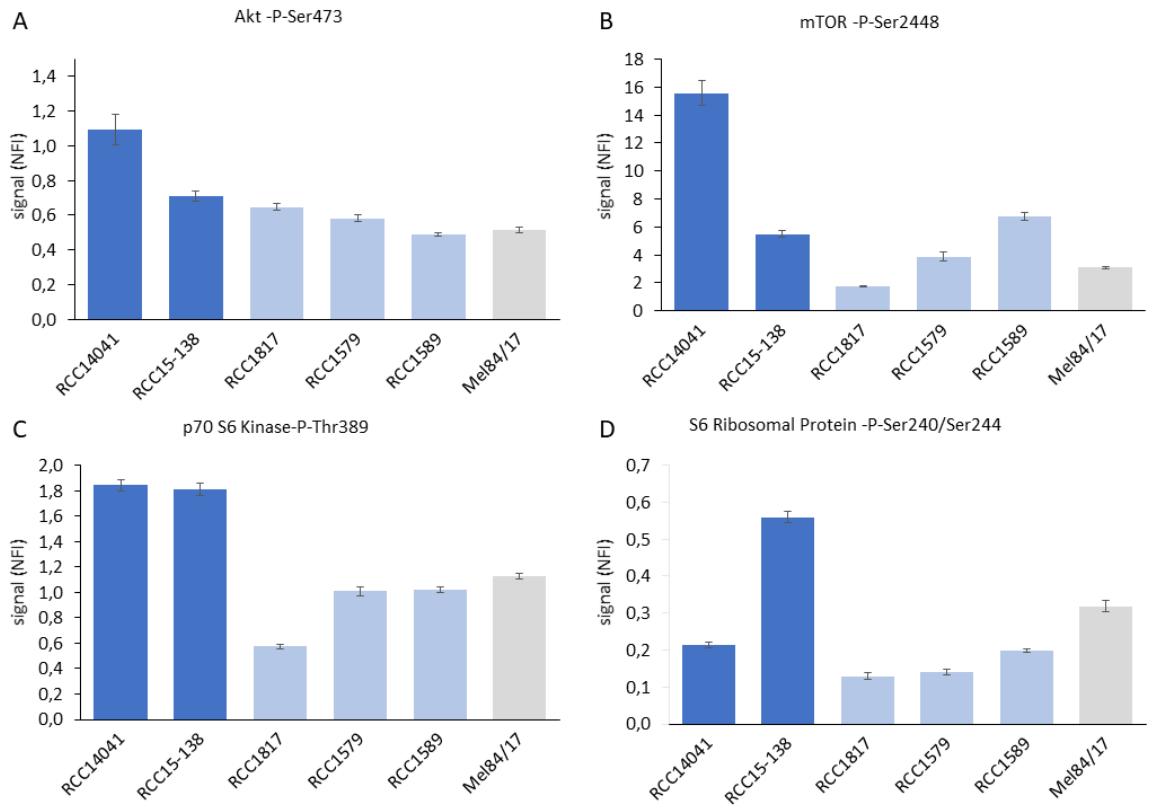

Figure 14: RPPA analysis of the Akt/mTOR pathway. **A** Analysis of the presence of phosphorylated Akt. **B** Analysis of the presence of phosphorylated S6 ribosomal protein **C** Analysis of the presence of phosphorylated mTOR **D** Analysis of the presence of phosphorylated p70 S6 kinase. The dark blue bars reflect the expression cluster group 1; the light blue bars reflect the expression cluster group 2; the grey bar reflects the malignant melanoma PDM Mel84/17.

In Figure 14 the grouping of the RCC PDM samples is observed as well. Figure 14A shows a slight upregulation of Akt phosphorylated at Ser473 in RCC14041 PDMs. For the activation of Akt, two different phosphorylation sites play an important role, Ser473 and Thr308. However, the different phosphorylation patterns correlate differently with survival and malignancy of cancer [152]. The activation of Akt correlates well with the observed upregulation of phosphorylated mTOR (Figure **14**B) in this sample as mTOR is a downstream protein of Akt [153]. The other group 1 PDM RCC15-138 does not show the same upregulation of phosphorylated Akt and mTOR. However, the same strong upregulation of the mTOR downstream protein p70 S6 kinase-P-Thr389, which is the

activation phosphorylation of the kinase [154], is observed for both group 1 PDM samples (Figure 14C). This indicates an Akt/mTor-independent activation of the p70 S6 kinase in RCC15-138 samples. For RCC15-138 samples the p70 S6 kinase seems to act on its known substrate, the S6 ribosomal protein (Figure 14D), leading to cell proliferation [153]. In RCC14041, on the other hand, the same upregulation of phosphorylated S6 ribosomal protein cannot be observed, which could indicate another downstream target of the p70 S6 kinase. One of these downstream targets could be the p90RSK1 [155], which is highly upregulated in the RCC14041 sample (Figure 13D). However, it could also be that the degradation of the phosphorylated S6 kinase is upregulated in RCC14041, thus inhibiting its phosphorylation abilities [154]. Neither group 2 RCC PDM models nor Mel84/17 show a distinct upregulation of this pathway.

5.4 Characterization of tumor-infiltrating lymphocytes

When working with fresh tumor tissue, one of the advantages is the possibility to isolate autologous tumor-infiltrating lymphocytes (TILs). During the preparation of the PDMs from the tumor sample, the flowthrough containing the TILs can collected and the TILs isolated (see method section 12.2.2). Due to the low amount of TILs retained in the tumor samples, they need to be expanded prior to performing experiments. During the expansion, it is important to maintain the TIL composition. Therefore, an expansion regiment using low-dose IL-2 in combination with Il-7 and IL-15 was chosen. After expanding the TILs for two weeks in culture, they could be analyzed regarding the cytotoxic T cell population and the expression of checkpoint inhibitor targets using flow cytometry (see method section 12.2). In order to do so, the cells were stained using fluorescently tagged antibodies against the antigen of interest.

When receiving RCC samples, peripheral blood of the patients was received as well. Therefore, tumor-reactive cytotoxic T cells could be isolated from the PBMCs. Thus, for co-culturing assays with RCC PDM models T cells isolated from the PBMC were used. These T cells were not further analyzed using flow cytometry.

As for the malignant melanoma samples, no peripheral blood was received. Therefore, TILs were isolated from the tumor material. These TILs were further analyzed using flow cytometry.

The benefit of being able to isolate T cells from either peripheral blood of the patient or the tumor tissue broadens the aspects that can be looked at in co-culturing experiments as it is still discussed which T cell population is more relevant in cancer treatment.

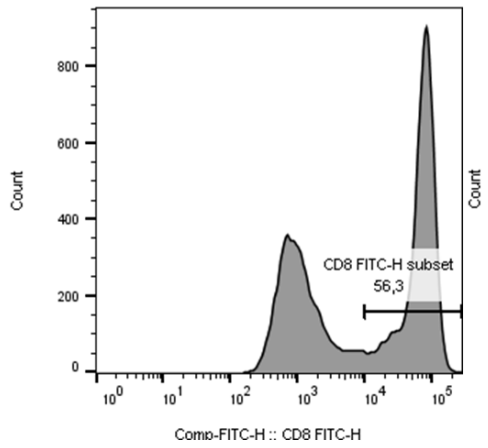

Figure 15: Flow cytometry histogram for determining the gating for the subsequent analysis of the expression of CD39, CTLA4 and PD1 on the expanded malignant melanoma TILs from Mel84/17 PDMs.

The gating for the subsequent performed analysis of the expression of CD39, CTLA4 and PD1 was based on the histogram of $CD8^+$ T cells (Figure 15). A parallel staining for $CD4^+$ T cells, to identify the double positive $CD4^+CD39^+$ population was not feasible due to laser restrictions of the available flow cytometer and the availability of T cells for further flow cytometry analysis.

A comparison of the gating with the unstained control was performed (Figure 16).

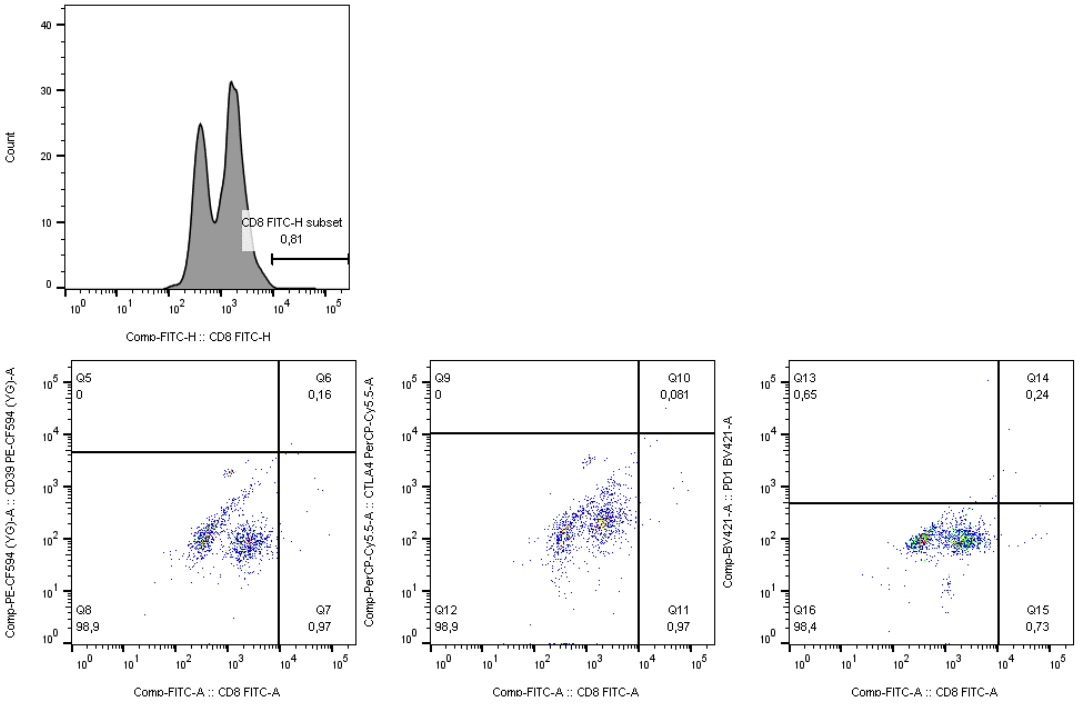

Figure 16: Unstained control of Mel84/17 TILs using the same gating parameters as for the stained samples.

The gating was performed to not incorporate unstained cells in the upper right quadrant which in the subsequently analyzed samples reflect the double positive T cell population.

In all cases, the signal is higher in the stained samples, indicating that the measured signal is not an artefact generated by the unstained cells. Unspecific binding of the antibodies is highly unlikely as the same signal would be observed for all samples.

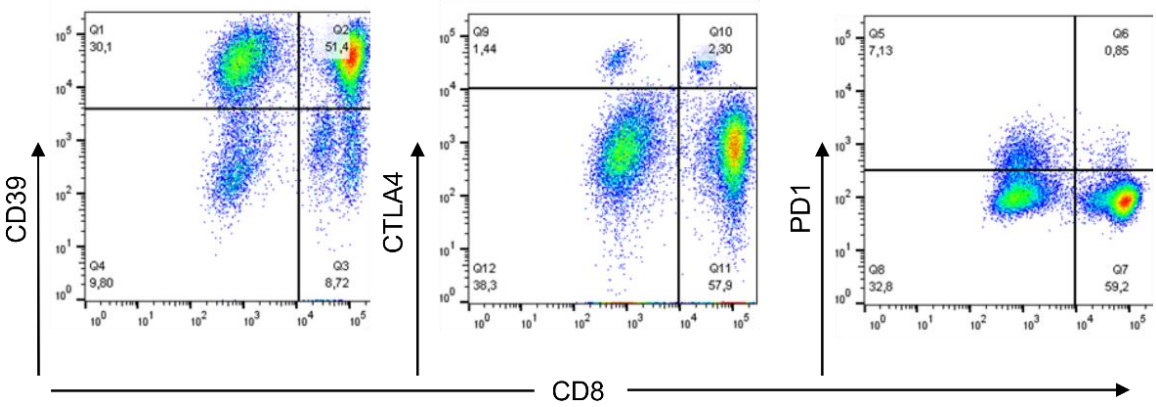

Figure 17: Flow cytometry analysis of Mel84/17 TILs. The cytotoxic TILs were identified by staining against CD8. This population was furthermore stained for CD39, CTLA4 and PD1. A cell population of 50,000 cells was recorded and the boundaries set according to the histogram of $CD8^+$ cells and the unstained control.

The cytotoxic TIL populations, which were CD8 positive, were stained against CD39, a marker for tumor-specific T cells that reside in the tumor. $CD39^+$ cells have been found to have distinct set T cell receptors (TCR) and are efficiently killing autologous tumor cells. The TCRs of these T cells were found to be more oligoclonal than of memory CD8 T cells in peripheral blood. This indicates a local activation and expansion of these cells at the tumor site. Furthermore, it has been shown that a high frequency of these cells leads to a better patient outcome [156]. Mel84/17 has a CD8 and CD39 double positive population of 51.4 %, indicating a susceptibility of the patients tumor to the effects of autologous T cells (Figure 17). The TILs were further characterized by staining for the presence of the checkpoint receptors CTLA4 and PD1. In Mel84/17 TILs, 2.3 % of the $CD8^+$ T cells express the checkpoint protein CTLA4, while only 0.85 % express the checkpoint protein PD1 (Figure 17).

Taken together, the isolation TILs from the tumor tissue during the PDM preparation is feasible. Furthermore, the expansion protocol can be used to maintain different subsets of T cells in the TIL culture, which reflect relevant expression profiles.

However, to deepen the analysis of TIL isolation, expansion, and flow cytometry analysis, more samples are needed. Having the ability to compare the results of multiple samples would further the understanding of the possibility to cultivate the TILs and compare the findings to the phenotypes already described in literature.

5.5 Effect of tumor-reactive T cells on isolated autologous PDMs

A critical merit of cancer therapy is the involvement of the immune system, specifically T lymphocytes [157]. Hence, the second question addressed in this thesis is whether the PDM model can be used to investigate the effect of isolated T cells on PDMs and thus also the efficacy of immunotherapeutic approaches of cancer treatment (see method section 12.3). In order to visualize the effect of the T cells on the autologous PDMs a single RCC15-138 PDM per condition was stained using CellTracker Green, as this cell dye is better retained in the cytoplasm (i.e. less "leaky") compared to Calcein-AM. Next, the RCC15-138 PDMs are incubated with autologous T cells, which were isolated from peripheral blood mononuclear cells (PBMCs) activated against the RCC tumor antigen Survivin (for details on the activation and isolation of the T cells see 12.2 Immune cell isolation). An Effector to Target cell (E:T) ratio of 2:1 and 10:1 has been tested as the use of a to high E:T ratio might diminish the physiological relevance of the assay [158, 159].

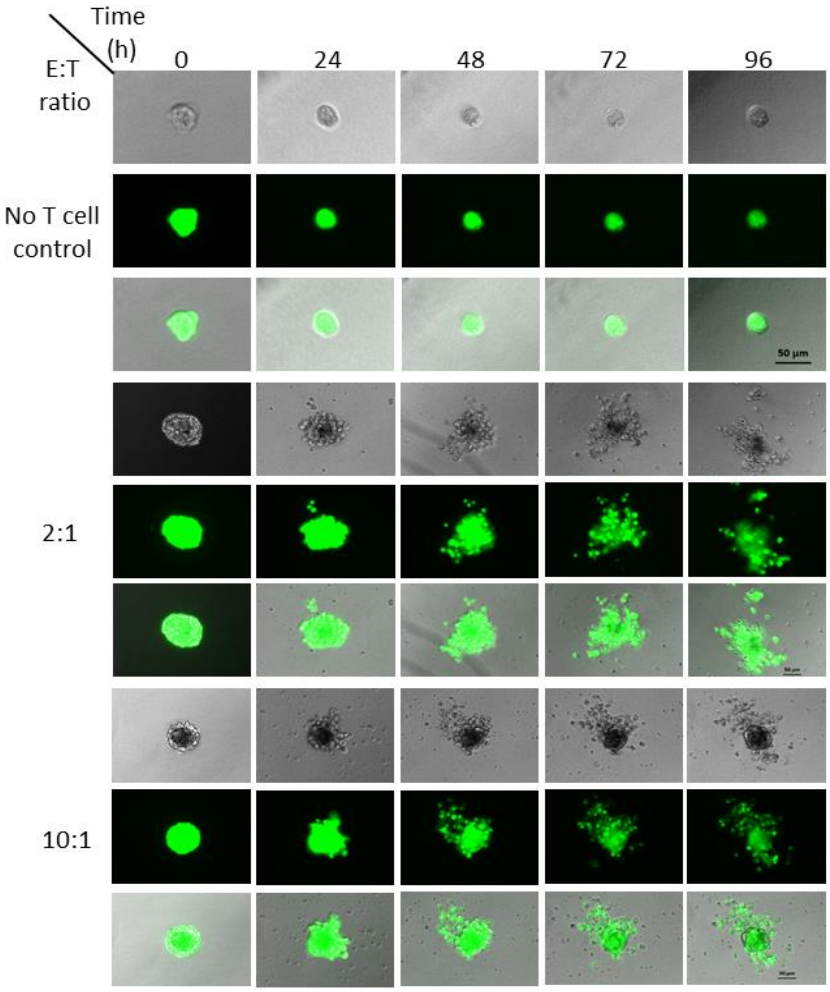

Figure 18: The effect of isolated tumor reactive T cells on single PDMs derived from RCC15-138. Single PDMs were incubated with two different E:T ratios over the course of four days to investigate the effect of the T cells on the PDMs. The PDMs were incubated without T cells (No T cell control), and an E:T ratio of 2:1 and 10:1. PDMs were stained with CellTracker green. Scale bar 50 µm.

At the beginning of the incubation period (t=0 h), no differences were observed with regard to mophology or degree of dye staining between the untreated PDMs and the PDMs incubated with tumor-reactive T cells.

Table 5: Analysis of the area and intensity change depending of the E:T ratio effect of isolated tumor reactive T cells on single PDM (see method section 12.3.3).

	Ctrl		**2:1**		**10:1**	
	area [px²]	Intensity [ROI]	area [px²]	Intensity [ROI]	area [px²]	Intensity [ROI]
0h	0.057	62.244	0.077	77.274	0.066	72.417
24h	0.03	58.728	0.096	70.890	0.093	66.151
48h	0.023	56.478	0.124	56.438	0.136	42.729
72h	0.023	45.306	0.156	42.777	0.143	29.973
96h	0.026	41.307	0.179	34.965	0.153	25.843

However, as early as 24 h after adding Survivin-specific T cells, the PDMs started to disintegrate and lose their spherical shape (Figure 18). Contrary to the control PDM, which is not treated with T cells the area of the 2:1 and 10:1-treated PDMs increased in size (Table 5). In contrast, it was observed that the area of the untreated control decreased over time. This could be due to the culturing conditions as single PDM in a 96 well plate. These effects grew stronger over the course of the incubation. At the end of incubation, the T cell-treated PDMs disintegrated to the extent of covering more than twice the area compared to t=0h. Furthermore, the flourecence diminishes. Even though the flourecence also diminishes by 33.6 % in the no T cell control (which might be caused by bleaching of the fluorescence upon repeated microscopy) the effect is higher in the 2:1-treated PDM (decrease by 54.8 %) and 10:1-treated PDM (decrease by 64.3 %).

This can be further illustrated when calculating the fluorescence per area and normalizing on the 0 h time point (Figure 19). The time-depandant decrease of flourescence per area in the Survivin T cell-treated co-cultures is clearly visible compared to the no T cell control. Furthermore, it can be observed that the effect of treating with 10:1 T cells is stronger than treating with 2:1.

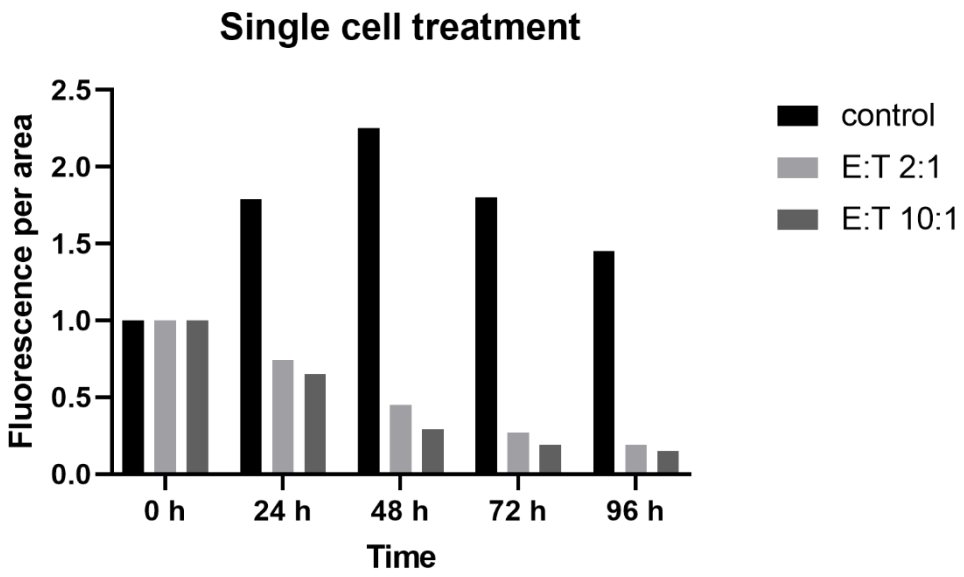

Figure 19: Analysis of the intensity change per area depending of the E:T ratio effect of isolated tumor reactive T cells on single PDM normalized to the starting time point 0h (see method section 12.3.3).

Thus co-culture of autologous Surivin-specific T cells with PDMs from RCC15-138 results in disintregration of respective PDMs over time as well as a loss of viability as compared to untreated PDM control.

As fluorescence imaging allows for mostly qualitative assessment of T cell response towards PDMs, the next step was to establish an assay approach for quantification of T cell-induced PDM killing in the presence and absence of compound treatment.

5.6 CellTox™ Green cytotoxicity assay

After showing the cytotoxic effect of the T cells to the PDMs by live cell fluorescence microscopy, a quantifiable method to determine cell death was the next step to take. A well described method is the dye-release assay. This can be either done by using ^{51}Cr loading of the target cells or by prestaining them with life-cell dyes like Calcein-AM [160]. Due to the need of radioactive labeling when using ^{51}Cr, Calcein-AM was used in the preliminary experiments.

The principle of a dye-release assay using Calcein-AM as a cell dye is to prestain the target cells, in this case the PDMs with a defined amount of Calcein-AM. Afterwards, the target cells are incubated with effector cells or a lysis agent as control. Upon cell death, the live cell dye Calcein is released into the supernatant. Using fluorescence plate readers, like the Envision Plate reader, allows to measure the released dye and thus the corresponding cell death [161]. As a critical amount of cells is needed in order to be able to measure the released dye, an initial experiment using Calcein-AM and an increasing amount of pooled PDMs was performed.

Therefore, to determine the minimal amount of PDMs to be pooled to obtain a reliable dead cell signal, a standard curve was established. For this purpose, an increasing amount of PDMs were pre-stained with Calcein-AM and subsequently lysed with a detergent.

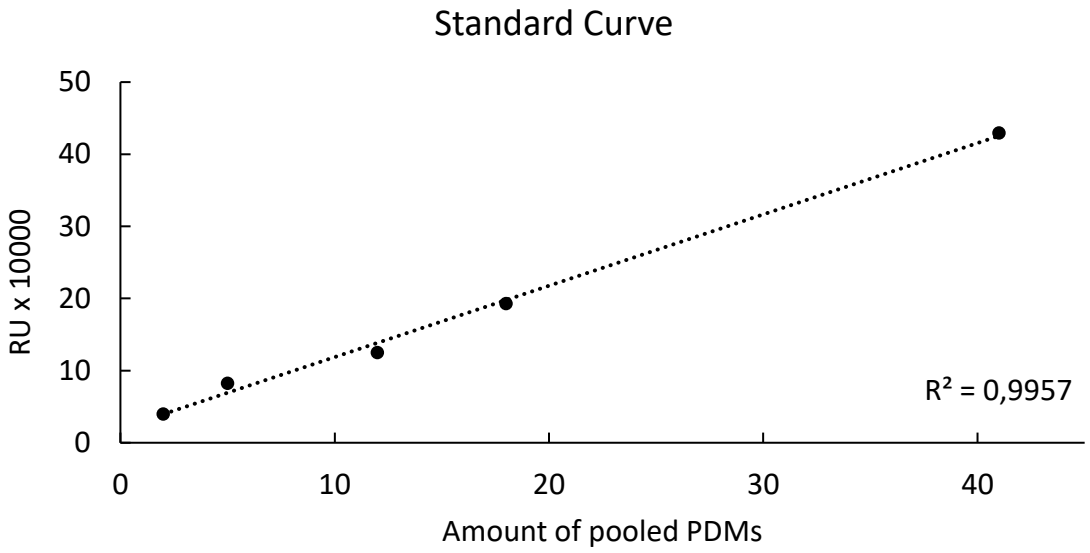

Figure 20: Standard curve of Calcein release into the media by respective amount of lysed PDMs per well of microtiter plate. The release of Calcein into the media is plotted as a function of PDM amount per well. A linear standard curve was added with the degree of determination of R^2=0.9957.

The standard curve (Figure 20) of Calcein release showed a good correlation between the amount of PDMs used and the Calcein signal measured in the culture supernatant. The correlation is reflected in the degree of determination of R^2=0.9957.

However, due to the described leakiness of Calcein from alive cells [161] over time, the subsequent experiments were performed with the CellTox Green reagent instead.

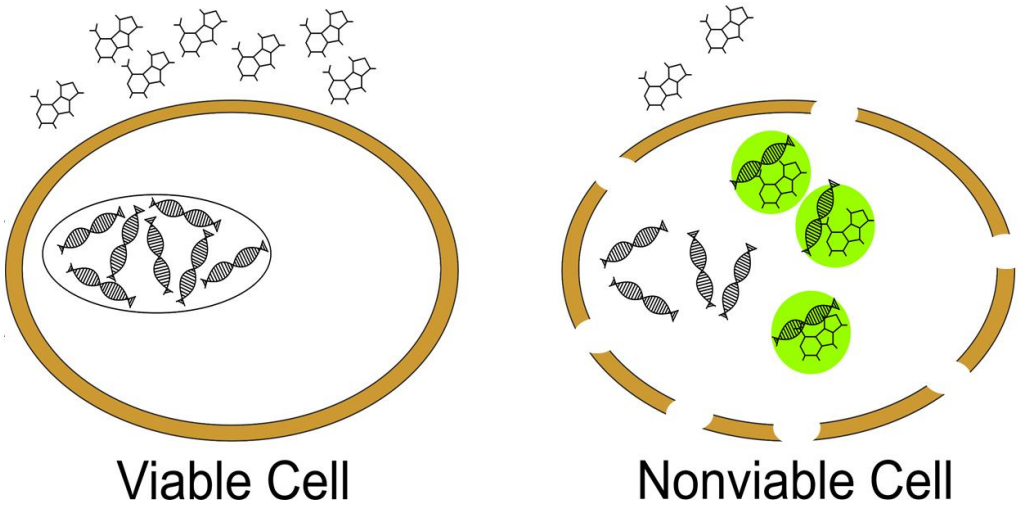

Figure 21: Principle of the CellTox Green reagent. The non-fluorescent dye is excluded from healthy cells with an intact cell membrane. In the presence of a cytotoxic event, the cell membrane loses its integrity and the CellTox green dye can bind to DNA. Upon binding to the DNA, the dye starts to fluoresce green, which can be measured using a plate reader. Adapted from manufacturer's manual.

The CellTox Green reagent cannot enter from healthy cells. It is non-fluorescent in the free DNA-unbound form. Upon cytotoxic cell death, the cell membrane loses its integrity, and the CellTox Green reagent binds to DNA, resulting in a green fluorescence signal, which can then be photometrically measured, e.g using a plate reader (Figure 21).

Nonetheless, for all subsequent assays, based on the initial Calcein-release assay (Figure 20), 15 PDMs were pooled per replicate and treatment. This was done to obtain a fluorescence signal which could be reliably measured using the Envision plate reader. Furthermore, the pooling of multiple PDMs allows to account for effects of size differences of the PDMs as well as accounts to the possible intratumoral heterogeneity of the original tumor.

Cancer displays a high degree of intratumoral heterogeneity [162, 163]. Therefore, it is possible that a part of the tumor exhibits a resistance to treatment whereas another part is affected by the treatment. Thus, the pooling of multiple PDMs also accounts for that heterogeneity and minimizes the risk of overestimating treatment effects.

5.6.1 Efficacy testing using standard of care and investigational compounds using isolated PDMs

Subsequently, experiments testing the possibility to measure the cytotoxic effects of standard of care (SOC) as well as investigational compounds on the PDMs were performed (for methods see method section 12.5.1 and 12.5.3). As a model for RCCs, PDMs from RCC1589 were treated with the second-line standard of care (SOC) agent for RCC tyrosine kinase (TK) inhibitor Axitinib as well as the investigational mTor inhibitor Torin-2.

According to the prescribing information for Axitinib, the oral dose is 2 to 10 mg given twice a day reaching a steady-state after two to three days of 27.8 ng/ml, corresponding to a C_{max} concentration of 71.9 nM.

As the mTOR inhibitor Torin-2 is still an investigational compound, no prescribing information is available. However, the IC_{50} described in literature for Torin-2 to PI3K is 200 nM [164]. The mTOR pathway is often dysregulated in cancer, and thus, the downstream proliferation pathways are activated. Furthermore, this pathway may be of particular interest in RCCs as the expression of the HIF protein depends on the mTOR pathway. The accumulation of HIF proteins is associated with tumorigenesis in RCC [165].

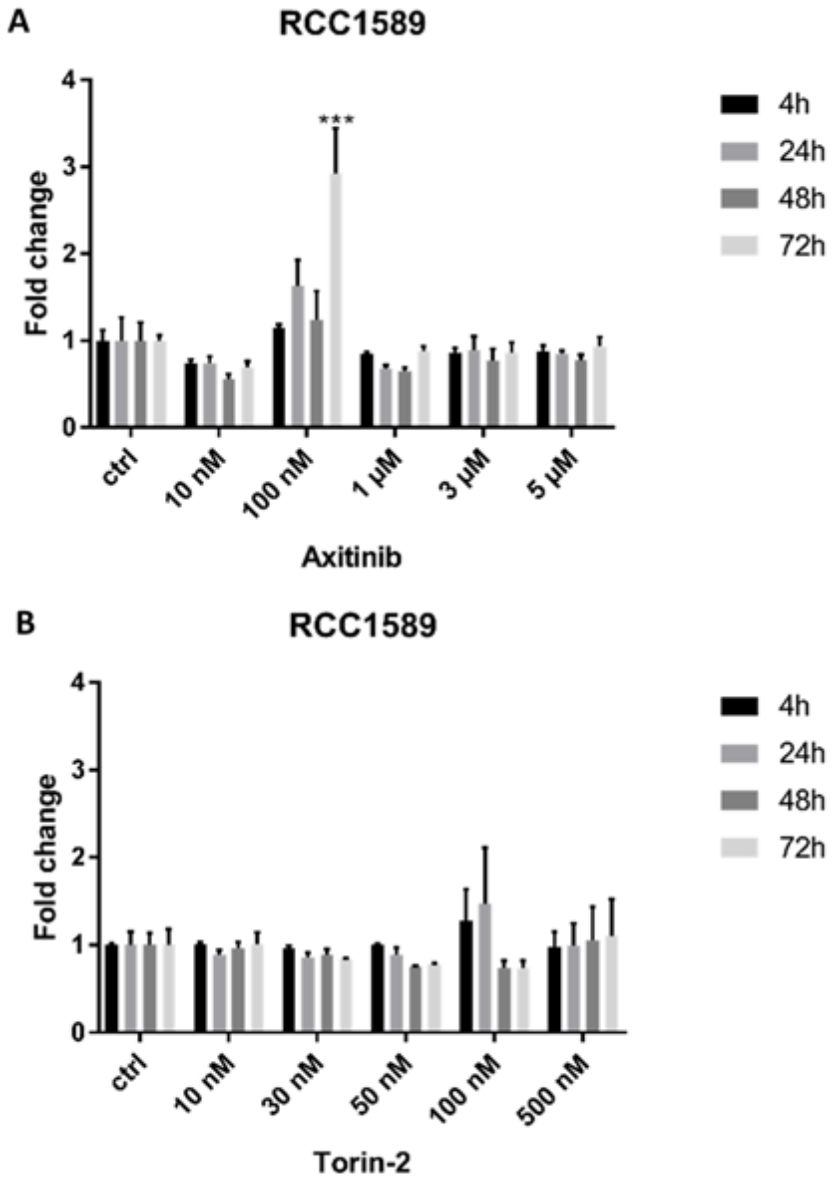

Figure 22: RCC1589 PDMs are treated with the second-line SOC Axitinib and the investigational compound Torin-2. Readouts are normalized to vehicle (DMSO) control. **A** Treatment of RCC1589 PDMs with the TK inhibitor Axitinib **B** RCC1589 PDMs treated with the investigational mTor inhibitor Torin-2. With n=3, statistical test used: 2-way ANOVA with Dunnett's multiple comparisons test *0.033, **0.002, ***0.001.

Treatment with 100 nM, which is the closest to the concentration of this drug reached in patients' blood (71.9 nM), of the second-line SOC Axitinib (Figure 22 A) resulted in a significant cytotoxic effect on PDMs of RCC1589. However, no dose-dependent increase of cytotoxicity could be observed.

The RPPA analysis of pathway alterations of RCC1589 PDMs did not show a distinct upregulation of the MAP kinase pathway (see Figure 13). Taken together with the significant cytotoxic effect of Axitinib treatment, this indicates that these PDMs exhibit no activating downstream mutation of this pathway. Thus, no resistance towards the treatment with the TK inhibitor is found in RCC1589 PDMs.

Furthermore, the RPPA analysis of the Akt/mTOR pathway (see Figure 14) does not suggest driving mutations, like Ser473-phosphorylated Akt, in the Akt/mTOR pathway in the RCC1589 PDMs. It has been shown that activating mutations of PI3K/Akt lead to a sensitivity towards the treatment with mTOR inhibitors [165]. This finding is reflected in the cytotoxicity assay by the fact that treatment of the RCC1589 PDMs with the investigational mTOR inhibitor Torin-2 did not lead to a significant cytotoxic effect.

In cancer therapy, malignant melanoma is still one of the diseases, which can only be successfully treated with excision in an early stage. In advanced melanoma, often, non-resectable metastases have formed, and treating the disease becomes difficult. There are treatment options available that depend on a certain mutational status of the tumor, such as Vemurafenib for the BrafV600E mutation, which activates the downstream MAP kinase signaling pathway. If a patient's tumor does not fit the mutational profile, treatment becomes even more challenging. A new approach in treating melanoma is the investigational PI3K inhibitor BKM-120 or Buparlisib [166]. In Figure 23A/B, Mel84/17 PDMs, which have no Braf mutation (see Table 3) are treated with the investigational compound BKM-120 alone and in combination with the MEK inhibitor Trametinib, respectively.

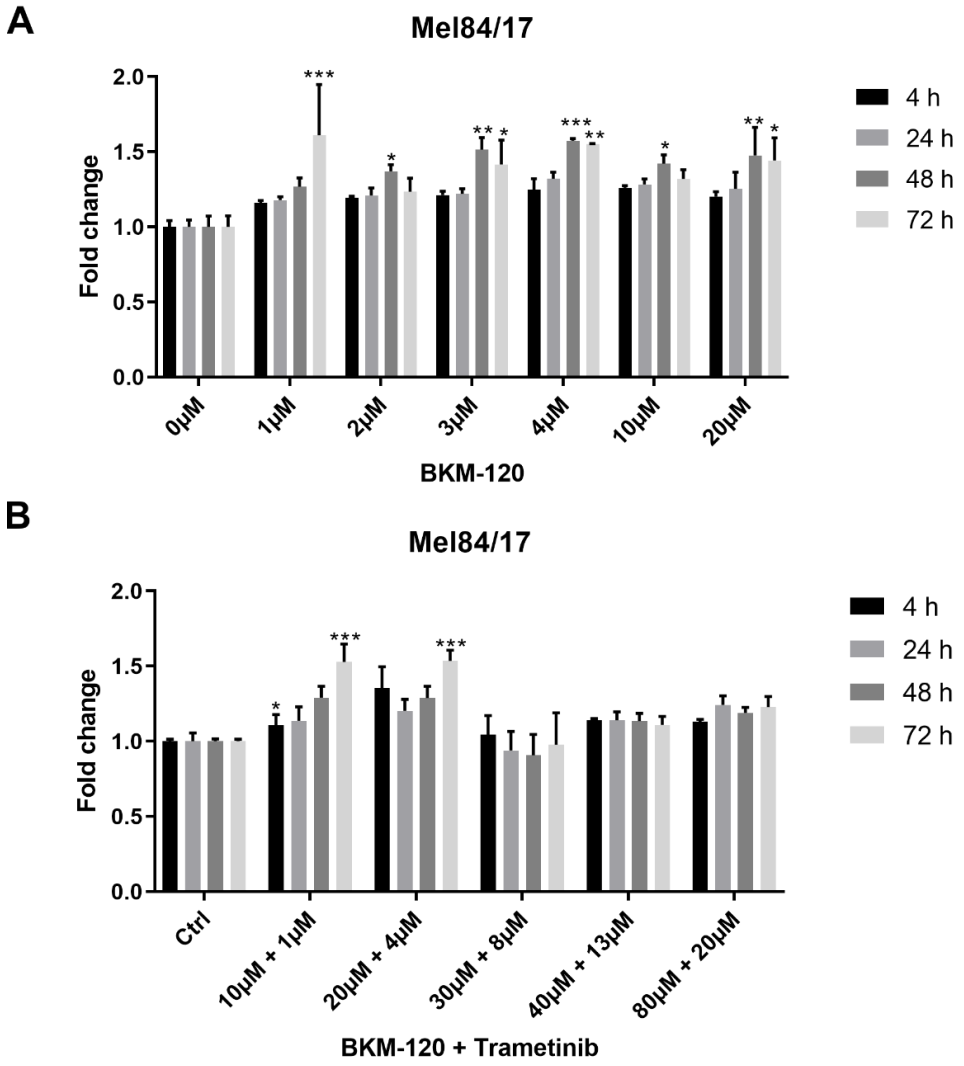

Figure 23: Melanoma 84/17 was treated with the investigational compound BKM-120 alone and in combination with the MEK inhibitor Trametinib. Readouts were normalized to the DMSO control. **A** The Mel84/17 PDMs were treated with BKM-120 over the time of 72h. **B** The PDMs were treated with similar BKM-120 concentrations in combination with the MEK inhibitor Trametinib at concentrations published melanoma cell line experiments. With n=3, statistic test used: 2-way ANOVA with Dunnett's multiple comparisons test *0.033, **0.002, ***0.001

Mel84/17 exhibited a strong cytotoxic response when treated with the investigational PI3K inhibitor BKM-120 (Figure 23 A). Even the lowest tested concentration resulted in significant cell death after 72 h. At higher concentrations of 2 µM, 3 µM, 4 µM, 10 µM and 20 µM, a significant cell death was already achieved after 48 h of treatment. However, a dose-dependent effect of the treatment could not be observed.

The concentration range used in this experiment was chosen to match the lower concentrations of published melanoma cell line experiments of the treatment with BKM-120 alone and in combination with Trametinib [167]. However, this concentration is not reached during patient treatment. The reported c_{max} in patients when given 100 mg BKM-120 once daily is 242.5 ng/ml, which corresponds to 590.9 nM [168, 169]. Furthermore, a study with 17 heavily pretreated

malignant melanoma patients found no benefit of survival when treated with 100 mg BKM-120 once daily [169]. Thus, the observed cytotoxic effects on the Mel84/17 PDMs cannot be reproduced in patients since the concentration could not be reached in patients' serum.

A beneficiary effect of the combination of BKM-120 and Trametinib can be observed in malignant melanoma cell lines [167]. Thus, different concentration combinations were tested in Mel84/17 PDMs.

The combination of the PI3K inhibitor BKM-120 with the MEK inhibitor Trametinib showed significant cell death in the combinations 10 µM Trametinib plus 1 µM BKM-120 and 20 µM Trametinib plus 4 µM BKM-120 after 72 h. The first combination also showed a significant increase in cell death after 4 h of treatment (Figure 23 B). However, the combination of BKM-120 with the MEK inhibitor Trametinib did not further increase the cytotoxicity compared to the treatment with BKM-120 alone (Figure 23 A&B). Furthermore, the concentration range of Trametinib cannot be reached in patients' serum as the reported c_{max} in the prescription information is 22.2 ng/ml corresponding to 36.1 nM. Nonetheless, the finding that the combination of BKM-120 and Trametinib has no beneficial effect in Mal84/17 PDMs is in line with the observation that no upregulation of phosphorylated MEK was found during the RPPA analysis of the MEL84/17 PDMs (Figure 13).

Taken together, the PDMs can be used in a 96-well format to test SOC as well as investigational compounds. The performed experiments result in robust data with a low standard deviation identifying significant cytotoxic compound effects. Furthermore, the observed cytotoxic effects are in line with protein profiles identified during RPPA analysis.

5.6.2 Co-culturing of PDMs with autologous PBMC-derived T cells

The effect of cytotoxic T cells on the tumor is another important aspect in cancer therapy. In most assays, effector to target cell (E:T) ratios up to 20:1 or 40:1 are used since the immune cells are merely HLA matched in such assays but not autologous to the used cell lines [170, 171]. Using PDMs with autologous cytotoxic T cells should allow to use lower, more physiologically relevant E:T ratios.

In order to show that the measured effects were due to the cytotoxic effect of the T cells on the PDMs and not the effect of dying T cells, an initial experiment with PDMs and T cells alone as well as in combination was performed.

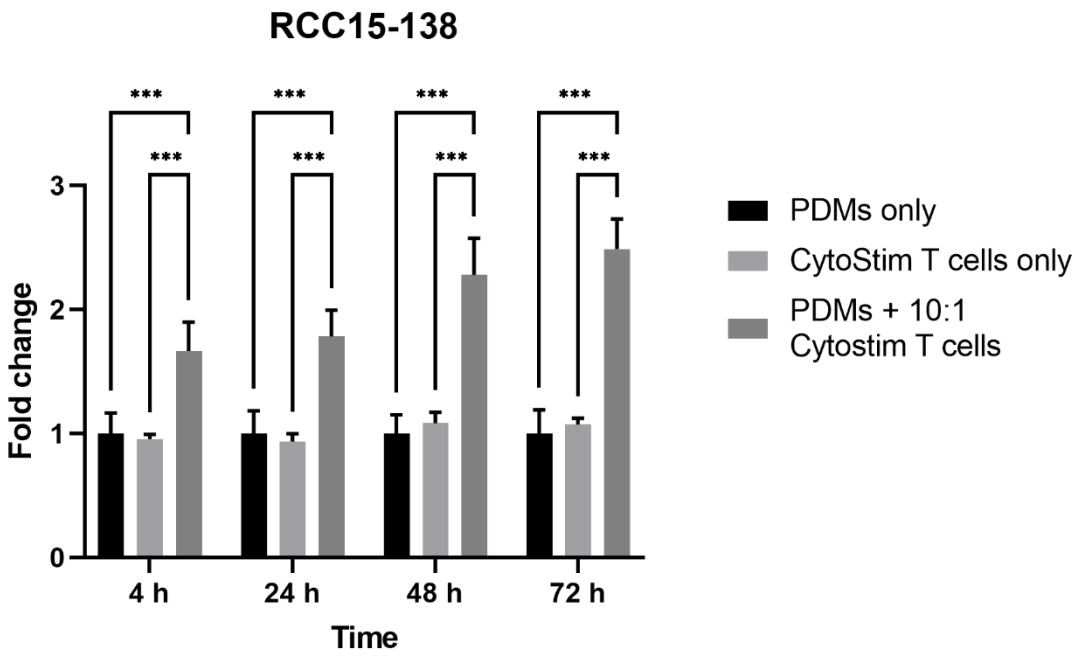

Figure 24: Initial experiment showing that the measured cytotoxic effect is not due to T cells dying during the observed time frame. The amount of autologous CytoStim T cells of RCC15-138 needed for the E:T ratio of 10:1 was incubated alone of the assay time frame of 72h as well as in combination with the respective PDMs. Readouts are normalized to PDM-only control. With n=3, statistic test used: 2-way ANOVA with Tukey's multiple comparisons test *0.033, **0.002, ***0.001

The results of the initial experiment in Figure 24 show that the measured rise in CellTox fluorescence values during the RCC15-138 PDM treatment with 10:1 autologous CytoStim T cells was due to the cytotoxic effect on the cancer cells and not due to T cells dying in the course of the assay time frame. Due to this finding and the fact that T cells cannot be expanded endlessly and are thus a limited resource, no T cell only control was performed in the subsequent experiments.

Prior to performing the CytoTox assay with Survivin T cells, the Survivin expression profile of the PDMs of RCC15-138 as well as RCC1589 was determined.

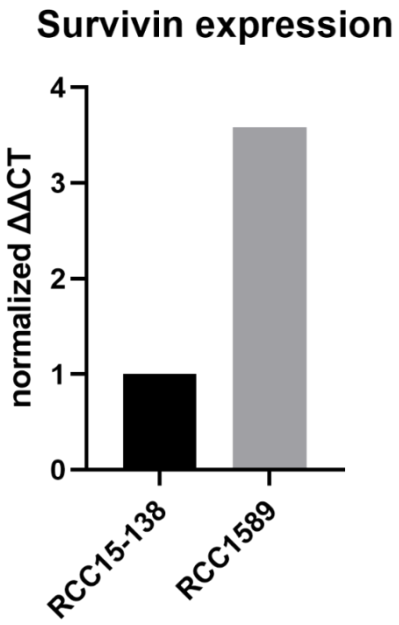

Figure 25: Survivin expression in RCC15-138 and RCC1589 PDMs. The Survivin expression was determined using qPCR and normalized to GAPDH expression, quantified according to the ΔΔCT method, and then normalized on RCC15-138 Survivin expression.

Both RCC PDM samples, RCC15-138 and RCC1589, used in the subsequent experiments express the diagnostic RCC marker Survivin (Figure 25). Thus, a treatment of the PDMs with Survivin T cells is worth pursuing.

Autologous T cells were directed against Survivin (hereafter named Survivin or Survivin T cells), which is reported to be a potential diagnostic marker for a poor prognosis and aggressiveness of the disease as well as a potential treatment target [172-174]. Survivin is an apoptosis-inhibiting protein, which is expressed by tumor cells of different origins to circumvent apoptosis. Furthermore, autologous T cells were broadly activated using the CytoStim reagent (hereafter named CytoStim or CytoStim T cells) by Miltenyi Biotec. This reagent is an antibody, which activates $CD4^+$ and $CD8^+$ T cells by crosslinking the T cell receptor with the major histocompatibility complex on antigen presenting cells [175]. Following, autologous Survivin and CytoStim T cells were tested at the E:T ratio of 4:1 and 10:1 to the RCC15-138 PDMs.

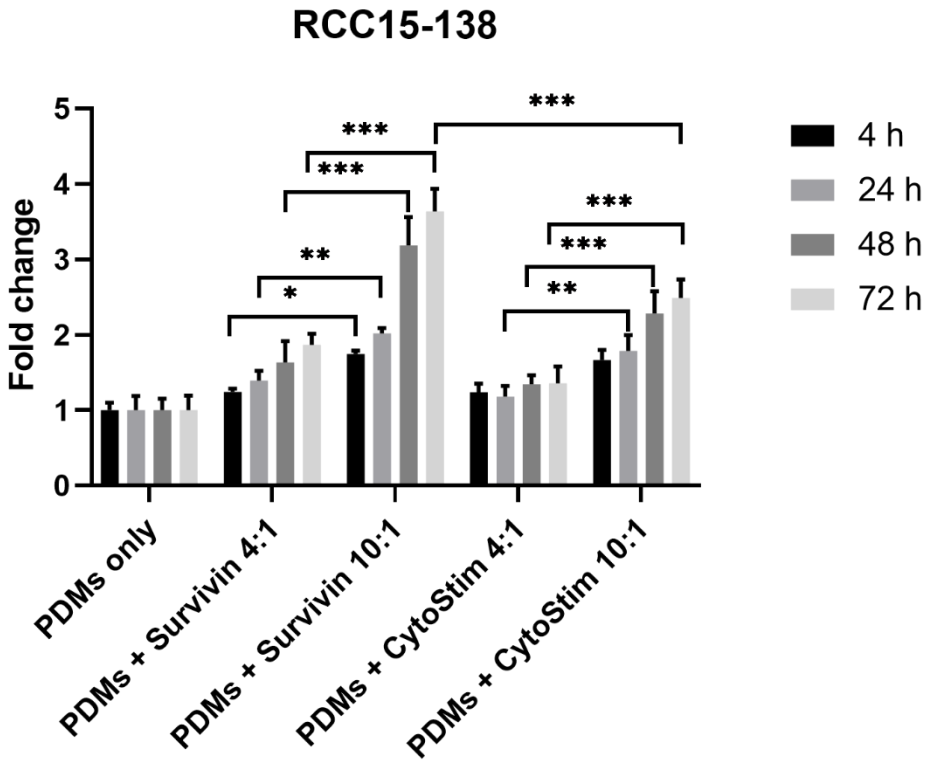

Figure 26: RCC15-138 PDMs were treated with Survivin and CytoStim T cells at an E:T ratio of 4:1 and 10:1 over the time course of 72 h. Readouts are normalized to PDM-only control. With n=3, statistic test used: 2-way ANOVA with Tukey's multiple comparisons test *0.033, **0.002, ***0.001.

Treatment with an E:T ratio of 4:1 Survivin-specific T cells did not show significant cell death but a clear trend of rising CellTox fluorescence values indicating cell death over the time course of 72 h. Treatment with an E:T ratio of 4:1 broadly, not antigen-specific, activated CytoStim T cells on the other hand had no cytotoxic effect on the PDMs. When treated with an E:T ratio of 10:1 Survivin-specific T cells, the PDMs exhibited significantly increased cell death compared to the E:T ratio of 4:1. The same effect could be observed for PDMs treated with an E:T ratio of 10:1 CytoStim T cells compared to 4:1 CytoStim T cells. After 72 h, treatment of the PDMs with 10:1 Survivin T cells resulted in a significantly higher fluorescence level, corresponding to cell death, than treatment with 10:1 CytoStim T cells (Figure 26).

The CytoTox assay showed a significant E:T ratio-dependent increase in CellTox fluorescence values indicating cell death over time. Furthermore, it shows that the antigen specific Survivin T cells in a ratio of 10:1 after 72h were significantly more efficient in tumor cell killing in a model that expresses the respective antigen than the broadly activated CytoStim T cells. Thus, the presented CytoTox assay system using PDMs and autologous T cells is capable of identifying such differences. Moreover, the low standard deviation of the results suggests a reliable assay system with low variability and high viability of the PDMs without treatment despite the complex co-culture system.

In order to have a closer look at the PDMs' response to T cell-specific immunotherapeutic treatment, the E:T ratio of 4:1 Survivin or CytoStim T cell treatment was combined with the checkpoint inhibitor aPD-1, Nivolumab, respectively.

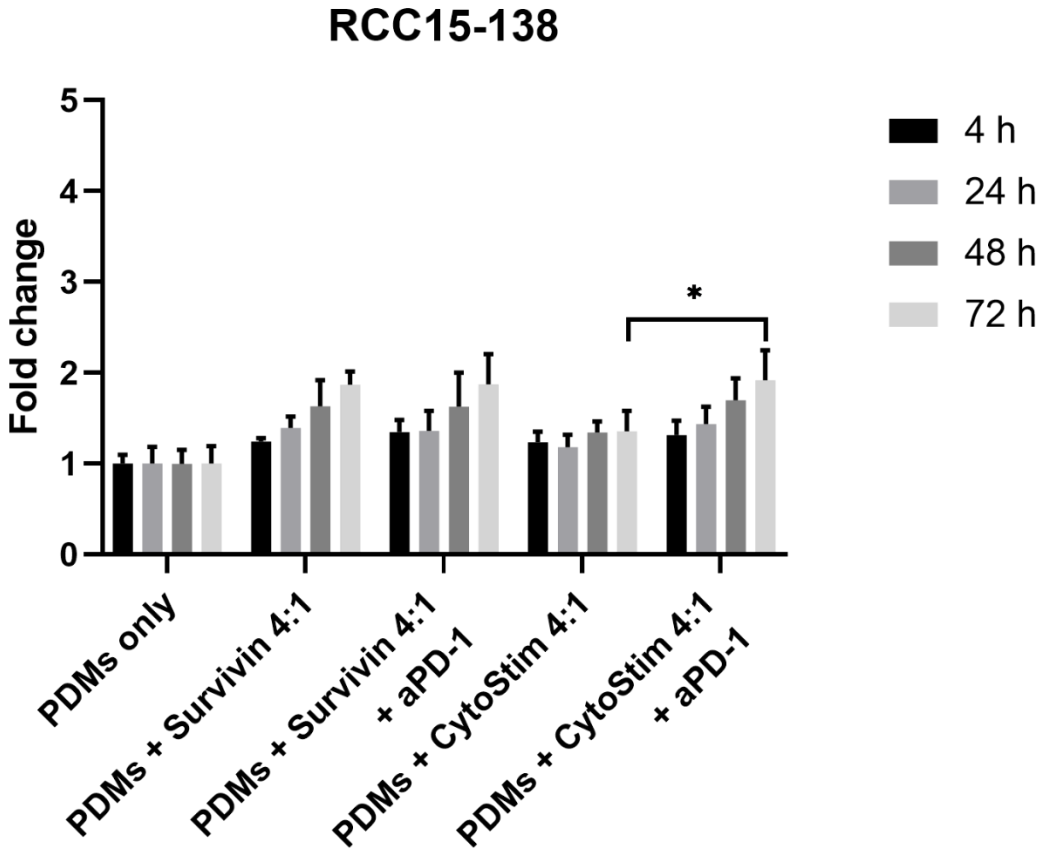

Figure 27: Treatment of RCC15-138 PDMs with Survivin and CytoStim T cells at a 4:1 ratio alone or in combination with checkpoint inhibitor aPD-1, respectively. Readouts were normalized to PDM-only control. With n=3, statistic test used: 2-way ANOVA with Tukey's multiple comparisons test *0.033, **0.002, ***0.001.

Treatment with Survivin specific T cells at a 4:1 ratio again showed no significant cell death but a clear trend to stronger fluorescence over the time course of 72 h, which was also observed in previous experiment (Figure 26). The antigen specific response could not be enhanced by combining the Survivin T cells with aPD-1, suggesting that either the cytotoxic effect of the Survivin T cells was already at a maximum or that the Survivin T cells do not express PD1.

Treating the PDMs with CytoStim T cells at a ratio of 4:1 had no cytotoxic effect. When combining nonspecifically activated CytoStim T cells with the checkpoint inhibitor aPD-1, the cytotoxic response was significantly increased after 72 h compared to treatment with CytoStim T cells alone (Figure 27) reaching a similar cytotoxic effect as the treatment with Survivin T cells, which indicates that the T cells do express PD1, and the treatment with Survivin indeed was not enhanced by aPD-1 as the maximum of the cytotoxic effect was reached.

Taken together, Figure 26 and Figure 27 show a good reproducibility of the performed CytoTox assay as the results of the 4:1 treatment with Survivin or CytoStim T cells are comparable, thus reflecting the reproducibility of the assay.

Next, using RCC1589 PDMs with autologous CytoStim T cells, the E:T ratios of 2:1 and 4:1 alone and in combination with the aPD-1 Nivolumab, respectively, were tested.

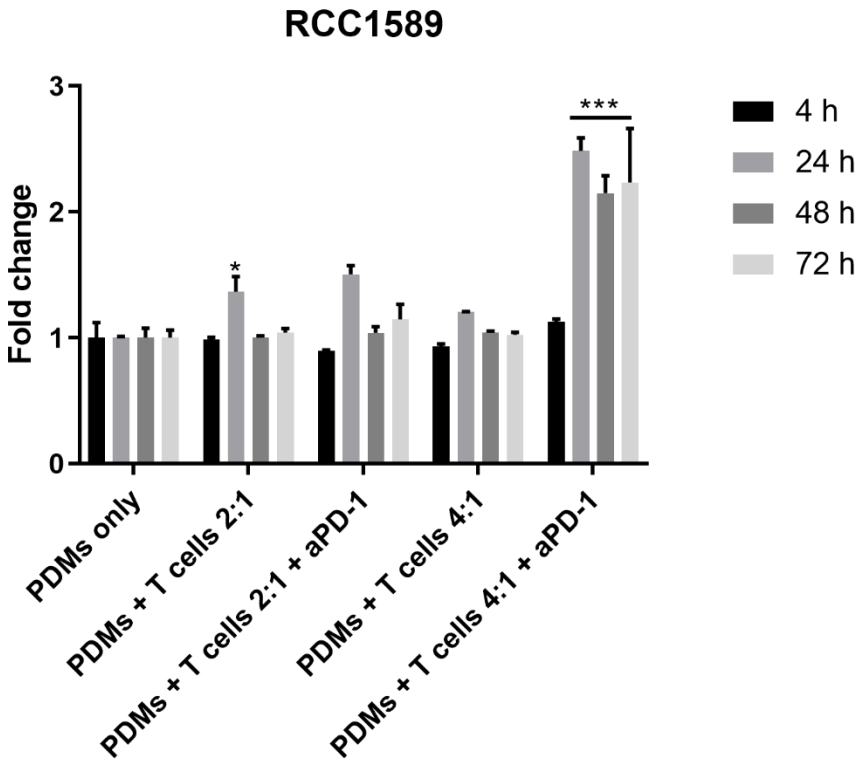

Figure 28: RCC1589 PDMs were treated with CytoStim T cells in E:T ratios of 2:1 and 4:1 alone and in combination with the checkpoint inhibitor aPD-1. All readouts were normalized to the PDM-only control. With n=3, statistic test used: 2-way ANOVA with Dunnett's multiple comparisons test *0.033, **0.002, ***0.001.

The treatment with an E:T ratio of 2:1 had a significant cytotoxic effect after 24 h, which was not enhanced over time or by the checkpoint inhibitor aPD-1. The treatment with 4:1 CytoStim T cells alone did not significantly increase cell death in this PDM model, thus no E:T ratio dependent increase in cell death could be observed. However, the combination of 4:1 CytoStim T cells with the checkpoint inhibitor aPD-1 resulted in a significant increase in cell death after 24 h. This indicates that the checkpoint blockade by PD1 resulted in the diminished cytotoxic effect of the increased E:T ratio of 4:1 compared to 2:1 (Figure 28).

Combination treatments were explored early on in cancer therapy and are continued today with newly available targeted cancer therapies as well as with immunotherapy and immunomodulatory treatment [176-178]. Therefore, the following experiments were performed to investigate if combinational therapies can be tested using the CytoTox assay system.

Next, the RCC1589 PDMs, which express the RCC marker Survivin as well (Figure 25), were treated with Survivin-specific T cells alone, in combination with aPD-1 and in combination with aPD-1 and the tyrosine kinase inhibitor Axitinib. The combination treatment with aPD-1 and Axitinib is currently evaluated in clinical trials (ClinicalTrials.gov Identifier: NCT03595124 & NCT03172754).

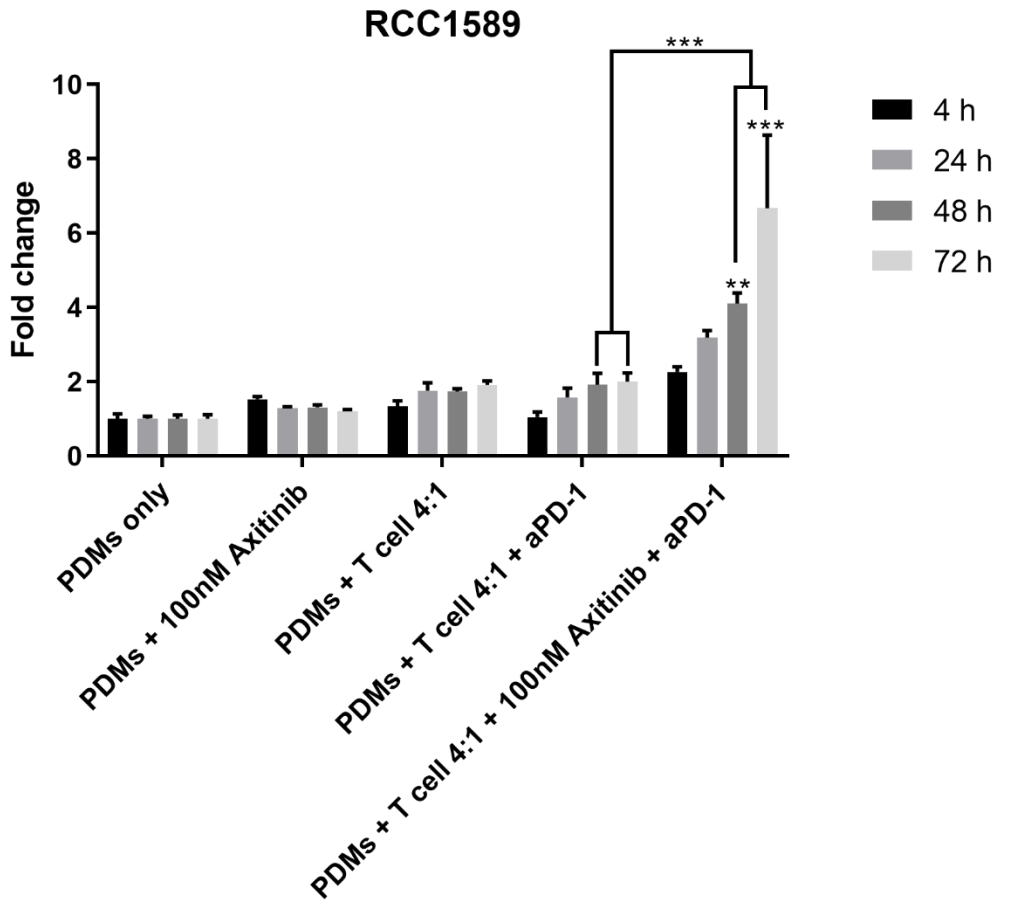

Figure 29: RCC1589 PDMs were treated with 100 nM Axitinib, Survivin T cells at a E:T ratio of 4:1 alone, in combination with aPD-1 and in combination with aPD-1 and 100 nM Axitinib. All readouts were normalized to the PDM-only control. With n=3, statistic test used: 2-way ANOVA with Dunnett's multiple comparisons test *0.033, **0.002, ***0.001.

The treatment of the PDMs with Axitinib or 4:1 Survivin T cells alone did not result in a significant increase in cell death, even though the PDMs express the Survivin antigen (Figure 25). However, a non-significant increase in fluorescence compared to the control could be observed for treatment with Survivin T cells. In contrast to the experiment performed with CytoStim T cells (Figure 28), the combination of the Survivin specific T cells with the checkpoint inhibitor aPD-1 did not further increase the cytotoxic effect of respective T cells. Strikingly, combining the Survivin T cells with aPD-1 and the TK inhibitor Axitinib showed a significant increase in cell death after 48 h and 72 h compared to the PDM-only control as well as to the treatment with Survivin T cells and aPD-1 (Figure 29). This increase in cell death strongly implicates a combinatorial effect since the mono-treatments with Axitinib and aPD-1 had no effect.

Taken together, the assay system detects significant effects of combinatorial treatment, with low standard deviation despite the complex co-culturing system. Furthermore, it is possible to identify additive effects of the combination treatment compared to the mono-treatment.

5.6.3 Co-culturing of PDMs with autologous TILs

When using the co-culture assays with malignant melanoma PDMs, tumor-infiltrating lymphocytes (TILs) instead of PBM-derived T cells were used (see method section 12.2). The different T cell population was chosen, because it is reported in melanoma that the state of TIL infiltration of the tumor is correlated with patient outcome [179]. Furthermore, autologous TILs are used in melanoma treatment for adoptive cell transfer (ACT) therapy. Thereby, isolated TILs from resected tumor tissue are expanded *ex vivo* for up to 6 weeks to obtain around 10^{11} lymphocytes, which can be subsequently reinfused into the patient [180].

Additionally, the treatment with checkpoint inhibitors like aCTLA-4 and aPD-1 is regularly performed in malignant melanoma patients and has advanced to one of the most favorable therapeutic option with an advanced disease [179].

PDMs from melanoma model Mel84/17 were treated with expanded tumor infiltrating lymphocytes (TILs) in an E:T ratio of 2:1 or 4:1 and in combination with the checkpoint inhibitors aPD-1 or aCTLA-4, respectively, as well as with the combination of both checkpoint inhibitors to see if an additive effect can be observed.

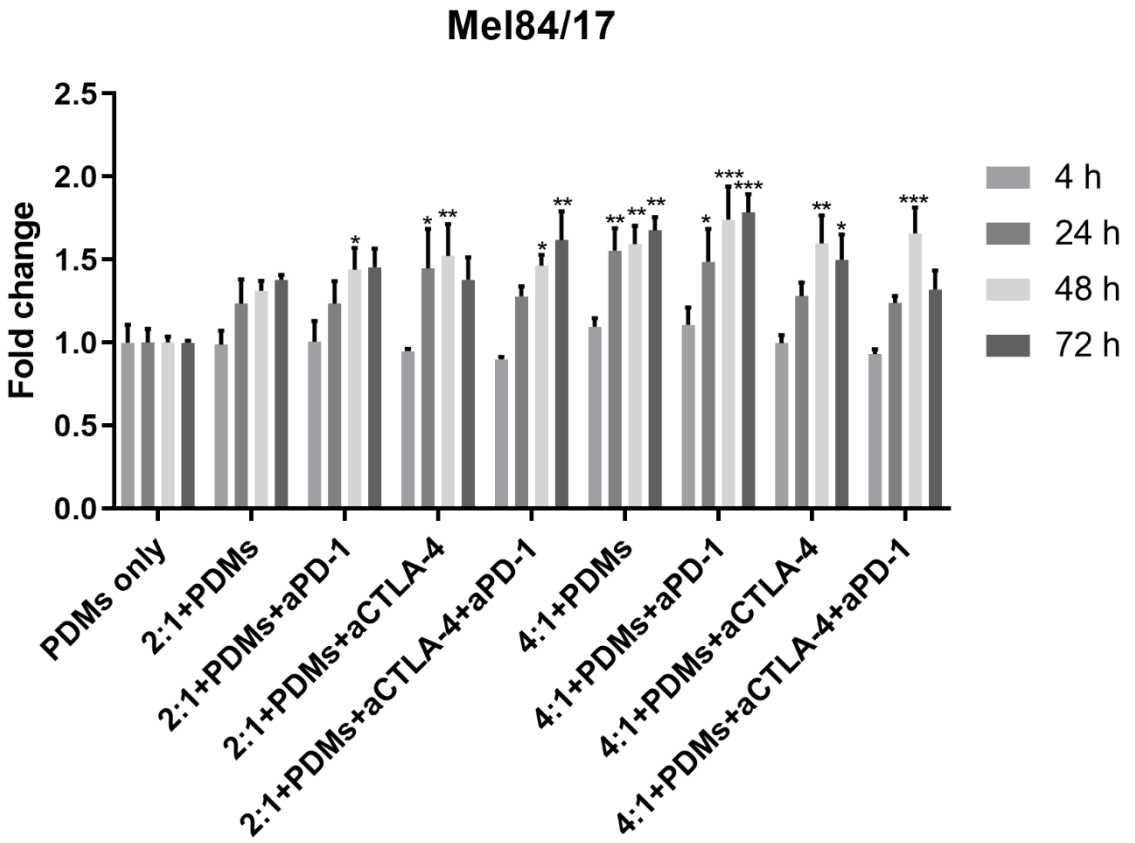

Figure 30: Mel84/17 PDMs were treated with an E:T ratio of 2:1 or 4:1 and in combination with the checkpoint inhibitors aPD-1 or aCTLA-4 as well as with the combination of both. All readouts were normalized to the PDM-only control. With n=4, statistic test used: 2-way ANOVA with Dunnett's multiple comparisons test *0.033, **0.002, ***0.001

Treating Mel84/17 PDMs with TILs at an E:T ratio of 2:1 alone did not result in a significant increase in cell death. Nonetheless, upon adding the checkpoint inhibitor aPD-1 the cytotoxicity after 48 h was significantly increased. Treating the PDMs with 2:1 TILs and aCTLA-4 showed a stronger significant increase after 24 h and 48 h than with adding aPD-1. Even though it resulted in a significant increase cell death after 48 h and 72 h (Figure 30), the combination of both checkpoint inhibitors had no additive effect. A stronger response to the checkpoint inhibitor aCTLA-4 is consistent with the flow cytometry analysis of the TILs. In Figure 17, a higher percentage of TILs expressing CTLA-4 than PD-1, regarding the $CD8^+$ population of T cells, was found.

When using an E:T ratio of 4:1, the cytotoxic effect of the TILs alone resulted in significant cell death as early as 24 h after treatment and remained significant over the whole-time course of 72 h. Upon adding aPD-1, the significant cytotoxic effect was slightly increased. Treating the PDMs with TILs and the checkpoint inhibitor CTLA-4 resulted in a significant increase of cell death after 48 h and 72 h. However, the cytotoxic effect when treating with aCTLA-4 alone was lower than treating the PDMs with TILs alone. The treatment of the PDMs with both aPD-1 and aCTLA-4 again had no additional effect and only resulted in a significant increase in cytotoxicity after 48 h (Figure 30).

Taken together, using the CytoTox assay, a cytotoxic response could be measured when treating Mel84/7 PDMs with autologous TILs alone and in combination with checkpoint inhibitors. However, an additional effect adding checkpoint inhibitors could only be observed with the E:T ratio of 2:1 as the cytotoxic effect by treating with 4:1 TILs resulted in a comparable cytotoxic effect.

These results show that the PDM-based CytoTox assay can also be used to investigate the cytotoxic effect of treating PDMs with autologous TILs and detect significant effects of combinatorial checkpoint inhibitor treatment, with a low standard deviation. Furthermore, it is possible to detect an additive effect of the additional treatment with checkpoint inhibitors.

5.6.4 Stronger anti-tumor activity by tumor antigen-specific expanded T cell populations

In a joined project with the group of Prof. Dr. Sine Reker Hadrup at the Denmark Technical University (DTU) in Copenhagen, T cells expanded from TILs using the classical high IL2 rapid expansion protocol (REP) [181, 182] are compared regarding their cytotoxic effects on the Mel100/17 PDMs to the technology to expand antigen-specific T cells using a scaffold-based method developed in the Hadrup Group [183, 184].

Isolated TILs were first analyzed using flow cytometry to check whether they were capable of binding to known shared melanoma antigens. If a T cell population is identified to recognize a melanoma antigen, the T cell population is specifically expanded using a scaffold, acting as an artificial APC, which is presenting the antigen as well as co-stimulatory agents to the T cells in order to activate cell proliferation.

Since, in this case, the focus was on the different kind of T cell populations, the treatments were normalized to the respective T cell-only control and not to PDMs-only controls.

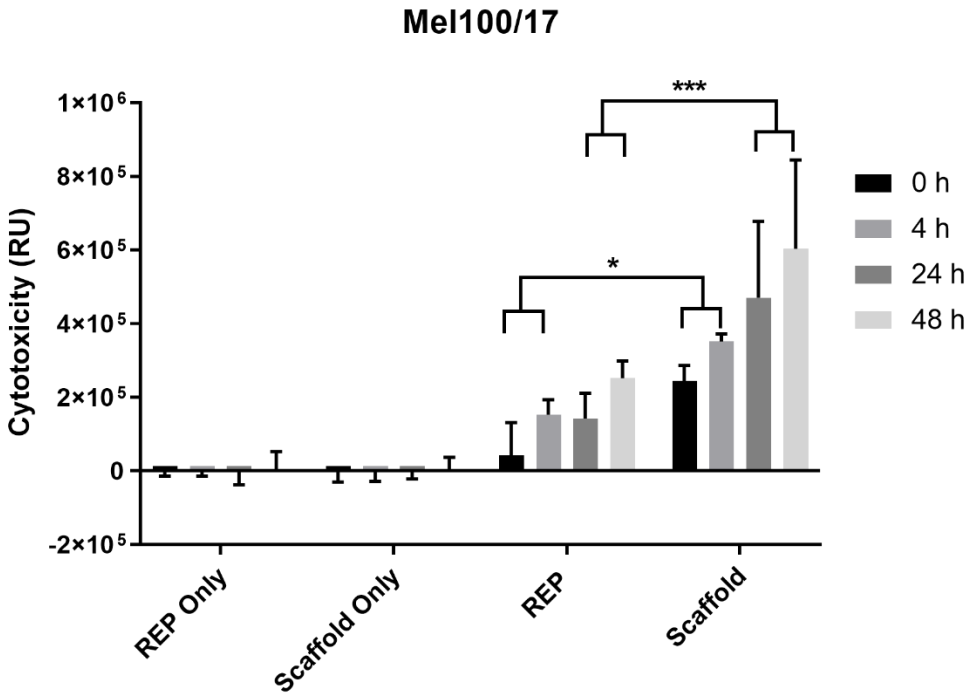

Figure 31: Treatment of Mel100/17 PDMs with REP expanded TILs and TILs expanded using an antigen-specific scaffold. Readouts were normalized to the respective T cell-only control. With n=3, statistic test used: 2-way ANOVA with Dunnett's multiple comparisons test *0.033, **0.002, ***0.001.

Although both treatments, REP and scaffold expanded T cells, showed an increase in cytotoxic response on Mel100/17 PDMs, the cytotoxic capability of the scaffold-based expanded T cells was significantly higher than that of the REP T cells towards Mel100/17 at every tested time point (Figure 31).

Taken together, the CytoTox assay can be used to investigate differently expanded T cell populations on their cytotoxic abilities. In this case, the measured fluorescence can be normalized on the T cell only control to eliminate possible viability differences due to the expansion method. The obtained results show a low standard deviation despite the complexity of the assay.

5.7 PDM infiltration assay

The cytotoxic effect of T cells is correlated with their infiltration of the tumor of patients. Tumors can be categorized into "cold" (non-inflamed) and "hot" (inflamed) tumors, which are rich in TILs. The last category can be further distinguished into brisk and nonbrisk TILs, in which the brisk TILs have the strongest significant tumor killing abilities. In the categories of nonbrisk TILs, the T cells are located around the tumor tissue, whereas brisk T cells are located around as well as inside the tumor [180]. Often T cell activation is compromised in response to checkpoint receptor ligation via proteins (e.g., PDL1) expressed on tumor cells and thus respective T cells cannot infiltrate the tumor. Time-lapse high-resolution microscopy was used to track the infiltration of T cells into the PDMs (Figure 32) (see method section 12.6).

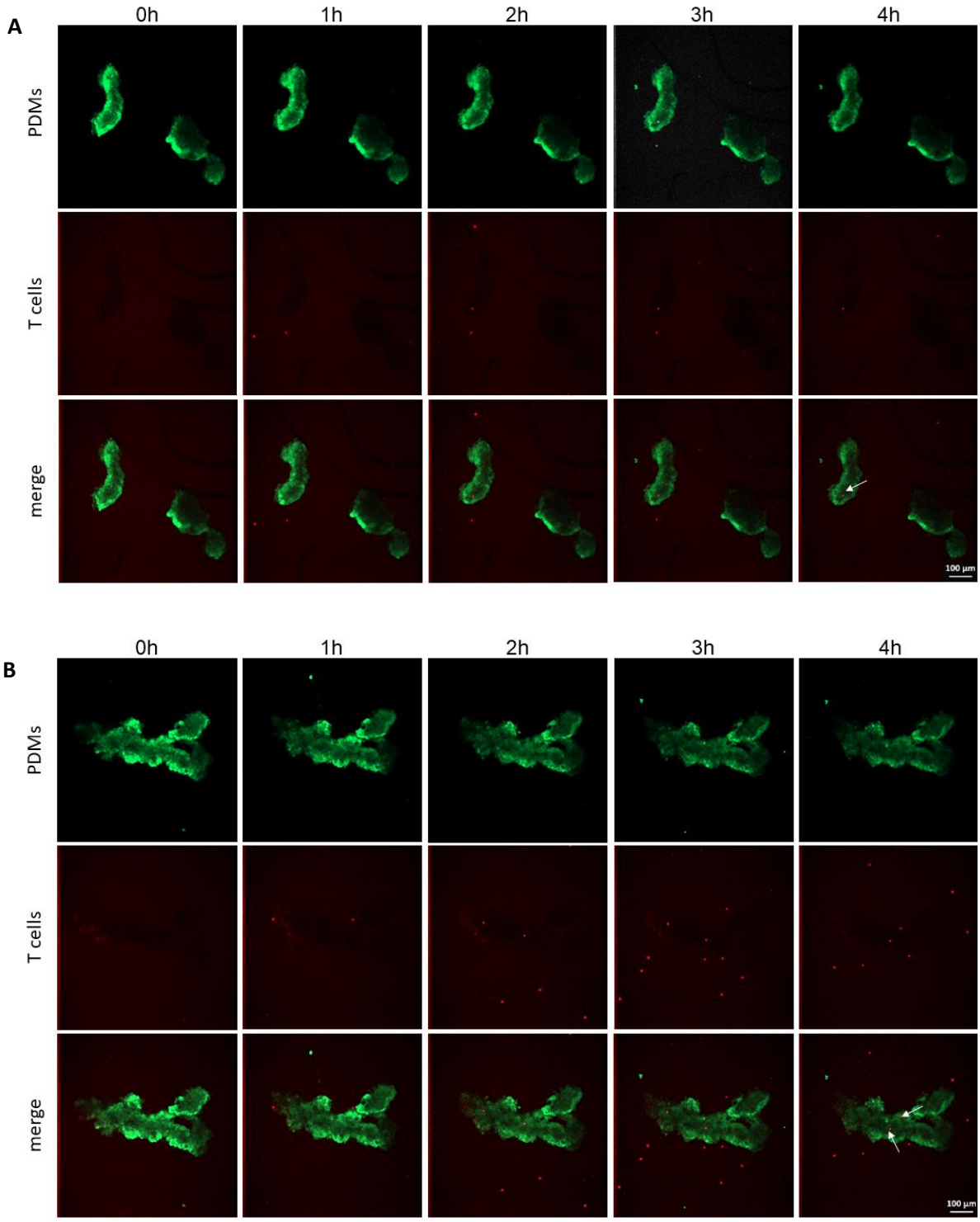

Figure 32: T cells treated with aPD-1 inhibitor infiltrated the PDMs over time. The infiltration of T cells (stained with CellTracker Deep Red) into the PDMs (stained with CellTracker Green) is followed using time-resolved microscopy. **A** Infiltration by T cells over the time frame of 4 h **B** Infiltration by T cells when treated with aPD-1 over the time frame of 4h. Scale bars: 100 µm.

The effect of checkpoint inhibitor treatment on the ability of T cells to infiltrate the PDMs can be measured using this assay. This effect can also be quantified by assessing the amount of T cells in the microtumors at a given time point (Figure 33).

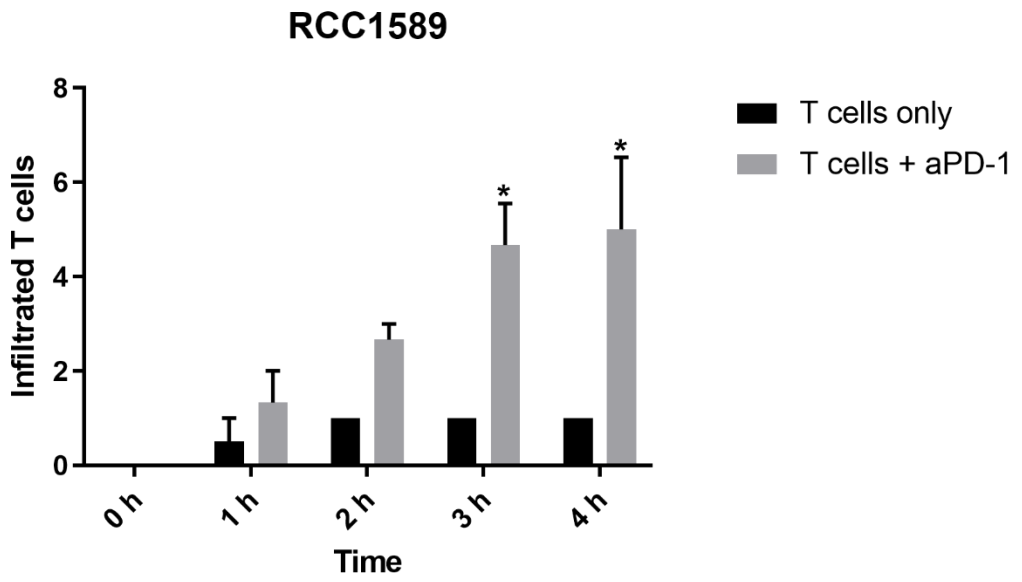

Figure 33: Quantification of PDM infiltration by the T cells. The amount of infiltrating T cells is assessed using the IMARIS software (see method section 12.6.3). With n=3, statistic test used: 2-way ANOVA with Dunnett's multiple comparisons test *0.033, **0.002, ***0.001.

For patient RCC1589, the infiltration of T cells into the PDMs was affected by aPD-1 treatment (Figure 33). As early as 1 h after adding the T cells to the PDMs, the infiltration in the aPD-1 treated sample was higher than in the untreated one. After 3 h the infiltration increase by aPD-1 was significant. This effect was even stronger after 4 h.

Thus, the PDMs can be utilized to measure the effect of checkpoint inhibitors on the infiltration of T cells into the tumor tissue. This effect can be closely followed using microscopic time laps imaging. The obtained results could then be matched to the results observed during the CytoTox assay.

6. Discussion

Cancer is a difficult-to-treat and heterogenous disease and 9.6 million people worldwide died 2018 due to it [185]. The currently applied 2D platforms are not a sufficient disease model as they do not accurately resemble human physiology. In 2D models, the tumor cells are usually immortalized by 'conditional reprogramming' and furthermore, due to the 2D culturing, the 3D architecture of the tumor is lost [93, 96, 97]. Moreover, it has been shown that drug effects can be more variable when treating 2D cultures compared to 3D cultures [98]. The xenograft (PDX) platforms have the drawback that the biopsy material is usually implanted in immunodeficient mice, thus the testing of immunomodulatory drugs is challenging. Additionally, the generation of PDX models is time and cost intensive and cannot be generated from all tumor biopsies and tumor specimens [100, 101].

A promising established 3D platform, regarding their generation as well as their resemblance of the original tumor [106], is the tumor organoids generation, during which a tumor organoid is formed from single cells in a scaffold, such as Matrigel™. However, this platform has several drawbacks. Firstly, tumor organoids can be started from single tumor cells obtained by needle biopsy, hence the intratumoral heterogeneity with unique tumor subpopulations in different geographical regions of the tumor can be lost [109, 186]. These subpopulations could entail inhomogeneously distributed tumor antigens. However, a recent study finds that tumor organoids can be used to predict the response to chemotherapy in metastatic colorectal cancer patients [107], suggesting that in some cases, when the fully resected tumor is used to generate the organoids, the heterogeneity of the tumor is retained [106]. In addition, the testing sensitivity using tumor organoids can differ from the patient's reaction, as the stroma as well as the immune system is absent. These components can influence treatment outcome in several ways. Culture methods, however, which allow to partially retain the tumor microenvironment could overcome these limitations [107].

Furthermore, the organoids are established using poorly defined Matrigel™ matrices as well as a multitude of inhibitors, which can prime the organoids to develop pathway alterations. Matrigel™ is naturally derived extracellular matrix extracted from Engelbreth-Holm-Swarm tumors in mice with a high lot-to-lot variability, making it poorly defined [187, 188]. During the cultivation of tumor organoids, inhibitors, like EGF, Wnt3A or R-spondin, are added to prohibit the growth of epithelial cells. The addition of these factors can prime the organoids into a dependency on specific signaling pathways. These factors are involved in signaling pathways, which can be altered in cancer, like EGF, which promotes tumor growth and proliferation of cancer cells; a dysregulated Wnt signaling promotes carcinogenesis and cancer progression, and R-spondin facilitates metastasis and cancer growth [113, 189].

Therefore, there is an urgent need for a platform, where a tumor and its microenvironment can be mimicked as closely to nature as possible. Therefore, starting from the methodology provided by Kondo *et al.*, the isolation of patient-derived microtumors is presented in this thesis [115]. Therein, due to an optimized digestion protocol using Liberase DH, the cancer cell-cell contacts are maintained, and solely the surrounding tissue is digested and can be separated from the tumor PDMs by a cell strainer. It could be shown that these PDMs retain cells from the tumor microenvironment (Figure 10) and CSC (Figure 11 and Figure 12). Furthermore, TILs of the respective patient could be isolated during the PDM generation from the single cell flow through (Figure 15 through Figure 17).

In this PhD thesis, a new assay platform using these PDMs and either TILs or autologous PBMC-derived T cells was implemented to test their cytotoxic effect on the PDMs in a co-culture system. Furthermore, compounds can be tested in a mono- or combination treatment towards their cytotoxic effect on the PDMs. Moreover, having the autologous T cells available, immunotherapeutic agents could be tested in co-culture with the PDMs as well.

6.1 Characterization of the viability and heterogeneity of the PDMs

Starting from the methodology of Kondo *et al.*, the isolation of PDMs from a multitude of different tumor entities could be achieved (Figure 7). The efficiency of PDM isolation from RCC and malignant melanoma tumor tissue was around 60 %. The PDMs isolated from malignant melanoma was in general larger than the RCC PDMs, which could be due to the isolation method. During isolation of the PDMs, the non-cancerous stroma cells between the cancerous cells are digested by the added Liberase DH. An explanation for the different size of the PDM could be that the cancerous cells in malignant melanoma are forming larger subsets divided by the stroma cells than they do in RCC.

The Live/Dead staining of six different RCCs as well as six different malignant melanoma PDMs revealed that the overall viability of the PDMs was between 84.1 % (RCC1518) and 99.3 % (RCC1817) (Figure 8A) and between 63.2 % (Mel102/17) and 99.9 % (Mel100/17) (Figure 8B). PDM samples with an overall viability above 80 % were selected to be suitable for subsequent experiments (Table **4**). This threshold was chosen to ensure that the measured cell death in the subsequently performed assays is not due to the low stability and viability of the PDM culture.

Using Immunohistochemical staining (IHC), the PDMs can be either stained for their overall structure, the expression of tumor antigens or the presence of immune cells. Furthermore, the staining can be compared to the parental tissue to determine whether the PDMs reliably reflect the patient's tumor. The RCC PDM samples RCC1589, RCC1579, RCC15-138 and RCC1817 were stained using H&E as well as for the tumor marker Vimentin (Figure 9). Based on the available clinical data

for respective tissue samples, the H&E staining of the PDMs displayed a clear correlation between the RCC type as well as the Fuhrman grading performed in the clinic. Furthermore, the expression of Vimentin as marker for papillary and clear cell RCC could be shown in RCC1589 and RCC15-138, respectively. Even though the expression of Vimentin in RCC15-138 was not as prominent as in RCC1589, it could be linked to the metastasis found in the patient [190]. RCC1579 and RCC1817 did not express Vimentin as expected for chromophobe RCC [123]. In case patient tumor tissue (PTT) is available, the staining of the primary tumor and the PDMs can be compared to determine to what degree the PDMs reflect the patient's tumor. Furthermore, having that comparison, it could be investigated wether the adaption of the culturing conditions could improve the comparability of the PDMs to the PTT.

Two malignant melanoma PDM samples were used for IHC staining. As parental tissue was available for the samples, a comparison could be made. The PDMs as well as the parental tissue was stained for the presence of PDL1, CD3 as a marker of T cells in the PDMs [126], CD163 as a marker of macrophages [127] and for the presence of fibroblasts (Figure 10). In the H&E staining, it can be observed that the Mel84/17 PDMs retained the melanocytes also found in the parental tumor tissue. In Mel100/17, no melanocytes are found, whereas in the parental tissue, melanocytes can be observed. However, the melanocytes found in the parental tissue of Mel100/17 are smaller and fewer than in the parental tissue of Mel 84/17. In contrast, the expression of MART-1 can be observed in both parental tissues but is almost completely lost in Mel84/17 PDMs, indicating, that either the PDMs result from tumor regions without MART-1 expression, as melanoma is a highly heterogeneous cancer, or that the MART-1 expression is lost in Mel84/17 PDMs [191]. In case the MART-1 expression is lost over time, the culturing conditions could be optimized e.g., by adding autologous serum of the patient, if available. Another possibility is to minimize the passaging of the PDMs prior to freezing or performing experiments.

For the subsequent staining for immune cell markers, it can be observed, that the retention of immune cells in the PDMs differs between the two samples, indicating that immune cells are not retained in all PDMs isolated from the parental tissue. However, a larger sample size of PDMs per model needs to be stained in order to confirm the observation. Another explanation for the absence of immune cells in the PDMs could be that the culturing conditions are optimized for PDM culture and not for the survival of immune cells. Thus, the optimization of the culturing conditions could improve the retention of immune cells in the PDMs. For this purpose the media could be supplemented with interleukins necessary for immune cell proliferation, like IL-2 for T cell proliferation and differentiation as well as proliferation and activation of NK cells, IL-7 for T cell proliferation, IL-15 for $CD8^+$ T cells proliferation or IL-21, which acts on multiple immune cells from

the innate and adaptive immune system [192]. Furthermore, if available, the culturing media could be supplemented with autologous serum of the patient.

It can be observed that the expression of PDL1 is only present in the PDMs of Mel84/17. Here, the parental tissue exhibits a strong expression of the checkpoint protein. In contrast the parental tissue of Mel100/17 exhibits a low expression of PDL1, which cannot be shown in the stained PDMs. However, to verify the finding that the PDL1 expression is lost in the PDMs, a larger number of PDMs must be stained and investigated for PDL1 expression. Furthermore, like with the expression of MART-1, an optimization of the culturing conditions could improve the expression profile of PDL1 in melanoma PDMs.

The presence of cancer-associated fibroblasts can alter the reaction of a tumor to therapy by inducing angiogenesis, recruiting inflammatory or immune cells and reshaping the extracellular matrix [193, 194]. Thus, it can be important that CAFs are retained in the PDMs. However, here, an anti-fibroblast antibody was used for staining; therefore, a distinction between normal fibroblasts and CAFs is not possible. In order to distinguish CAFs from fibroblasts, an additional marker, like the fibroblast activation protein (FAP) could be stained. FAP is a type II membrane-bound serin protease, which has recently gained attention as a possible therapeutic target in CAFs [195].

In the parental tissue of Mel84/17, a defined structure and localization of the fibroblasts can be seen, whereas in the parental tissue of Mel100/17, the fibroblasts are spread over the entire tissue. In the PDMs, only Mel84/17 could retain fibroblasts.

Taken together, it could be shown that the PDM models can be processed and stained as FFPE slices, which allows them to be directly compared to the processed FFPE slices of the PTT. Furthermore, it could be shown that some markers are retained in the PDMs from the patient's tumor. However, some markers are lost in the PDMs, which could be counteracted by adapting the preparation protocol and the culturing condition for each tumor type and purpose. Importantly, the IHC staining shows a cellular heterogeneity of the PDM models; thus, the PDMs contain not only tumor cell but also cells of the tumor microenvironment like immune cells and fibroblasts. Therefore, the PDM model has a considerable advantage over 3D cell line spheroids or mouse xenografts.

6.2 Retention of cancer stem cells in the PDMs

There is the hypothesis that a tumor not only consists of the fast-dividing tumor cells but also of a slow-dividing cell population, which exhibits stem cell-like characteristics [31, 32]. This stem cell-like character is in line with the clinical observation of the almost inevitable relapse of the disease after initial response to chemotherapy or radiation [33]. A multitude of markers, including distinct cancer stem cell (CSC) markers as well as common stem cell markers have been identified. Since

the occurrence of CSC is extremely low (less than 0.04 % of tumor cells [36]), they have so far been overseen in cancer therapy. Most of the classical chemotherapeutics are incapable of targeting the low-cycling CSCs, which explains the cases in which the tumor relapsed after an initial reduction of tumor mass. Hence, the goal now is to find a therapy to target the CSCs. However, CSC-specific treatment is not approved for cancer treatment, yet. However, several approaches to target the CSC are in clinical trials [32, 33].

The presence of cancer stem cells in the PDMs was demonstrated using two different approaches: Using qPCR as well as RPPA protein profiling, tumor stem cells could be detected, and a difference in stem cell markers could be shown between the different samples (Figure 11 & Figure 12).

Using both methods, it could be shown that PDMs express different subsets of CSC marker RNA. However, it was observed that strong transcription of a CSC protein did not necessarily result in a high protein level of the same marker. Thus, when targeting certain CSC proteins, it should be kept in mind that a protein-based analysis of the expression profile could be more accurate.

Taken together, it could be shown on the RNA as well as protein level that the PDMs contain CSCs. Thus, the PDMs can be used to investigate compounds and treatment strategies targeting CSCs.

6.3 Alterations in cancer related signaling pathways

Using RPPA protein profiling, not only the presence of tumor stem cells was shown, the method was also used to investigate for cancer-promoting pathway mutations in the PDMs. One major observation was that the same grouping that was observed during stem cell expression analysis could also be found in the mutational profile of the PDMs (Figure 13 & Figure 14). Group 1 containing RCC14-041 and RCC15-138 displayed an upregulation in the investigated stem cell marker as well as in the MAP kinase pathway and in the Akt/mTOR pathway. Knowing this, treatment options for the patient could be based on the protein expression profile, i.e. utilizing the upregulated Akt/mTOR pathway the patients could be treated with mTOR inhibitors, like Temsirolimus or Everolimus, which are approved for the use in RCC [54]. Additionally, it would also be an option to treat with the kinase inhibitors Vemurafenib, Dabrafenib or Trametinib, which are approved for melanoma [196].

Group 2 containing RCC1817, RCC1579 and RCC1589 show no upregulation in most investigated stem cell markers, neither MAP kinase pathway nor Akt/mTOR pathway, but a downregulation in apoptosis proteins and an upregulation in the Wnt signaling pathway. Using these findings, agents to counteract the upregulated Wnt pathway, such as Niclosamide, Sulindac or Pyrivinium, which are all FDA-approved for off-label use [197], could be beneficial for the patient. Another way to treat these patients would be to activate apoptosis using DNA-damaging agents like 5-flourouracil,

Doxorubicin or Carboplatin [198]. However, this is only feasible in p53 WT cancers; otherwise, the tumor can escape the DNA damage-mediated apoptosis pathway.

Altogether, it can be said that the protein profiling can be used to determine pathway alterations in the PDMs as well as investigate possible links to up- or downregulation of stem cell markers. Furthermore, this information could be used to cluster PDMs regarding their expression profile and thereby determine which PDM model could be used concerning their expression profile to test investigational compounds regarding their cytotoxic effect. Moreover, the clustering of stem cell marker expression to signaling pathways could be used to investigate combinatorial effects of targeting the CSC as well as the dysregulated signaling pathway.

6.4 Characterization of tumor infiltrating lymphocytes

In order to include immune cells, which plays a crucial role in tumor biology by either supporting or killing the tumor, into the assay system, TILs isolated from the patient's tumor were also characterized in terms of specific markers, such as percentage of $CD8^+$ T cells as well as for the percentage of $CD39^+$ tumor-specific T cells [156], using flow cytometry analysis (Figure 15 & Figure 17). Furthermore, the cytotoxic T cells were stained and analyzed for the expression of checkpoint proteins like CTLA4 and PD1. This analysis can be used to determine the susceptibility of a coculture with PDMs and therefore the patient towards checkpoint inhibitors (Figure 17). In Mel84/17, 51% of the $CD8^+$ cells were also $CD39^+$, reflecting a tumor-reactive T cell population that starts to get downregulated by the tumor [156]. 2.3% of the TIL population expressed the checkpoint protein CTLA4 and 0.85% expressed PD1, indicating that this patient may benefit from an aCTLA-4 therapy. Following, the susceptibility of the tumor to towards with an aCTLA-4 checkpoint inhibitor could be analyzed using the PDM-based CellTox Green assay.

6.5 The CellTox Assay measures cytotoxic effect of SOC

In order to prove that the CellTox Green reagent is suitable for testing the cytotoxic response of the PDMs, two of the SOC molecules (Axitinib and Torin-2) were tested with RCC1589 PDMs. Using this setup, it could be shown that treating RCC1589 PDMs with 100 nM Axitinib results in a significantly increased cell death. However, no dose dependent effect could be observed. This could be explained with the fact, that contrary to cell lines, the PDMs consist of multiple cell types which can react differently towards Axitinib leading to the observation that a certain concentration has the strongest effect. Furthermore, neither in mice nor in patients, which are the systems the PDMs should be compared to, a dose-dependency of drug treatment is investigated.

This cytotoxic reaction is especially interesting, since it is close to the concentration that the drug reaches in patients' blood (71.9 nM), according to the prescription information (Figure 22) [199].

The fact that the significant increase in cell death could be measured, taken together with the result from the RPPA analysis, which did not show an upregulation in the MAP Kinase pathway, indicates that the RCC1589 PDMs exhibit no activating downstream mutation of the MAK Kinase pathway.

The RCC1589 PDMs were treated with the mTor inhibitor Torin-2. However, their treatment with Torin-2 did not result in higher cell death with any of the tested concentrations. This can be explained at the protein profiling of pathway alterations (Figure 14). RCC1589 can be sorted into group 2, which has no upregulation in the Akt/mTor pathway. Hence, treatment with SOCs targeting this pathway has no cytotoxic effect.

The assay was also tested on another tumor entity, malignant melanoma. Mel84/17 PDMs were treated with the investigational compound BKM-120 and in combination with the targeted therapy agent Trametinib. BKM-120 targets the PI3 kinase, whereas Trametinib is a MEK inhibitor. The concentration range was chosen based on the publication from the dermatology department at the Universitätsklinik Tübingen (UKT) [200]. A viability reduction by BKM-120 could be observed in cell lines starting from 1 µM after 72 h and reached a maximum of roughly 70 % reduction in viability with 10 µM BKM-120. Mel84/17 was treated with up to 20 µM BMK-120. Mel84/17 showed a significant increase in cell death after 72 h at 1 µM, which is in concordance with the findings in melanoma cell lines. Using higher concentrations, significant cell death could be reliably reached after 48 h.

Niessner *et al.* also found a combinatorial effect for treatment with the PI3 kinase inhibitor BKM-120 together with the MEK inhibitor Binimetinib [200]. In order to test wether this effect can also be observed in the PDMs, Mel84/17 was treated with BKM-120 in combination with the MEK inhibitor Trametinib, resulting in a significant cytotoxic response. However, the overall cytotoxic response of the combination did not exceed treatment with BKM-120 alone. This finding suggests that in this patient, the response to an PI3K inhibitor is significantly stronger than the response to the MEK inhibitor and therefore, in a predictive manner, treatment with the PI3K inhibitor would be preferred over treatment with the MEK inhibitor (Figure 23).

Thus, the PDM-based assay system can be used to test the cytotoxic effect of compounds as mono- and combinatorial treatment. Furthermore, RPPA data can be matched to the observed drug responses.

6.6 Effect of autologous PBMC-derived T cells on PDM models

The critical merit of the PDM platform is to co-culture PDM models with the autologous T cells to observe the ability of T cells to kill the tumor cells. Incubation of single PDMs with different E:T ratios of antigen-specific T cells revealed that the effect of the T cells on the PDM could be observed

by microscopy. The treatment with T cells led to a disintegration and loss of fluorescence intensity over time (Figure 18). This effect could be measured by the increase of the fluorescent area and the decrease in fluorescence intensity. It could be observed that the treatment with an E:T ratio of 10:1 led to a stronger decrease in fluorescence (64.3 %) compared to the treatment with the E:T ratio of 2:1 (54.8 %). In conclusion, the treatment with autologous tumor-reactive cytotoxic T cells affects the PDM integrity as well as the viability of the tumor cells. Thus, the PDM models can be used to establish a fluorescence-based assay to investigate the effect of cytotoxic T cells on the tumor.

The CellTox Green assay was used to quantify the observation made when treating single PDMs from RCC15-138 with different E:T ratios of Survivin-specific T cells (Figure 18). The E:T ratios used in the following assays were based on several reports testing E:T ratios between 20:1 to ratios as low as 0.625:1 in 2D assay systems to be more physiologically relevant [158, 201]. Furthermore, to exclude that the measured fluorescence is due to T cells dying in the PDM assay media, an initial experiment with the highest tested E:T ratio 10:1 was performed comparing the fluorescence measured in T cell only controls to PDMs incubated with the respective T cells. The results clearly showed that the T cells were stable in the PDM assay media for up to 72 h without significant cell death (Figure 24). Therefore, the following measured effects on the co-culture can be attributed to the cytotoxic effect of the T cells on the PDMs.

RCC15-138 expresses the tumor antigen Survivin (Figure 25). Therefore, a higher cytotoxic response towards Survivin T cells than to the broadly activated CytoStim T cells was expected.

The cytotoxic effect of the E:T ratio of 10:1 Survivin T cells is significantly higher than treating with 4:1 Survivin T cells at every tested time point. When treating with nonspecifically activated CytoStim T cells, the overall cytotoxic effect was, as expected, lower than when treated with the Survivin T cells. 72 h treatment with 10:1 Survivin specific T cells resulted in significantly higher cell death than treatment with 10:1 CytoStim T cells (Figure 26). This finding reflects the expectation of antigen-specific T cells being more effective in tumor cell killing when the target cells express the antigen. Furthermore, the experiment shows a dose- and time-dependent effect of the T cell on the PDMs for the antigen-specific as well as broadly activated T cells. Thus, the presented CytoTox assay system using PDMs and autologous T cells is capable of identifying such differences.

Furthermore, the additional effect of the checkpoint inhibitor aPD-1 was investigated in RCC15-138 when treated with 4:1 Survivin or CytoStim T cells. The first observation was that the cytotoxic effect was in the same range (up to a 2-fold increase after 72 h) as in the previous assay with this model, showing the reproducibility of this assay. The second striking observation was that the cytotoxic effect of the Survivin-specific T cells could not be enhanced using the checkpoint inhibitor, whereas the cytotoxic effect of the CytoStim T cells could be significantly enhanced after 72 h with the checkpoint inhibitor aPD-1 then being in the same range as the cytotoxic effect of the Survivin

T cells (Figure 27). This points towards the cytotoxic effect being already at a maximum or the Survivin-specific T cells not being downregulated by the PD1/PD-L1 checkpoint axis. This can be explained by the fact that the antigen-specific T cells are isolated from PBMCs and hence have not been in the tumor vicinity and therefore have not been in contact with PD-L1 expressed by the tumor. The cytotoxic effect of the CytoStim T cells, on the other hand, were enhanced by adding aPD-1. This observation leads to the conclusion that the RCC15-138 subset of nonspecifically activated T cells from PBMCs comprises T cells, which have been in the vicinity of the tumor expressing PD-L1. The tumor-reactive subset of T cells has been downregulated by the PD-L1 of the tumor and could therefore be reactivated by aPD-1 [202].

In order to check if an E:T ratio lower than 4:1 is also suitable to be tested in this assay setup, RCC1589 PDMs were treated with 2:1 and 4:1 CytoStim T cells alone and in combination with the checkpoint inhibitor aPD-1. A significant additive effect of aPD-1 was observed with an E:T ratio of 4:1, but not when treated with 2:1 CytoStim T cells (Figure 28). This led to the conclusion that in this assay set-up the E:T ratio of 4:1 is optimal in RCC PDMs.

After determining the optimal E:T ratio of 4:1, RCC1589 PDMs were treated with 4:1 Survivin T cells alone, with the checkpoint inhibitor aPD-1 and with aPD-1 plus 100 nM Axitinib. The last combination is currently evaluated in different clinical trials (ClinicalTrials.gov Identifiers: NCT02133742, NCT03172754). Even though the RCC1589 PDMs express the RCC marker Survivin (Figure 25), the treatment of the PDM with Survivin T cells did not show significant cell death. This could be due to the fact that the T cells are downregulated by checkpoint proteins, like PD-L1. However, adding aPD-1 to the co-culture did not enhance the cytotoxic response, indicating that the downregulation is most likely not through the PD1/PD-L1 axis. Treatment with the combination of aPD-1 and 100 nM Axitinib resulted in a significantly higher cell death compared to the PDM-only control as well as compared to the single treatment with aPD-1 or Axitinib alone. This result is in line with the findings of Atkins *et al.*, who found that the combination of Pembrolizumab, an approved aPD-1 checkpoint inhibitor, and Axitinib had favorable outcome for patients in a phase Ib study. Interestingly, they found significant clinical benefit for patients who did not express the PD-L1 ligand [203, 204]. This combinatorial effect of a TK inhibitor with immunotherapy is due to the reducing effect of the TKI on T_{reg} as well as the improvement of type 1 T cell cytokine response [205].

6.7 Effect of autologous TILs on melanoma PDMs

Mel84/17 PDMs were treated with 2:1 and 4:1 expanded TILs alone and in combination with aPD-1, aCTLA-4, and a combination of both checkpoint inhibitors. The treatment with 2:1 TILs alone did not result in a significant cell death, while combinatorial treatment with aPD-1 and aCTLA-4 resulted

in significant cell death. When treated with aCTLA-4, a significant cytotoxic effect was measured after 24 h and further enhanced after 48 h. In contrast, the treatment with only aPD-1 resulted in significant cell death after 48 h. Taken together, these observations were in line with the results from the flow cytometry analysis of the Mel84/17 TILs, in which a higher CTLA4 than PD-1 expression was found. Combining both checkpoint inhibitors did not enhance the cytotoxic effect further. Compared to the E:T ratio of 2:1 treatment with 4:1 TILs resulted in a significant cell death after 24 h. In the case of a 4:1 T cell ratio, the cytotoxic effect could not be enhanced by adding checkpoint inhibitors, indicating that the maximal cytotoxic effect was already reached (Figure 30). This indicates that the cytotoxic effect of the T cells alone did not reach the maximal cell death in case of the E:T ratio of 2:1 and can therefore be enhanced by adding the checkpoint inhibitors.

These results show that the PDM-based CytoTox assay can be used to investigate the cytotoxic effect of treating PDMs with autologous TILs and detect significant effects of combinatorial checkpoint inhibitor treatment.

6.8 Effect of antigen-specific expanded TILs on melanoma PDMs

In ACT, TILs are expanded using high concentrations of IL-2, which can lead to an exhausted state of the T cells and also promotes stronger proliferation in virus-specific T cells, possibly leading to the loss of tumor-specific T cells [206]. In cooperation with the DTU, antigen-specific T cell populations from TILs were expanded using an artificial antigen-presenting scaffold. In order to test wether the specifically expanded T cells have a higher efficiency in tumor cell killing, they were compared to T cells expanded using the REP protocol. Using the PDM-based cytotoxicity assay it could be shown that the scaffold-expanded T cells have a significantly higher cytotoxic effect on the tumor cells (Figure 31). Thus, the CytoTox assay can be used to investigate differently expanded T cell populations on their cytotoxic abilities. In this case, the measured fluorescence could be normalized on the T cell-only control to eliminate possible viability differences due to the expansion method.

6.9 Infiltration of immune cells into PDMs

Additionally, to the cytotoxicity testing, the PDMs are a versatile tool, which can also be used during microscopy experiments to investigate the interacting between the immune cells and the tumor. It is reported [207] that the ability of immune cells to infiltrate the tumor is generally correlated to a positive patient outcome. However, the positive effect also depends on the composition of the immune cell infiltrate. Hence, it is an important question to answer whether or not a treatment can enhance the T cell infiltration. Using single PDMs, the infiltration of T cells can be tracked using time-laps-imaging. Treatment with checkpoint inhibitors can significantly enhance the infiltration

of T cells into the PDM (Figure 32). This demonstrated that the PDMs can be used to study the tumor infiltration of T cells and to test if this infiltration can be enhanced. This could be used to show the reported enhancement of immune cell infiltration in tumors when treated with an antiangiogenic, like Axitinib, in combination with an checkpoint inhibitor, like aPD-1, into the tumor [208, 209]. These findings could be correlated to the observation that the combination of aPD-1 and Axitinib treatment in RCC1589 PDM co-culture showed a significant increase in cytotoxic effect.

7. Conclusion

Taken together, PDMs display a high viability and express tumor markers of the original tumor, which can be further improved by adapting the isolation protocol and the culturing conditions. It was shown on the RNA as well as protein level that cells of the PDMs express cancer stem cell markers; thus, CSCs are retained in the PDM models. This finding makes the PDMs a suitable model to test agents targeting this subset of cancer cells. Using RPPA protein analysis, additional information on pathway alterations in PDMs can be gained and used to either find suitable PDM models for the compound to be tested or to match the observed cytotoxic response to pathway alterations.

After showing that antigen-specific T cells have an effect on PDMs, an assay system to measure the cytotoxic effect was set up. Using the CellTox Green assay, the effect of SOC compounds as well as immune cells on PDMs can be tested as mono- or combinatorial treatment. Additionally, in case peripheral blood of the patient is available, tumor-reactive T cells can be isolated from autologous PBMCs. Being able to isolate and test TILs as well as tumor-reactive T cells from the periphery allows to account for both T cell populations in a cancer patient, since it is still under debate which T cell population is more relevant for immune therapy as TILs predominantly express checkpoint proteins like, PD1 and CTLA4 and thus, are impaired in their antitumoral response [210, 211].

Moreover, PDMs can be used to assess the ability of drugs to improve tumor infiltration by T cells.

8. Outlook

The use of immune cells needs to be broadened in research in order to expand the array of possible applications of the PDM assay in cancer research, since in the human body not only T cells are able to influence the outcome of a cancerous disease. The innate immune system plays a vital part in the development as well as in the prevention of cancer. Development of immune-modulatory anti-cancer drugs has picked up on the importance of this part of the immune system, and a relevant test system for the efficacy of these drugs is needed. One advantage when working with the innate

immune system is that it does not need to be HLA-matched to the patient. Hence, stem cell-originated immune cells are feasible to be used, and therefore, the availability of these cells, contrary to autologous material, is not limited. Overall, the field of application for the PDM assay can be expanded by verifying the predictive nature as well as by broadening the use of immune cell types.

As the next step, an important goal for the PDM assay would be to validate it regarding its predictive nature in patient therapy. In order to be a predictive assay for personalized cancer therapy, firstly, the correlation between the mutational profile found by RPPA analysis and the cytotoxicity and/or viability assays in the respective PDMs must be shown. Secondly, the patient outcome in the clinic must be matched to the respective treatment of the PDMs in a patient cohort large enough to validate a correlation and thus a predictive nature of the PDM assay.

9. Summary

After years of extensive research, cancer is still a devastating disease. Even though the knowledge on cancer and its development is growing, a valid close-to-*in vivo* test system for new drugs is still missing. The aim of this thesis was the successful isolation of 3D patient derived microtumors (PDMs) from various cancer entities and the establishment of a PDM based test system using RCC and malignant melanoma PDMs improving the mentioned shortcomings in cancer drug discovery.

PDMs from 11 different tumor entities could be successfully isolated and cultured. The isolated PDMs of RCC and malignant melanoma models are characterized for their viability as well as compared to the patient tumor tissue using Immunohistochemistry. An interesting finding is the presence of cancer stem cells in the PDMs, making it feasible to test agents targeting this subset of cancer cells. By RPPA protein analysis, pathway mutations in the PDMs of different patients were determined and clustered. This information could be used to decide on appropriate PDM models for the testing of novel chemotherapeutic compounds. In future, possible treatment options for patients could be decided on using the RPPA information, ranging from approved SOCs for the specific cancer type to off-label use of approved drugs.

Treating single PDMs with different E:T ratios of antigen-specific T cells resulted in disintegration of the PDM and diminished live cell dye fluorescence, reflecting cell death. Based on these findings, a quantitative way to measure cell death was found by using the CellTox Green reagent, which starts to fluoresce green upon binding to free DNA. The established CytoTox assay can be used to test standard of care agents as well as novel chemotherapeutic compounds alone or in combination as well as in an immune cell co-culture. Furthermore, using autologous T cells the effects of checkpoint inhibitors on the ability to target the cancer cells could be investigated. Despite the complex assay

condition due to the co-culture set-up, the assay results were reproducible and significant effects were detected with a low standard deviation.

During the isolation of the PDMs from patient tissue, TILs can be isolated and cultured for subsequent testing. Furthermore, the isolated TILs can be characterized using flow cytometry analysis to plan the treatment options to be verified using the CellTox™ Green cytotoxicity assay.

Moreover, not only cell death could be quantified using the PDMs, but also the PDM infiltration by T cells could be investigated and whether the infiltration can be enhanced by chemotherapeutic compounds or checkpoint inhibitors.

Taken together, the presented PDM-based assay is a valid test system for new anti-cancer or immunomodulatory drugs and, in future, if a large enough cohort could be tested, a possible predictive tool for treatment decisions in the clinic.

10. Zusammenfassung

Nach Jahren intensiver Forschung ist Krebs noch immer eine verheerende Krankheit. Obwohl das Wissen über Krebs und dessen Entwicklung stetig wächst, fehlt ein valides nahe-*in vivo*-Testsystem für neue Medikamente. Das Ziel dieser Arbeit war die erfolgreiche Isolierung von 3D-Patientenabgeleiteten-Mikrotumoren (PDMs) aus verschiedenen Krebsentitäten und die Etablierung eines PDM-basierten Testsystems unter Verwendung von RCC- und malignen Melanom-PDMs, um die genannten Defizite in der Krebsmedikamentenentwicklung zu verbessern.

PDMs von 11 verschiedenen Tumorarten konnten erfolgreich isoliert und kultiviert werden. Die isolierten PDMs von RCC- und malignen Melanom-Modellen wurden auf ihre Lebensfähigkeit hin untersucht, sowie mittels Immunhistochemie mit dem Tumorgewebe der Patienten verglichen. Ein interessanter Fund ist der Nachweis von Tumorstammzellen in den PDMs, was es möglich macht, Wirkstoffe zu testen, welche auf diese Untergruppe von Krebszellen abzielen. Unter Verwendung von RPPA-Protein-Analyse konnten Signalwegs-Mutationen in den PDMs verschiedener Patienten bestimmt und geclustert werden. Diese Informationen könnten genutzt werden, um über geeignete PDM-Modelle für das Testen neuartiger chemotherapeutischer Wirkstoffe zu entscheiden. Zukünftig könnte anhand der RPPA-Informationen über mögliche Behandlungsoptionen für Patienten entschieden werden, die von zugelassenen SOCs für die jeweilige Krebsart bis hin zum Off-Label-Einsatz zugelassener Medikamente reichen.

Die Behandlung von einzelnen PDMs mit unterschiedlichen E:T-Verhältnissen antigenspezifischer T-Zellen führte zum Zerfall des PDMs und einer Verminderung der Fluoreszenz des Lebendzellfarbstoffes, was den Zelltod widerspiegelte. Basierend auf diesen Erkenntnissen wurde ein quantitativer Weg zur Messung des Zelltods mit dem Reagenz CellTox Green gefunden, das bei

Bindung an freie DNA grün zu fluoreszieren beginnt. Der etablierte CytoTox-Assay kann sowohl für den Test von Standardmedikamenten als auch von neuartigen Chemotherapeutika allein oder in Kombination sowie in einer Immunzell-Co-Kultur eingesetzt werden. Darüber hinaus kann unter Verwendung autologer T-Zellen der Effekt von Checkpoint-Inhibitoren auf die Fähigkeit, die Krebszellen zu bekämpfen, untersucht werden. Trotz der komplexen Assay-Bedingungen aufgrund des Co-Kultur-Aufbaus sind die Assay-Ergebnisse reproduzierbar und es werden signifikante Effekte mit einer geringen Standardabweichung nachgewiesen.

Während der Isolierung der PDMs aus Patientengewebe können TILs isoliert und für nachfolgende Tests kultiviert werden. Darüber hinaus können die isolierten TILs mittels Durchflusszytometrie charakterisiert werden, um die Behandlungsoptionen zu planen, die mit dem CellTox™ Green Cytotoxicity Assay überprüft werden.

Darüber hinaus kann mit den PDMs nicht nur der Zelltod quantifiziert werden, sondern auch die Infiltration von T-Zellen in das PDM untersucht werden und ob die Infiltration durch Chemotherapeutika oder Checkpoint-Inhibitoren verstärkt werden kann.

Zusammengenommen ist der vorgestellte PDM-basierte Assay ein valides Testsystem für neue Krebsmedikamente oder immunmodulatorische Wirkstoffe und in Zukunft, wenn eine ausreichend große Kohorte getestet werden könnte, ein mögliches prädiktives Werkzeug für Behandlungsentscheidungen in der Klinik.

11. Materials

11.1 Equipment and consumables

Equipment and consumables	Supplier
Absolutely RNA Nanoprep Kit	Agilent Technologies, USA
Biopsy Cassettes	Medite Cancer Diagnostics, USA
CD137 beads for the MACS system	Milteniy Biotech, Germany
CD3 beads for the MACS system	Milteniy Biotech, Germany
Cell Observer Spinning Disc Microscope	Zeiss, Germany
Cell culture dish 10 cm	Corning, USA
Cell culture flask T25, T75	Corning, USA
Cell culture 96 well plate ultra-low attachment	Corning, USA
Cell culture µclear bottom 96-well plate	Corning, USA
Cell culture 96-well plate clear V-bottom	Corning, USA
Cell culture 96-well plate, black	Corning, USA
Cell strainer 40 µm	Corning, USA
Centrifuge 5810R	Eppendorf, Deutschland
Coverslides Superfrost Ultra Plus 25x75x1mm)	Thermo Fisher Scientific, USA
CytoStim	Milteniy Biotech, Germany
DNAse	Qiagen, Germany
Dynabeads Human T-Activator CD3/CD28	Thermo Fisher Scientific, USA
Dynabeads Human T-Activator CD3/CD28/CD137	Thermo Fisher Scientific, USA
Envision Multilabel Reader	Perkin Elmer, USA
Erlenmeyer flask, steril	Corning, USA
FACS Melody	BD, USA
Fume hood	Erlab, France
Freezer -80°C	Sanyo, Japan
Hoechst 33342	Thermo Fisher Scientific, USA
Incubator	Binder, Germany
Liquid nitrogen tank	teclab GmbH, Worthington Industry, USA
Librase DH	Roche, Switzerland
LS column	Milteniy Biotech, Germany
LSRFortessa	BD, USA
Lymphoprep	StemCell, Canada
Magnetic stirrer	IKA Labortechnik, Germany

Micro scale	Mettler Toledo, USA
Microscope Axiovert 200M	Zeiss, Germany
Microtome Blades S35/C35	Feather, Japan
Microwave	Sharp, Japan
NanoPlotter 2	SESMOS Ltd., GB
pH meter	Mettler Toledo, USA
Nucleocounter	Chemometec, Denmark
Nanodrop2000	Thermo Fisher Scientific, USA
PepTivator Survivin	Miteniy Biotech, Germany
pH meter	Mettler Toledo, USA
Pipet (5 ml, 10 ml, 25 ml, 50 ml)	Corning, USA
Pipet (0.5-10 ml, 10-100 µl, 100-1000 µl)	Eppendorf, Germany
Pipetboy 2	Integra Biosciences, USA
Pipet tips	SARSTEDT AG & Co., Germany
Rotary Microtome 2165 Leica Biosystems	Leica Biosystems, Germany
Scale	Mettler Toledo, USA
Scalpel	Schreiber Instrumente, Germany
Sepmate tubes	Stemcell, Canada
Sterile Bench HERAsafe	Thermo Fisher Scientific, USA
Steel mesh 500 µm	VWR, USA
SuperScriptTM VILO™ cDNA Synthesis Kit	Thermo Fisher Scientific, USA
Tube 15 ml, 50 ml	Greiner Bio one, Germany
Tube 50 ml	Corning, USA
Tissue Embedding System TES 99	Medite GmbH, Germany
Tissue Floating Bath TFB 45	Medite GmbH, Germany
Tissue Tek® Cyromolds	Sakura Finetek, Japan
Water bath	GFL, Germany

11.2 Chemicals

Chemical	Supplier
2-Mercaptoethanol	Gibco, GB
bFGF	Gibco, GB
BD™ CS&T Beads RUO	BD Biosciences, USA
BD™ Pharmingen™ Propidium-Iodide	BD Biosciences, USA
BSA: Albumin Fraktion 5	Roth, Germany
Calcein AM	Invitrogen, USA
Carboplatin 1mM	Selleckchem, USA
CD3 MicroBeads for MACS system	Miltenyi Biotech, Germany
Celltox Green Dye	Promega, USA
Celltracker Green	Invitrogen, USA
Celltracker DeepRed	Invitrogen, USA
Cholera toxin	Sigma Aldrich, Germany
DMEM	Gibco, GB
DMSO	Roth, Germany
Docetaxel 1mM	Selleckchem, USA
Dynabeads Human T Cell Activation CD3/CD28	Thermo Fisher Scientific, USA
eBioscience™ Fixation/Permeabilization Concentrate (4x)	Invitrogen, USA
eBioscience™ Fixation/Permeabilization Diluent	Invitrogen, USA
eBioscience™ Permeabilization Buffer (10x)	Invitrogen, USA
EDTA	Roth, Deutschland
Eosin (Alcohol)	Leica Biosystems, Germany
Ethanol ≥99	Roth, Germany
Ethidium Homodimer	Invitrogen, USA
FCS	Gibco, GB
Glutamin	Gibco, GB
Harris Hematoxylin	Leica Biosystems, Germany
HBSS	Gibco, GB
HistoGel™ - Richard-Allan Scientific™	Thermo Fisher Scientific, USA
IL15	Peprotech, USA
IL2	Peprotech, USA
IL7	Peprotech, USA

Ipilimumab	Selleckchem, USA
Liberase DH	Roche, Switzerland
Lymphoprep	Stemcell, USA
MEM Vitamin	Thermo Fisher Scientific, USA
Mounting Media CV Mount	Leica Biosystems, Germany
Nivolumab 5mg/ml	Selleckchem, USA
NGS	Jackson ImmunoResearch
Novocastra™ Avidin	Leica Biosystems, Germany
Novocastra™ Biotin	Leica Biosystems, Germany
Novolink™ DAB Substrate Buffer	Leica Biosystems, Germany
Novocastra™ DAB Chromogen	Leica Biosystems, Germany
Novocastra™ Hematoxylin	Leica Biosystems, Germany
Novocastra™ NovoPen (NCL-Pen)	Leica Biosystems, Germany
Novocastra™ Peroxidase Block	Leica Biosystems, Germany
Novocastra™Streptavidin-HRP	Leica Biosystems, Germany
Pen-Strep	Gibco, GB
PBS	Gibco, GB
Primocin	Invivogen, USA
Renaissance essential Tumor Media	Cellaria, USA
RETM Media phenolredfree	Thermo Fisher Scientific, USA
Roti®-Histol	Roth, Germany
Roti Histofix 4%	Roth, Germany
RPMI Advanced Media	Gibco, GB
RPMI Advanced Phenolred-free Media	Thermo Fisher Scientific, USA
StemPro hESC SFM Media	Gibco, GB
Sytox Orange 5mM in DMSO	Invitrogen, USA
Triton X100	Roth, Germany
Trizma base	Sigma Aldrich, USA
Tween 20	Roth, Germany
Trypsin-EDTA 0.05 %	Gibco, GB

11.3 Antibodies

Antibody	Source	Application	Usage
Rabbit anti-human PDL1		IHC	1:200
Mouse monoclonal anti-human CD3	Abcam (ab17143)	IHC	1:10-1:25
Rabbit monoclonal anti-human Ki67	CellSignaling (9027)	IHC	1:400
Mouse monoclonal anti-human Fibroblasts (TE-7)	EMD Millipore (CBL271)	IHC	1:400
a-CD163 rabbit	Cell Signaling Technologies (93498)	IHC	1:500
a-Vimentin mouse	Cell Signaling Technologies (5741)	IHC	1:100
a-CA9 mouse	NSJ Bioreagents (V2939)	IHC	1:200
a-MART1 mouse	NSJ Bioreagents (V2116)	IHC	1:200
Mouse Anti-human CD3, FITC	BD Biosciences (345763)	FACS	1:40
Mouse anti-human CD8, PerCP	Thermofisher Scientific (MHC0831)	FACS	1:40
Mouse anti-human CD8, FITC	BioLegend (301005)	FACS	1:20
Mouse anti-human CD4, PE-Cy7	BioLegend (344611)	FACS	1:20
Mouse anti-human CD25, PerCP	BioLegend (356131)	FACS	1:20
Mouse anti-human CD137, PE	Miltenyi Biotec (130-098-878)	FACS	1:11
Mouse anti-human CD39, PE/Dazzle 594	BioLegend (328223)	FACS	1:20
Mouse anti-human PD1, BV421	BioLegend (329919)	FACS	1:20
Mouse anti-human CEACAM1, PE-Cy7	BioLegend (342309)	FACS	1:20
Mouse anti-human CTLA4, PerCP-Cy5.5	BioLegend (369607)	FACS	1:20
Goat anti-mouse IgG (H+L) Biotin-SP	Jackson ImmunoResearch (115-066-062)	IHC	1:1,000
Goat anti-rabbit IgG (H+L) Biotin-SP	Jackson ImmunoResearch (111-065-144)	IHC	1:1,000
Goat anti-rat IgG (H+L) Biotin-SP	Jackson ImmunoResearch (112-065-167)	IHC	1:1,000

11.4 Media

Digestion Media

20 ml	DMEM
40 µl	Primocin
430 µl	Liberase DH

Microtumor Media (StemPro® hESC SFM Medium)

451 ml	DMEM/F-12 + GlutaMAX™
10 ml	StemPro® hESC Supplemen
36 ml	BSA (25%)
400 µl	bFGF (10µg/ml)
909 µl	2-Mercaptoethanol (55mM)
1 ml	Primocin (50mg/ml)

T Cell Media

500 ml	Advanced RPMI 1640 (1x)
5 ml	Glutamin (200mM)
5 ml	MEM Vitamins
25 ml	Human Serum
1 ml	Primocin (50mg/ml)

CellTox Assay Media

500 ml	RPMI Advanced Phenolred-free Media
5 ml	Glutamin (200mM)
5 ml	MEM Vitamins
25 ml	Human Serum
1 ml	Primocin (50mg/ml)

11.5 Buffer

FACS Staining Buffer

PBS
+ 10 % FCS

MACS Buffer

PBS
+ 0.5 %BSA
+ 2 mM EDTA

12. Methods

12.1 Microtumor preparation and characterization

12.1.1 Microtumor preparation

Microtumors are isolated from fresh tumor material received from the clinic. The protocol for the isolation was adapted from Kondo *et al*. [115]. For the isolation, the tumor material is minced into 5-10 mm pieces and washed with 20 ml HBSS. The minced tissue is incubated for 2 h in 20 ml of Liberase media (see 11.4) containing 0.28 U/ml of Liberase DH®. Following the 2 h incubation, the digest is filtered through a 500 µm mesh to remove undigested connective tissue. The rough flowthrough is then filtered through a 40 µm cell strainer. The microtumors are retained by the strainer, whereas the single cells and the TILs are in the flowthrough. The cell strainer containing the microtumors is transferred into a 10 cm dish containing 20 ml of HBSS, and the microtumors are collected using a 1 ml pipette. The collected microtumors are washed twice with 20 ml HBSS and transferred into 5 ml of culture media.

12.1.2 Cultivation of patient-derived microtumors

For cultivation, the PDMs are transferred into 6 cm non-treated culture dishes and incubated in a 5% CO2-humidified chamber at 37 °C. Every three days the culture media is exchanged by collecting the PDMs in a 15 ml tube and the culture dish is washed twice with 1 ml HBSS ensure the total transfer of PDMs. The PDMs are then spun down at 200 g for 5 min. The media is removed, and the pelleted PDMs are resuspended in 4 ml of culture media and transferred in a fresh 6 cm non-treated culture dish. The falcon is washed with 1 ml of media to ensure the total transfer of the PDMs.

12.1.3 q-PCR of target gene expression

In order to identify the expression of target genes in the microtumors, a q-PCR is performed. For the isolation of sufficient amounts of RNA, approximately 300 microtumors are pooled. The RNA is isolated using the "Absolutely RNA Nanoprep Kit" from Agilent Technologies according to manufacturers' protocol. In brief, 100 µl freshly prepared lysis buffer is added to the microtumor pellet and homogenized by pipetting. After adding an equal amount of 80 % sulfolane, the mixture is transferred to the RNA-binding nano-spin cup. Following a 60 s spin at full seed, the filtrate is discarded, and the sample is treated with DNase to remove residual DNA. In order to do so, the column is prepared by washing with Low-Salt Wash Buffer. Then 2.5 µl RNase-free DNaseI in 12.5 µl DNase Digestion Buffer is added and the mixture incubated for 15 min at 37°C. After the digestion, the column is washed with High-Salt Wash Buffer and again with Low-Salt Wash Buffer. Next, the column is dried by centrifuging for 3 min at full speed and transferred into a fresh 1.5 ml Eppendorf

tube. The RNA is eluted with 10 µl of Elution Buffer. The concentration is measured using a Nanodrop2000.

The RNA is transcribed into cDNA using the SuperScript™ VILO™ cDNA Synthesis Kit according to the manufacturer's protocol. In brief, up to 2.5 µg of RNA are mixed with 4 µl 5x VILO™ Reaction Mix, 2 µl of 10x SuperScript™ Enzyme Mix and filled up to 20 µl with RNase-free water. The mixture is incubated at 42°C for 60 min, and the reaction is terminated at 85°C for 5 min.

Taqman assays are used for the qPCR. For this, 1.25 µl of the 20x Gene Expression assay is mixed with 10 µl of Nuclease-free water and 12.5 µl of PCR Master Mix. 1.25 µl of the sample is added to this mixture.

Gene expression is calculated relative to GAPDH as internal control, and the relative gene expression analyzed using the ΔΔCT method [212]. The result is then normalized to the Survivin expression of RCC15-138.

12.1.4 Viability assay

Microtumors are stained with a Live/Dead marker to test for their viability. Approximately 5 microtumors are transferred into a clear bottom 96-well plate containing 150 µl of culture media. The microtumors are now stained using 2 µM Calcein and 4 µM Ethidium Homodimer. After 30 min, images are taken on the spinning disc confocal Zeiss Cell Observer Z1 microscope using the 10x air objective.

The diameter of the PDMs is determined using the middle image of the image stack and analyzed using the Zeiss Zen software.

In order to determine the fluorescence, the ImageJ software was used. The image of the respective fluorescence channel was selected, the outer rim of the PDM marked and the fluorescence measured using the ImageJ tool. Followed by calculation of the percentage.

12.1.5 Immunohistochemical staining of the microtumors and parental tissue

12.1.5.1 Embedding of microtumors in HistoGel

After collecting the PDMs in a 15 ml falcon they are washed twice and fixed with 4 % Roti Histofix for 1 h at RT. Afterwards, the PDMs are transferred into Hematoxylin for 5 min to make them visible for the cutting of the paraffin block. The PDMs are washed in H_2O and then incubated two times in 50 % and two times in 70 % ethanol for 15 min each. During the incubation, the HistoGel is warmed in the microwave. Using a microscope, the PDMs are transferred into a cryomold. After the remaining ethanol is evaporated, the warm HistoGel is added carefully to allow the PDMs to remain

on the bottom of the cryomold. The rest of the cryomold is filled up with HistoGel after allowing the PDMs to settle. Next, the HistoGel solidifies at RT for 10 min and can be put on 4°C for 1 min to allow for easer retrieval of the HistoGel from the cryomold. The HistoGel can be stored in 70 % ethanol for up to two weeks. Finally, the HistoGel is embedded into paraffin.

12.1.5.2 Tissue processing for paraffin embedding

The tissue processing for the paraffin embedding is performed at the Frauenklinik in Tübingen at the group of Prof. Dr. Schenke-Layland using the automatic processor overnight. The procedure is as follows:

Table 6: Tissue processing steps for the paraffin embedding.

Solution	**Time**
70 % Ethanol	1 h
90 % Ethanol	1 h
96 % Ethanol	1 h
2-Propanol absolute I	1 h
2-Propanol absolute II	1 h
Xylol/2-Propanol absolute	1:30 h
Xylol I	1 h
Xylol II	1 h
Paraffin I	1:30 h
Paraffin II	1:30 h

12.1.5.3 Paraffin embedding and cutting

The processed tissue is stored in a solid paraffin block. For the embedding of the HistoGel into paraffin, the block has to be melted at 60°C to retrieve the HistoGel, which then can be embedded into paraffin. Afterwards, the sample can be cut using a microtome. The most frequently used thickness of the paraffin slices is 3 µm to visualize the cellular structures.

12.1.5.4 Hematoxylin/Eosin (HE)-Staining

HE staining is a way to visualize the cells on the slides and compare the structures to the HE staining od the primary tumor tissue (PTT). After baking the slides in the heating cabinet at 60°C for 30 min, the slides are incubated according to Table 7:

Table 7: Processing steps of HE-Staining

Processing step	**Solution**	**Time**
Dewaxing	Xylene	3 min
	Xylene	3 min
	100%EtoH	2 min
	100%EtOH	2 min
	95% EtoH	2 min
	70%EtoH	2 min
Washing	Tap Water	2 min
	Aqua Dest	30sec
Staining	Harris Hematoxylin	2 min
Washing – Bluing	Tap Water	3 min
Differentiator	Acetic Acid 2%	1 – 2 min
Washing	Tap water	4 min
Neutralizing	95% EtOH	2 min
Staining	Eosin alk	2 min
Washing	Tap water	15sec
Dehydrating	95% EtOH	1 min
	100%EtOH	1 min
	100%EtOH	2 min
	Xylene	2 min
	Xylene	2 min

12.1.5.5 Immunohistochemical staining of paraffin-embedded sections

In order to be able to stain antigens on the paraffin slides, they first need to be deparaffinated. Therefore, the slides are baked for 30 min in a heating cabinet at 60°C and then processed following Table 8.

Table 8: Processing steps for deparaffinization

Solution	**Time**
Xylene	3-5 min
Xylene	3-5 min
100 % Ethanol	2 min
100 % Ethanol	2 min
95 % Ethanol	1 min
70 % Ethanol	2 min

After shortly washing the slides with deionized water, they are put into tap water until antigen retrieval. From now on, drying out of the slides should be avoided. For epitope retrieval, the slides are incubated in TE buffer at 95-98°C in a water bath or heating cabinet and then cooled down to RT in water.

For the first part of DAB staining, the slides are washed two times with H_2O and dried with a lint-free cloth. After circling the sample with a NovoPen, Peroxidase Block is added for 5 min to neutralize the endogenous peroxidases. Next, the slides are washed twice with PBS for 2 min and then blocked for 1 h at RT in a humidified chamber with 200-300 µl blocking medium to prevent unspecific binding of the antibody. The slides are then washed twice with PBS for 2 min. Afterwards 200-300 µl of primary antibody diluted in PBS+1 % BSA is added to each section as well as 4 drops of biotin solution and incubated overnight at 4°C in a humidity chamber.

The second part of the DAB staining is the secondary antibody staining. After removing the primary antibody by washing twice with PBS for 2 min, 200-300 µl of secondary antibody diluted 1:1000 in PBS+1 % BSA áre added and the staining is incubated for 30 min at RT. Next, the slides are washed twice with PBS and then incubated with Streptavidin-HRP for 30 min. The slides are again washed twice with PBS, then the signal is developed by incubating with DAB working solution for about 5 min. For counterstaining, the slides are incubated with Hematoxylin for 7 min. After rinsing with tap water, the slides are dehydrated and cleared by incubating for 1 min in each of the following solutions: 70 % ethanol, 95 % ethanol, 100 % ethanol and Xylene. The slides are then mounted using

CV mounting media. The bright field images are obtained with a microscope (Zeiss ApoTome.2) with a 20x/0.8 air objective, 40x/1.1 oil objective and 63x/1.3 oil objective.

12.2 Immune cell isolation

12.2.1 PBMC isolation

PBMCs are isolated from Lithium-Heparin blood from tumor patients. 15 ml of Lymphoprep are filled into 50 ml SepMate columns. The blood is diluted 1:2 in PBS with 2 % FCS and a maximum of 30 ml is layered on top of 15 ml of Lymphoprep. For the separation of the PBMCs from the red blood cells, the SepMate columns are spun at 1200 g for 20 min. Following that, the supernatant containing the PBMCs can be poured into a 50 ml falcon. The PBMCs are pelleted at 300 g for 10 min. After washing once with 15 ml of PBS with 2 % FCS the PBMCs are resuspended in T cell media. The PBMCs are then frozen with 10^7 cells/ml in freezing media.

12.2.2 TIL isolation

In the flow-through after microtumor preparation, tumor-infiltrated lymphocytes can be found. These TILs can be expanded by culturing them in T cell-culturing media and adding 2 µl of Dynabeads Human T-Activator CD3/CD28. After two weeks, the expanded T cells can be used for co-culture assays or cryoconserved.

12.2.3 Antigen or unspecific activation of cytotoxic T cells

For the antigen specific stimulation, the PBMCs are treated for 24 h with 20 µl of 30 nmol/ml PepTivator Survivin 1 per 10^7 cells. For unspecific activation, the PBMCs are treated for 6 h with 20 µl CytoStim per 10^7 cells.

12.2.4 Isolation of immune cell populations using MACS

The activated cytotoxic T cells from PBMCs, PepTivator Survivin 1 or CytoStim-treated PBMCs are isolated using CD137 beads for the MACS system according to the manufacturer's protocol. In brief, the PBMCs are collected and spun down at 300 g for 10 min and resuspended in 40 µl MACS buffer and 10 µl of CD137-PE is added. After incubating for 10 min in the refrigerator, the cells are washed with 1 ml of MACs buffer and resuspended in 80 µl of MACs buffer. 20 µl of anti-PE Micro-Beads are added and incubated for 15 min in the refrigerator. Following a washing step, the pellet is resuspended in 500 µl of MACS buffer and applied to the equilibrated LS column. The activated T cells will be bound to the magnetic column. After washing, the cells are flushed from the column using the plunger.

For the isolation of $CD3^+$ T cells from PBMCs, CD3 beads for the MACS system are used according to the manufacturers' protocol. In brief, the PBMCs are harvested at 300 g for 10 min and

resuspended in 80 µl of MACS buffer. 20 µl of CD3 MicroBeads are added to the PBMCs and incubated for 15 min at 4-8°C. After washing the cells with 1 ml of MACS buffer, they are resuspended in 500 µl of MACS buffer and applied to the equilibrated LS column. The labeled CD3 cells are bound to the column. After washing the column, the CD3 positive cells are flushed from the column using a plunger.

12.2.5 T cell cultivation

The T cells are cultivated in Advanced RPMI containing human serum. Before every media change, 100 U IL-2, 10 U IL-7 and 23.5 U IL-15 are added. For T cell expansion, CD3/Cd28/CD137 Dynabeads are added. The media is exchanged every second day.

12.2.6 Identification of tumor reactive T cells using tetramer staining

The identification of tumor-reactive T cells by tetramer staining is performed in a collaboration with Hadrup Laboratory at DTU in Copenhagen. Following is a brief description of the method used there.

In order to identify tumor antigen-specific T cells in TILs, roughly 10^6 TILs are unspecifically expanded using CD3/CD28 Dynabeads. Recombinant MHC I, which is bound to a photo-labile antigen, is incubated under UV light together with shared melanoma antigens. By binding to the rescue epitopes, the MHC I is stabilized, MHCI without bound antigen denatures and can be removed by centrifugation. Next, the epitope-laden MHCI are bound via a biotin-tag to fluorescently labeled streptavidin beads. Importantly, MHCI bound to the same epitope are bound to two differently labeled streptavidin beads. That way, T cells binding to this epitope can be identified by two different colors. Before incubating the T cells with the MHCI clusters, they are treated with Desatinib to force the TCR translocation to the cell surface. Afterwards, the T cells are added to the MHCI cluster and then stained with an antibody mix, to identify the cytotoxic T cell population as well as a live cell dye. The mixture is analyzed on the BD LSRFortessa.

12.2.7 Target-specific expansion of T cell populations

The target-specific expansion of an antigen-specific T cell population is done by Hadrup Laboratory at DTU in Copenhagen.

In brtief, to expand only antigen-specific populations of T cells, MHC I bound to the antigen is immobilized in a streptavidin-dextran backbone via a biotin-tag. For the expansion, stimulatory molecules, such as IL-2 and IL-21 are also immobilized on the backbone using a biotin-tag to form an expansion multimer. The T cells are incubated with the expansion multimer for two weeks. After that period, the specifically expanded T cells can be tested in the CytoTox assay.

12.3 T cell effect on single PDMs

12.3.1 Staining of PDMs

Microtumors needed are pooled and washed with HBSS. After a spin of 5 min at 300 g, the microtumors are resuspended in 1 ml of HBSS, and 10 µM CellTracker Green is added and incubated for 1 h at 37°C.

Microtumors are washed three timed with HBSS and then resuspended in 100 µl media per well for a statistical amount of one PDM per well.

12.3.2 Cell culture plate preparation and microscopy

The PDMs are distributed on the 96-well plate for a statistical amount of one PDM per well and the wells checked by microscopy to contain only one PDM. Next, the amount of T cells needed for an E:T ratio of 2:1 and 10:1 is collected, spun down and resuspended in 50 µl media per well and added to the wells containing a single PDM. Furthermore, 50 µl of media is added to single PDMs for the no T cell control.

The plates are monitored over a time course of 69 h and microscopy pictures of the PDMs are taken.

12.3.3 Quantification of the T cell effect

In order to determine the diameter and fluorescence, the ImageJ software was used. The image of the fluorescence channel was selected, the outer rim of the PDM marked and the diameter as well as fluorescence measured using the ImageJ tool.

12.4 Calcein staining for standard curve determination

Microtumors are collected and washed with HBSS. After a second spin for 5 min at 300 g, the microtumors are resuspended in 500 µl HBSS, and 30 µM Calcein-AM are added. After 30 min incubation at 37°C, the microtumors are washed three times with HBSS to remove the excess Calcein-AM. The stained microtumors are resuspended in the appropriate amount of assay media.

In order to determine the optimal amount of PDMs for the assay, a standard curve is generated. PDMs are stained with Calcein-AM, and an increasing number of PDMs is pooled and subsequently lysed by Triton-X100. The released Calcein is measured.

Determined by the standard curve, the assay is performed containing approximately 15 microtumors per well and in triplicates per treatment.

12.5 CellTox™ Green Cytotoxicity Assay

The assay is performed in triplicates per treatment and approximately 15 microtumors per replicate. The advantage of this assay is that there is no need for pre-staining of the microtumors.

12.5.1 SOC testing

For SOC testing, the needed amount of wells is filled with 50 µl of assay media and the Celltox™ Green Dye is added in a 1:1000 dilution to a final volume of 150 µl. Next, the SOCs are added in 50 µl media containing the tested concentrations. Lastly, the microtumors are taken up in 50 µl per well and added to the 96 well plate. Green fluorescence, corresponding to dead cells, is measured after 4 h, 24 h, 48 h and 72 h using the Envision plate reader from Perkin Elmer according to the CellTox™ Green Cytotoxicity Assay protocol.

12.5.2 Co-culturing with autologous T cells

In the co-culture assay, the needed wells are prefilled with 50 µl Co-culture assay media containing 1:1000 CellTox™ Green Dye to a final volume of 150 µl. The T cells, the amount depending on the desired E:T ratio, are resuspended in 50 µl media per well and distributed in the corresponding wells. Additional treatment with SOC or a-PD-1 antibody is added to the wells. Finally, the microtumors are added with 50 µl media per well. Green fluorescence is measured after 4 h, 24 h, 48 h and 72 h using the Envision plate reader from Perkin Elmer according to the CellTox™ Green Cytotoxicity Assay protocol.

12.5.3 Analysis of CellTox™ Green Cytotoxicity Assay

To obtain the fold change read-out, the mean of the measured fluorescence value of the PDM-only control is calculated. Next, the measured results of the different treatments are normalized to the PDM-only mean value.

These values are then analyzed using the GraphPad Prism software (see 12.8).

12.6 Infiltration Assay

12.6.1 Staining of microtumor and Immune cells

The infiltration assay is performed in triplicates with 15 microtumors per replicate in a µ-clear U-bottom ultra-low attachment 96-well plate. The T cells are used at an E:T ratio of 4:1. The microtumors needed are pooled and washed with HBSS. After a spin of 5 min at 300 g, the microtumors are resuspended in 1 ml of HBSS, and 10 µM CellTracker Green is added and incubated for 1 h at 37°C. The needed amount of T cells is pooled and pelleted for 5 min at 300 g and

resuspended with 100 µl of co-culture assay media. After adding CellTracker Deep Red to a final concentration of 25 µM, the T cells are incubated for 1 h at 37°C.

Both microtumors and T cells are washed three timed with HBSS. The microtumors are resuspended in 100 µl media per well and distributed on a µ-clear U-bottom ultra-low attachment 96-well plate. If a treatment or combination of SOC with checkpoint inhibitors is tested, the agents are added next. The T cells are resuspended in 50 µl per well and distributed in the corresponding wells.

12.6.2 Time-lapse spinning disc microscopy

The infiltration is observed on the Zeiss Cell Observer spinning disc confocal microscope. The infiltration is imaged every hour for 4 to 6 h and after 24 h, 48 h and 72 h. Tiles are set for the wells containing the microtumors. Z-stacks covering the microtumor are set in 488 nm laser channel. The T cells are imaged in the 545 nm laser channel. The z-stacks are adjusted for z-stack shift before imaging.

12.6.3 Analysis using IMARIS Software

The infiltration assay is analyzed using the IMARIS software. Using this software, a mask for green and one for the Cy5 channel, reflecting the microtumors and T cells, respectively, are generated. That way, the software can analyze the masks for T cells included in the mask for the microtumors. Using this software, a bias-free count of the infiltrated T cells for each time point and z-stack is generated.

12.7 Protein profiling using RPPA

RPPA profiling was performed to determine the presence of cancer stem cells as well as mutations in driving pathways.

12.7.1 PDM collection and lysis

Roughly 1000 PDMs were collected and pooled in a 1.5 ml Eppendorf tube and washed twice with PBS to remove the media. Following the washing steps, the pellet is flash-frozen and stored at -80°C until further processing. The following steps are performed according to Bader and Willibald [213, 214] and described in brief here. The pellets are lysed using 100 µl cell lysis buffer CLB1 and incubating for 30 min at RT. The protein concentration is determined using a Bradford Assay and adjusted to the same concentration with CLB1 in 10-fold RPPA spotting buffer CSBL1.

12.7.2 Array printing and analysis

The samples are subsequently printed on the hydrophobic chip arrays in four dilutions (starting at 0.3 µg/µl plus 1.6-fold dilutions) in two replicates using the NanoPlotter 2. The microarrays are then

blocked with 3 % *w/v* albumin followed by thorough washing with distilled water and dried in a stream of nitrogen. The arrays can be stored at 4°C until further use. The arrays are incubated for 15 h at RT with the respective primary antibody. After washing once, the array is incubated for 45 min with Alexa647-labled secondary antibody. Followed by a washing step, the arrays are imaged using the ZeptoREADER in the red laser channel with typical exposure time between 0.5 to 16 s. Samples without primary antibody are used as negative controls. The analysis of the obtained data is performed using the ZeptoVIEW 3.1 software. Signals are quantified as protein-normalized, blank-corrected mean fluorescence intensities [213, 214].

12.8 Statistics

Statistical analysis is done using the GraphPad Prism version 9.0.0 for Windows, GraphPad Software, San Diego, California USA, www.graphpad.com. The analytical tests used are specified for each graph in the figure legend. The significance is evaluated according to the obtained p-value and demonstrated in the following way: p value ≤ 0.033 *; ≤ 0.02 **; ≤ 0.001 ***.

13. Acknowledgements

Christian, vielen Dank für all Deine Unterstützung in den vergangenen Jahren. Du hast mich nicht nur während meiner aktiven Laborphase unterstützt und Anregungen gegeben, sondern mich auch in der weiteren Zeit beim Schreiben der Arbeit unterstützt.

Lena, Pauline, Riccarda, Nicole, Jenny und Simge, vielen Dank für die gemeinsame Zeit am NMI. Ohne euch hätte die Zeit nur halb so viel Spaß gemacht.

Ursu, Tine, Roswitha und Sybille, vielen Dank für eure Unterstützung im Labor und das ihr bei Fragen rund um Zellkultur, Mikrobiologie und Zellfärbungen immer Antworten und Ideen parat hattet.

Rest der NMI Truppe, vielen Dank für die lustigen Ausflüge zum freitags Döner, die Gillabende sowie die gemeinsam getrunkenen Kaffees.

Meinen **Kooperationspartnern in der Urologie und Hautklinik sowie innerhalb des NMI**, möchte ich für die gute und erfolgreiche Zusammenarbeit danken.

Michael, vielen Dank fürs Korrekturlesen der Arbeit.

Felix, vielen Dank für deine immerwährende Unterstützung und auch das gelegentliche in Hintern treten, so dass die Arbeit doch noch ein gutes Ende gefunden hat.

Emilia, dafür, dass es dich gibt und du mir den Antrieb gegeben hast, die Arbeit zu einem Ende zu bringen.

Vielen Dank an meine **Familie und insbesondere meine Eltern** deren Unterstützung und Rückhalt ich mir immer sicher sein konnte und die meine Entscheidungen immer unterstützt haben!

14. References

1. Greaves, M., *Evolutionary determinants of cancer.* Cancer Discov, 2015. **5**(8): p. 806-20.
2. Hajdu, S.I., *Greco-Roman thought about cancer.* Cancer, 2004. **100**(10): p. 2048-2051.
3. Stewart B.W., W.C.P., *World cancer report 2014.* International Agency for Research on Cancer, 2014.
4. Jonsson, B., et al., *The cost and burden of cancer in the European Union 1995-2014.* Eur J Cancer, 2016. **66**: p. 162-70.
5. Nicole Scholz, M.R.S. *European Union action on cancer*. 2017 02.02.2017 23.03.2019]; Available from: http://www.europarl.europa.eu/RegData/etudes/ATAG/2017/599246/EPRS_ATA%282017%29599246_EN.pdf.
6. Commission, E. *Horizon 2020*. 25.07.2018 23.03.2019]; Available from: https://ec.europa.eu/programmes/horizon2020/en/news/latest-update-work-programme-2019-now-online.
7. MacDonald, T., *Pediatric Cancer: A Comprehensive Review. Part I: Biology, Epidemiology, Common Tumours, Principles of Treatment and Late Effects.* Canadian Pharmacists Journal / Revue des Pharmaciens du Canada, 2010. **143**(4): p. 176-183.
8. Anand, P., et al., *Curcumin and cancer: an "old-age" disease with an "age-old" solution.* Cancer Lett, 2008. **267**(1): p. 133-64.
9. Narayanan, D.L., R.N. Saladi, and J.L. Fox, *Ultraviolet radiation and skin cancer.* Int J Dermatol, 2010. **49**(9): p. 978-86.
10. Furrukh, M., *Tobacco Smoking and Lung Cancer: Perception-changing facts.* Sultan Qaboos Univ Med J, 2013. **13**(3): p. 345-58.
11. Liao, J.B., *Viruses and human cancer.* Yale J Biol Med, 2006. **79**(3-4): p. 115-22.
12. Scott, R.E., J.J. Wille, Jr., and M.L. Wier, *Mechanisms for the initiation and promotion of carcinogenesis: a review and a new concept.* Mayo Clin Proc, 1984. **59**(2): p. 107-17.
13. Berenblum, I., *Sequential Aspects of Chemical Carcinogenesis: Skin*, in *Cancer. A Comprehensive Treatise: Volume 1. Etiology: Chemical and Physical Carcinogenesis*, F.F. Becker, Editor. 1975, Springer US: Boston, MA. p. 323-344.
14. Becker, F.F., *Presidential address. Recent concepts of initiation and promotion in carcinogenesis.* Am J Pathol, 1981. **105**(1): p. 3-9.
15. Hennings, H., et al., *Malignant conversion of mouse skin tumours is increased by tumour initiators and unaffected by tumour promoters.* Nature, 1983. **304**(5921): p. 67-9.
16. Greenman, C., et al., *Patterns of somatic mutation in human cancer genomes.* Nature, 2007. **446**(7132): p. 153-8.
17. Haber, D.A. and J. Settleman, *Drivers and passengers.* Nature, 2007. **446**: p. 145.
18. Davies, H., et al., *Mutations of the BRAF gene in human cancer.* Nature, 2002. **417**(6892): p. 949-54.
19. Kastan, M.B. and J. Bartek, *Cell-cycle checkpoints and cancer.* Nature, 2004. **432**(7015): p. 316-23.
20. Bartkova, J., et al., *Oncogene-induced senescence is part of the tumorigenesis barrier imposed by DNA damage checkpoints.* Nature, 2006. **444**(7119): p. 633-7.
21. Lowe, S.W., E. Cepero, and G. Evan, *Intrinsic tumour suppression.* Nature, 2004. **432**(7015): p. 307-15.
22. Halazonetis, T.D., V.G. Gorgoulis, and J. Bartek, *An oncogene-induced DNA damage model for cancer development.* Science, 2008. **319**(5868): p. 1352-5.
23. Fearon, E.R. and B. Vogelstein, *A genetic model for colorectal tumorigenesis.* Cell, 1990. **61**(5): p. 759-767.
24. L.P. Bignold, B.L.D.C., H.P.A. Jersmann, *David Paul von Hansemann: Contributions to Oncology*. 2007: Birkhäuser Basel.
25. Foo, J., K. Leder, and F. Michor, *Stochastic dynamics of cancer initiation.* Phys Biol, 2011. **8**(1): p. 015002.

26. Berenblum, I. and P. Shubik, *A new, quantitative, approach to the study of the stages of chemical cartinogenesis in the mouse's skin.* Br J Cancer, 1947. **1**(4): p. 383-91.
27. Slaga, T.J., et al., *Studies on the mechanism of skin tumor promotion: evidence for several stages in promotion.* Proc Natl Acad Sci U S A, 1980. **77**(6): p. 3659-63.
28. Cooper, G.M., *Cellular transforming genes.* Science, 1982. **217**(4562): p. 801-6.
29. Conheim, J., *Congenitales, quergestreiftes muskelsarkon der nireren.* Virchows Arch, 1875. **65**: p. 64.
30. Visvader, J.E., *Cells of origin in cancer.* Nature, 2011. **469**(7330): p. 314-22.
31. Allegra, A., et al., *The cancer stem cell hypothesis: a guide to potential molecular targets.* Cancer Invest, 2014. **32**(9): p. 470-95.
32. Franco, S.S., et al., *In vitro models of cancer stem cells and clinical applications.* BMC Cancer, 2016. **16**(Suppl 2): p. 738.
33. Batlle, E. and H. Clevers, *Cancer stem cells revisited.* Nat Med, 2017. **23**(10): p. 1124-1134.
34. Dayem, A.A., et al., *Role of oxidative stress in stem, cancer, and cancer stem cells.* Cancers (Basel), 2010. **2**(2): p. 859-84.
35. Reya, T., et al., *Stem cells, cancer, and cancer stem cells.* Nature, 2001. **414**(6859): p. 105-11.
36. Ishizawa, K., et al., *Tumor-initiating cells are rare in many human tumors.* Cell Stem Cell, 2010. **7**(3): p. 279-82.
37. Rowan, K., *Are Cancer Stem Cells Real? After Four Decades, Debate Still Simmers.* JNCI: Journal of the National Cancer Institute, 2009. **101**(8): p. 546-547.
38. Jordan, C.T., *Cancer stem cells: controversial or just misunderstood?* Cell Stem Cell, 2009. **4**(3): p. 203-5.
39. Hanahan, D. and R.A. Weinberg, *Hallmarks of cancer: the next generation.* Cell, 2011. **144**(5): p. 646-74.
40. Hanahan, D. and R.A. Weinberg, *The hallmarks of cancer.* Cell, 2000. **100**(1): p. 57-70.
41. Cheng, N., et al., *Transforming growth factor-beta signaling-deficient fibroblasts enhance hepatocyte growth factor signaling in mammary carcinoma cells to promote scattering and invasion.* Mol Cancer Res, 2008. **6**(10): p. 1521-33.
42. Sherr, C.J. and R.A. DePinho, *Cellular senescence: mitotic clock or culture shock?* Cell, 2000. **102**(4): p. 407-10.
43. Burkhart, D.L. and J. Sage, *Cellular mechanisms of tumour suppression by the retinoblastoma gene.* Nat Rev Cancer, 2008. **8**(9): p. 671-82.
44. Steinbichler, T.B., et al., *Tumor-associated fibroblast-conditioned medium induces CDDP resistance in HNSCC cells.* Oncotarget, 2016. **7**(3): p. 2508-18.
45. Wee, I., et al., *Role of tumor-derived exosomes in cancer metastasis.* Biochim Biophys Acta Rev Cancer, 2019. **1871**(1): p. 12-19.
46. Lamouille, S., J. Xu, and R. Derynck, *Molecular mechanisms of epithelial-mesenchymal transition.* Nat Rev Mol Cell Biol, 2014. **15**(3): p. 178-96.
47. Polyak, K. and R.A. Weinberg, *Transitions between epithelial and mesenchymal states: acquisition of malignant and stem cell traits.* Nat Rev Cancer, 2009. **9**(4): p. 265-73.
48. Hugo, H., et al., *Epithelial--mesenchymal and mesenchymal--epithelial transitions in carcinoma progression.* J Cell Physiol, 2007. **213**(2): p. 374-83.
49. Moharil, R.B., et al., *Cancer stem cells: An insight.* J Oral Maxillofac Pathol, 2017. **21**(3): p. 463.
50. Ferrara, N., *Vascular endothelial growth factor.* Arterioscler Thromb Vasc Biol, 2009. **29**(6): p. 789-91.
51. Baluk, P., H. Hashizume, and D.M. McDonald, *Cellular abnormalities of blood vessels as targets in cancer.* Curr Opin Genet Dev, 2005. **15**(1): p. 102-11.
52. Cory, A.H. and J.G. Cory, *Understanding interactions between and among apoptosis inducing pathways in tumor cells.* In Vivo, 2007. **21**(2): p. 245-9.
53. WHO, I.A.f.R.o.C. *Germany*. 2021 March, 2021 2021.04.04]; Available from: https://gco.iarc.fr/today/data/factsheets/populations/276-germany-fact-sheets.pdf.

54. Koch-Institut, R., *Krebs in Deutschland für 2013/2014*. 2017, Robert Koch-Institut.
55. Doehn, C., et al., *The Diagnosis, Treatment, and Follow-up of Renal Cell Carcinoma.* Dtsch Arztebl Int, 2016. **113**(35-36): p. 590-6.
56. Cairns, P., *Renal cell carcinoma.* Cancer Biomark, 2010. **9**(1-6): p. 461-73.
57. Onkologie, L. *S3-Leitlinie Diagnostik, Therapie und Nachsorge des Nierenzellkarzinoms*. 2017 February 2017 13.04.2019]; Kurzversion 1.1 – Februar 20 1:[Available from: https://www.awmf.org/leitlinien/detail/ll/043-017OL.html.
58. Arrangoiz, R., et al., *Melanoma review: epidemiology, risk factors, diagnosis and staging.* J Cancer Treat Res, 2016. **4**(1): p. 1-15.
59. Onkologie, L. *Arbeitsgemeinschaft der Wissenschaftlichen Medizinischen Fachgesellschaften. S3-Leitlinie: Diagnostik, Therapie und Nachsorge des Melanoms, Version 3.1*. 2019 29.01.2019 [cited 2019 23.3.2019]; 3.1:[Available from: https://www.leitlinienprogramm-onkologie.de/fileadmin/user_upload/Downloads/Leitlinien/Melanom/Melanom_Version_3/LL_Melanom_Langversion_3.1.pdf.
60. Domingues, B., et al., *Melanoma treatment in review.* Immunotargets Ther, 2018. **7**: p. 35-49.
61. Fehleisen, F., *Ueber die Züchtung der Erysipelkokken auf künstlichem Nährboden und ihre Übertragbarkeit auf den Menschen.* Dtsch Med Wochenschr, 1882. **8**: p. 553-554.
62. Busch, W., *Aus der Sitzung der medicinischen Section vom 13 November 1867.* Berl Klin Wochenschr, 1868. **5**: p. 137.
63. Oelschlaeger, T.A., *Bacteria as tumor therapeutics?* Bioeng Bugs, 2010. **1**(2): p. 146-7.
64. Morales, A., D. Eidinger, and A. Bruce, *Intracavitary Bacillus Calmette-Guerin in the treatment of superficial bladder tumors.* The Journal of urology, 1976. **116**(2): p. 180-182.
65. Vesely, M.D., et al., *Natural innate and adaptive immunity to cancer.* Annu Rev Immunol, 2011. **29**: p. 235-71.
66. Oiseth, S.J. and M.S. Aziz, *Cancer immunotherapy: a brief review of the history, possibilities, and challenges ahead.* Journal of Cancer Metastasis and Treatment¦ Volume, 2017. **3**: p. 251.
67. Burnet, F.M., *The concept of immunological surveillance.* Prog Exp Tumor Res, 1970. **13**: p. 1-27.
68. Thomas, L. and H. Lawrence, *Cellular and humoral aspects of the hypersensitive states.* New York: Hoeber-Harper, 1959: p. 529-532.
69. Kitamura, T., B.Z. Qian, and J.W. Pollard, *Immune cell promotion of metastasis.* Nat Rev Immunol, 2015. **15**(2): p. 73-86.
70. Noy, R. and J.W. Pollard, *Tumor-associated macrophages: from mechanisms to therapy.* Immunity, 2014. **41**(1): p. 49-61.
71. Shiga, K., et al., *Cancer-Associated Fibroblasts: Their Characteristics and Their Roles in Tumor Growth.* Cancers (Basel), 2015. **7**(4): p. 2443-58.
72. Talmadge, J.E. and D.I. Gabrilovich, *History of myeloid-derived suppressor cells.* Nat Rev Cancer, 2013. **13**(10): p. 739-52.
73. Yang, P., et al., *TGF-beta-miR-34a-CCL22 signaling-induced Treg cell recruitment promotes venous metastases of HBV-positive hepatocellular carcinoma.* Cancer Cell, 2012. **22**(3): p. 291-303.
74. Karavitis, J., et al., *Regulation of COX2 expression in mouse mammary tumor cells controls bone metastasis and PGE2-induction of regulatory T cell migration.* PLoS One, 2012. **7**(9): p. e46342.
75. Novitskiy, S.V., et al., *TGF-beta receptor II loss promotes mammary carcinoma progression by Th17 dependent mechanisms.* Cancer Discov, 2011. **1**(5): p. 430-41.
76. Chung, A.S., et al., *An interleukin-17-mediated paracrine network promotes tumor resistance to anti-angiogenic therapy.* Nat Med, 2013. **19**(9): p. 1114-23.
77. Ribas, A. and J.D. Wolchok, *Cancer immunotherapy using checkpoint blockade.* Science, 2018. **359**(6382): p. 1350-1355.

78. Chambers, C.A., et al., *CTLA-4-mediated inhibition in regulation of T cell responses: mechanisms and manipulation in tumor immunotherapy.* Annu Rev Immunol, 2001. **19**: p. 565-94.
79. Walunas, T.L., et al., *CTLA-4 can function as a negative regulator of T cell activation.* Immunity, 1994. **1**(5): p. 405-13.
80. Schadendorf, D., et al., *Pooled Analysis of Long-Term Survival Data From Phase II and Phase III Trials of Ipilimumab in Unresectable or Metastatic Melanoma.* J Clin Oncol, 2015. **33**(17): p. 1889-94.
81. Baumeister, S.H., et al., *Coinhibitory Pathways in Immunotherapy for Cancer.* Annu Rev Immunol, 2016. **34**: p. 539-73.
82. Oncotrends. *EU-Zulassung für Pembrolizumab als Monotherapie zur adjuvanten Behandlung des Melanoms im Stadium III mit Lymphknotenbeteiligung nach vollständiger Resektion*. 15.01.2019 23.03.2019]; Available from: https://www.oncotrends.de/eu-zulassung-fuer-pembrolizumab-als-monotherapie-zur-adjuvanten-behandlung-des-melanoms-im-stadium-iii-mit-lymphknotenbeteiligung-nach-vollstaendiger-resektion-427479/.
83. Oncotrends. *Europäische Kommission erteilt Zulassung von Nivolumab zur adjuvanten Behandlung des Melanoms mit Lymphknotenbeteiligung oder Metastasierung nach vollständiger Resektion bei Erwachsenen*. 27.08.2018 23.03.2019]; Available from: https://www.oncotrends.de/europaeische-kommission-erteilt-zulassung-von-nivolumab-zur-adjuvanten-behandlung-des-melanoms-mit-lymphknotenbeteiligung-oder-metastasierung-nach-vollstaendiger-resektion-bei-erwachsenen-427119/.
84. Meiliana, A., N.M. Dewi, and A. Wijaya, *Cancer immunotherapy: a review.* The Indonesian Biomedical Journal, 2016. **8**(1): p. 1-20.
85. Miescher, S., et al., *In situ characterization, clonogenic potential, and antitumor cytolytic activity of T lymphocytes infiltrating human brain cancers.* J Neurosurg, 1988. **68**(3): p. 438-48.
86. Rosenberg, S.A., et al., *Use of tumor-infiltrating lymphocytes and interleukin-2 in the immunotherapy of patients with metastatic melanoma.* New England Journal of Medicine, 1988. **319**(25): p. 1676-1680.
87. Rosenberg, S.A. and N.P. Restifo, *Adoptive cell transfer as personalized immunotherapy for human cancer.* Science, 2015. **348**(6230): p. 62-8.
88. Ocana, A., et al., *Preclinical development of molecular-targeted agents for cancer.* Nature Reviews Clinical Oncology, 2010. **8**: p. 200.
89. Kola, I. and J. Landis, *Can the pharmaceutical industry reduce attrition rates?* Nat Rev Drug Discov, 2004. **3**(8): p. 711-5.
90. Blucher, A.S., et al., *Evidence-Based Precision Oncology with the Cancer Targetome.* Trends Pharmacol Sci, 2017. **38**(12): p. 1085-1099.
91. Deng, X. and Y. Nakamura, *Cancer Precision Medicine: From Cancer Screening to Drug Selection and Personalized Immunotherapy.* Trends Pharmacol Sci, 2017. **38**(1): p. 15-24.
92. Shrager, J. and J.M. Tenenbaum, *Rapid learning for precision oncology.* Nat Rev Clin Oncol, 2014. **11**(2): p. 109-18.
93. Liu, X., et al., *Conditional reprogramming and long-term expansion of normal and tumor cells from human biospecimens.* Nat Protoc, 2017. **12**(2): p. 439-451.
94. Palechor-Ceron, N., et al., *Radiation induces diffusible feeder cell factor(s) that cooperate with ROCK inhibitor to conditionally reprogram and immortalize epithelial cells.* Am J Pathol, 2013. **183**(6): p. 1862-1870.
95. Kodack, D.P., et al., *Primary Patient-Derived Cancer Cells and Their Potential for Personalized Cancer Patient Care.* Cell Rep, 2017. **21**(11): p. 3298-3309.
96. Mbeunkui, F. and D.J. Johann, *Cancer and the tumor microenvironment: a review of an essential relationship.* Cancer chemotherapy and pharmacology, 2009. **63**(4): p. 571-582.
97. Tung, K.H., et al., *A Review of Exosomes and their Role in The Tumor Microenvironment and Host-Tumor.* 2019.

98. Mitra, A., L. Mishra, and S. Li, *Technologies for deriving primary tumor cells for use in personalized cancer therapy.* Trends Biotechnol, 2013. **31**(6): p. 347-54.
99. Srivastava, P., M. Kumar, and P.K. Nayak, *ROLE OF PATIENT DERIVED CELL LINES AND XENOGRAFT IN CANCER RESEARCH.*
100. Lai, Y., et al., *Current status and perspectives of patient-derived xenograft models in cancer research.* J Hematol Oncol, 2017. **10**(1): p. 106.
101. Byrne, A.T., et al., *Interrogating open issues in cancer medicine with patient-derived xenografts.* Nat Rev Cancer, 2017. **17**(10): p. 632.
102. Meijer, T.G., et al., *Ex vivo tumor culture systems for functional drug testing and therapy response prediction.* Future Sci OA, 2017. **3**(2): p. Fso190.
103. Majumder, B., et al., *Predicting clinical response to anticancer drugs using an ex vivo platform that captures tumour heterogeneity.* Nat Commun, 2015. **6**: p. 6169.
104. Corning. *Corning Matrigel Matrix*. 14.04.2019]; Cells behave better on Corning Matrigel matrix—the original, trusted extracellular matrix (ECM).

Nearly 30 years ago, researchers were looking for a way to grow mouse sarcoma cells. The solution? The development of Corning Matrigel matrix, a solubilized basement membrane preparation extracted from the Engelbreth-Holm-Swarm (EHS) mouse sarcoma, a tumor rich in such ECM proteins as laminin (a major component), collagen IV, heparin sulfate proteoglycans, entactin/nidogen, and a number of growth factors.

Today, this natural ECM-based hydrogel is among the most widely used models for 2D and 3D cell culture in vitro, enabling you to:

Improve the attachment and differentiation of both normal and transformed anchorage-dependent epitheliod cells, as well as other cell types.

Better mimic in vivo environments for 2D and 3D cell culture applications]. Available from: https://www.corning.com/emea/de/products/life-sciences/products/surfaces/matrigel-matrix.html.
105. Nunes, A.S., et al., *3D tumor spheroids as in vitro models to mimic in vivo human solid tumors resistance to therapeutic drugs.* Biotechnol Bioeng, 2019. **116**(1): p. 206-226.
106. Yachida, S., et al., *Distant metastasis occurs late during the genetic evolution of pancreatic cancer.* Nature, 2010. **467**: p. 1114.
107. Ooft, S.N., et al., *Patient-derived organoids can predict response to chemotherapy in metastatic colorectal cancer patients.* Science Translational Medicine, 2019. **11**(513): p. eaay2574.
108. Devarasetty, M., A.R. Mazzocchi, and A. Skardal, *Applications of Bioengineered 3D Tissue and Tumor Organoids in Drug Development and Precision Medicine: Current and Future.* BioDrugs, 2018. **32**(1): p. 53-68.
109. Aboulkheyr Es, H., et al., *Personalized Cancer Medicine: An Organoid Approach.* Trends in Biotechnology, 2018. **36**(4): p. 358-371.
110. Pauli, C., et al., *Personalized In Vitro and In Vivo Cancer Models to Guide Precision Medicine.* Cancer Discov, 2017. **7**(5): p. 462-477.
111. Vlachogiannis, G., et al., *Patient-derived organoids model treatment response of metastatic gastrointestinal cancers.* Science, 2018. **359**(6378): p. 920-926.
112. Gao, D., et al., *Organoid cultures derived from patients with advanced prostate cancer.* Cell, 2014. **159**(1): p. 176-87.

113. Drost, J. and H. Clevers, *Organoids in cancer research.* Nature Reviews Cancer, 2018. **18**(7): p. 407-418.
114. Neal, J.T., et al., *Organoid Modeling of the Tumor Immune Microenvironment.* Cell, 2018. **175**(7): p. 1972-1988 e16.
115. Kondo, J., et al., *Retaining cell-cell contact enables preparation and culture of spheroids composed of pure primary cancer cells from colorectal cancer.* Proc Natl Acad Sci U S A, 2011. **108**(15): p. 6235-40.
116. Gantenbein-Ritter, B., et al., *Confocal imaging protocols for live/dead staining in three-dimensional carriers.* Methods Mol Biol, 2011. **740**: p. 127-40.
117. Thakur, S., D.I. Cattoni, and M. Nollmann, *The fluorescence properties and binding mechanism of SYTOX green, a bright, low photo-damage DNA intercalating agent.* Eur Biophys J, 2015. **44**(5): p. 337-48.
118. Sirenko, O., et al., *High-Content Assays for Characterizing the Viability and Morphology of 3D Cancer Spheroid Cultures.* ASSAY and Drug Development Technologies, 2015. **13**: p. 402-414.
119. Delahunt, B., *Advances and controversies in grading and staging of renal cell carcinoma.* Mod Pathol, 2009. **22 Suppl 2**: p. S24-36.
120. Delahunt, B., et al., *Grading of renal cell carcinoma.* Histopathology, 2019. **74**(1): p. 4-17.
121. Shen, S.S., et al., *Role of immunohistochemistry in diagnosing renal neoplasms: when is it really useful?* Arch Pathol Lab Med, 2012. **136**(4): p. 410-7.
122. Fuhrman, S.A., L.C. Lasky, and C. Limas, *Prognostic significance of morphologic parameters in renal cell carcinoma.* Am J Surg Pathol, 1982. **6**(7): p. 655-63.
123. Williams, A.A., et al., *CD 9 and vimentin distinguish clear cell from chromophobe renal cell carcinoma.* BMC clinical pathology, 2009. **9**: p. 9-9.
124. Kidd, M.E., D.K. Shumaker, and K.M. Ridge, *The role of vimentin intermediate filaments in the progression of lung cancer.* American journal of respiratory cell and molecular biology, 2014. **50**(1): p. 1-6.
125. Haynes, B.F., *Phenotypic characterization and ontogeny of components of the human thymic microenvironment.* Clin Res, 1984. **32**(5): p. 500-7.
126. Chetty, R. and K. Gatter, *CD3: Structure, function, and role of immunostaining in clinical practice.* The Journal of Pathology, 1994. **173**(4): p. 303-307.
127. Fabriek, B.O., et al., *The macrophage scavenger receptor CD163 functions as an innate immune sensor for bacteria.* Blood, 2009. **113**(4): p. 887-892.
128. Busam, K.J., et al., *Expression of melan-A (MART1) in benign melanocytic nevi and primary cutaneous malignant melanoma.* Am J Surg Pathol, 1998. **22**(8): p. 976-82.
129. Patel, S.P. and R. Kurzrock, *PD-L1 Expression as a Predictive Biomarker in Cancer Immunotherapy.* Molecular Cancer Therapeutics, 2015. **14**(4): p. 847-856.
130. Meng, X., et al., *Predictive biomarkers in PD-1/PD-L1 checkpoint blockade immunotherapy.* Cancer Treatment Reviews, 2015. **41**(10): p. 868-876.
131. Edin, S., et al., *The Distribution of Macrophages with a M1 or M2 Phenotype in Relation to Prognosis and the Molecular Characteristics of Colorectal Cancer.* PLOS ONE, 2012. **7**(10): p. e47045.
132. Liu, T., et al., *Cancer-Associated Fibroblasts Build and Secure the Tumor Microenvironment.* Frontiers in Cell and Developmental Biology, 2019. **7**: p. 60.
133. Koury, J., L. Zhong, and J. Hao, *Targeting Signaling Pathways in Cancer Stem Cells for Cancer Treatment.* Stem Cells International, 2017. **2017**: p. 2925869.
134. Miyazaki, Y., et al., *Efficient elimination of pancreatic cancer stem cells by hedgehog/GLI inhibitor GANT61 in combination with mTOR inhibition.* Molecular Cancer, 2016. **15**(1): p. 49.
135. Glumac, P.M. and A.M. LeBeau, *The role of CD133 in cancer: a concise review.* Clinical and translational medicine, 2018. **7**(1): p. 18-18.
136. Siddique, H.R. and M. Saleem, *Role of BMI1, a stem cell factor, in cancer recurrence and chemoresistance: preclinical and clinical evidences.* Stem Cells, 2012. **30**(3): p. 372-8.

137. Wang, L., et al., *The Role of CD44 and Cancer Stem Cells.* Methods Mol Biol, 2018. **1692**: p. 31-42.
138. Jaggupilli, A. and E. Elkord, *Significance of CD44 and CD24 as Cancer Stem Cell Markers: An Enduring Ambiguity.* Clinical and Developmental Immunology, 2012. **2012**: p. 708036.
139. Tomita, H., et al., *Aldehyde dehydrogenase 1A1 in stem cells and cancer.* Oncotarget, 2016. **7**(10): p. 11018-11032.
140. Rasti, A., et al., *Co-expression of Cancer Stem Cell Markers OCT4 and NANOG Predicts Poor Prognosis in Renal Cell Carcinomas.* Scientific reports, 2018. **8**(1): p. 11739-11739.
141. Cane, R., *Characterization of Cancer Stem Cells in Renal Clear Cell Carcinoma.* J Stem Cell Regen Biol, 2019. **5(1): 6-18**.
142. Goldman, D.C., et al., *BMP4 regulates the hematopoietic stem cell niche.* Blood, 2009. **114**(20): p. 4393-4401.
143. Kim, W.-T. and C.J. Ryu, *Cancer stem cell surface markers on normal stem cells.* BMB reports, 2017. **50**(6): p. 285-298.
144. Braicu, C., et al., *A Comprehensive Review on MAPK: A Promising Therapeutic Target in Cancer.* Cancers, 2019. **11**(10): p. 1618.
145. Owusu-Brackett, N., M. Shariati, and F. Meric-Bernstam, *Role of PI3K/AKT/mTOR in Cancer Signaling*, in *Predictive Biomarkers in Oncology: Applications in Precision Medicine*, S. Badve and G.L. Kumar, Editors. 2019, Springer International Publishing: Cham. p. 263-270.
146. Oda, K., et al., *A comprehensive pathway map of epidermal growth factor receptor signaling.* Molecular systems biology, 2005. **1**: p. 2005.0010-2005.0010.
147. McCubrey, J.A., et al., *Roles of the Raf/MEK/ERK pathway in cell growth, malignant transformation and drug resistance.* Biochimica et biophysica acta, 2007. **1773**(8): p. 1263-1284.
148. Guo, Y.J., et al., *ERK/MAPK signalling pathway and tumorigenesis (Review).* Exp Ther Med, 2020. **19**(3): p. 1997-2007.
149. Cargnello, M. and P.P. Roux, *Activation and function of the MAPKs and their substrates, the MAPK-activated protein kinases.* Microbiology and molecular biology reviews : MMBR, 2011. **75**(1): p. 50-83.
150. Sette, G., et al., *Tyr1068-phosphorylated epidermal growth factor receptor (EGFR) predicts cancer stem cell targeting by erlotinib in preclinical models of wild-type EGFR lung cancer.* Cell death & disease, 2015. **6**(8): p. e1850-e1850.
151. Wang, F., et al., *Phosphorylated EGFR expression may predict outcome of EGFR-TKIs therapy for the advanced NSCLC patients with wild-type EGFR.* Journal of Experimental & Clinical Cancer Research, 2012. **31**(1): p. 65.
152. Freudlsperger, C., et al., *Phosphorylation of AKT(Ser473) serves as an independent prognostic marker for radiosensitivity in advanced head and neck squamous cell carcinoma.* Int J Cancer, 2015. **136**(12): p. 2775-85.
153. Wittenberg, A.D., et al., *Phosphorylated Ribosomal Protein S6 Is Required for Akt-Driven Hyperplasia and Malignant Transformation, but Not for Hypertrophy, Aneuploidy and Hyperfunction of Pancreatic beta-Cells.* PLoS One, 2016. **11**(2): p. e0149995.
154. Sridharan, S. and A. Basu, *Distinct Roles of mTOR Targets S6K1 and S6K2 in Breast Cancer.* International journal of molecular sciences, 2020. **21**(4): p. 1199.
155. Leighton, I.A., et al., *Comparison of the specificities of p70 S6 kinase and MAPKAP kinase-1 identifies a relatively specific substrate for p70 S6 kinase: the N-terminal kinase domain of MAPKAP kinase-1 is essential for peptide phosphorylation.* FEBS Lett, 1995. **375**(3): p. 289-93.
156. Duhen, T., et al., *Co-expression of CD39 and CD103 identifies tumor-reactive CD8 T cells in human solid tumors.* Nat Commun, 2018. **9**(1): p. 2724.
157. Gun, S.Y., et al., *Targeting immune cells for cancer therapy.* Redox biology, 2019. **25**: p. 101174-101174.
158. Cerignoli, F., et al., *In vitro immunotherapy potency assays using real-time cell analysis.* PLoS One, 2018. **13**(3): p. e0193498.

159. Davenport, A.J., et al., *CAR-T cells are serial killers.* Oncoimmunology, 2015. **4**(12): p. e1053684-e1053684.
160. Nelson, D.L., C.C. Kurman, and D.E. Serbousek, *51Cr Release Assay of Antibody-Dependent Cell-Mediated Cytotoxicity (ADCC).* Current Protocols in Immunology, 1993. **8**(1): p. 7.27.1-7.27.8.
161. Lichtenfels, R., et al., *CARE-LASS (calcein-release-assay), an improved fluorescence-based test system to measure cytotoxic T lymphocyte activity.* Journal of Immunological Methods, 1994. **172**(2): p. 227-239.
162. Parker, T.M., et al., *Cell competition and tumor heterogeneity.* Seminars in Cancer Biology, 2020. **63**: p. 1-10.
163. Easwaran, H., H.-C. Tsai, and Stephen B. Baylin, *Cancer Epigenetics: Tumor Heterogeneity, Plasticity of Stem-like States, and Drug Resistance.* Molecular Cell, 2014. **54**(5): p. 716-727.
164. Xie, J., X. Wang, and C.G. Proud, *mTOR inhibitors in cancer therapy.* F1000Research, 2016. **5**: p. F1000 Faculty Rev-2078.
165. Battelli, C. and D.C. Cho, *mTOR inhibitors in renal cell carcinoma.* Therapy (London, England : 2004), 2011. **8**(4): p. 359-367.
166. Meier, F.E., et al., *The PI3K inhibitor BKM120 has potent antitumor activity in melanoma brain metastases in vitro and in vivo.* Journal of Clinical Oncology, 2013. **31**(15_suppl): p. e20050-e20050.
167. Aasen, S.N., et al., *Effective Treatment of Metastatic Melanoma by Combining MAPK and PI3K Signaling Pathway Inhibitors.* Int J Mol Sci, 2019. **20**(17).
168. Armstrong, A.J., et al., *Phase II trial of the PI3 kinase inhibitor buparlisib (BKM-120) with or without enzalutamide in men with metastatic castration resistant prostate cancer.* European Journal of Cancer, 2017. **81**: p. 228-236.
169. Amaral, T., et al., *An open-label, single-arm, phase II trial of buparlisib in patients with melanoma brain metastases not eligible for surgery or radiosurgery-the BUMPER study.* Neuro-oncology advances, 2020. **2**(1): p. vdaa140-vdaa140.
170. Hussain, R.F., A.M.E. Nouri, and R.T.D. Oliver, *A new approach for measurement of cytotoxicity using colorimetric assay.* Journal of Immunological Methods, 1993. **160**(1): p. 89-96.
171. Yamashita, M., et al., *A novel method for evaluating antibody-dependent cell-mediated cytotoxicity by flowcytometry using cryopreserved human peripheral blood mononuclear cells.* Scientific Reports, 2016. **6**: p. 19772.
172. Pu, Z., et al., *Clinicalpathological and prognostic significance of survivin expression in renal cell carcinoma: a meta-analysis.* Oncotarget, 2017. **8**(12): p. 19825-19833.
173. Garg, H., et al., *Survivin: a unique target for tumor therapy.* Cancer Cell Int, 2016. **16**: p. 49.
174. Xie, Y., et al., *Prognostic and Clinicopathological Significance of Survivin Expression in Renal Cell Carcinoma: A Systematic Review and Meta-Analysis.* Scientific Reports, 2016. **6**(1): p. 29794.
175. Mazza, G., et al., *Isolation and characterization of human interleukin-10-secreting T cells from peripheral blood.* Human immunology, 2010. **71**(3): p. 225-234.
176. Doroshow, J.H. and R.M. Simon, *On the Design of Combination Cancer Therapy.* Cell, 2017. **171**(7): p. 1476-1478.
177. Vanneman, M. and G. Dranoff, *Combining immunotherapy and targeted therapies in cancer treatment.* Nat Rev Cancer, 2012. **12**(4): p. 237-51.
178. Khalil, D.N., et al., *The future of cancer treatment: immunomodulation, CARs and combination immunotherapy.* Nature Reviews Clinical Oncology, 2016. **13**(5): p. 273-290.
179. Lee, N., et al., *Tumour-infiltrating lymphocytes in melanoma prognosis and cancer immunotherapy.* Pathology, 2016. **48**(2): p. 177-187.
180. Roncati, L. and B. Palmieri, *Adoptive cell transfer (ACT) of autologous tumor-infiltrating lymphocytes (TILs) to treat malignant melanoma: the dawn of a chimeric antigen receptor T (CAR-T) cell therapy from autologous donor.* International Journal of Dermatology, 2020. **59**(7): p. 763-769.

181. Nguyen, L.T., et al., *Expansion and characterization of human melanoma tumor-infiltrating lymphocytes (TILs).* PLoS One, 2010. **5**(11): p. e13940.
182. Somerville, R.P., et al., *Clinical scale rapid expansion of lymphocytes for adoptive cell transfer therapy in the WAVE(R) bioreactor.* J Transl Med, 2012. **10**: p. 69.
183. Kladis, G., et al., *39P - TCR engaging antigen-scaffolds for targeted expansion of functionally improved T cells for adoptive cell therapy.* Annals of Oncology, 2019. **30**: p. xi13.
184. Rafa, V.M., et al., *Abstract B039: Peptide-MHC-directed expansion of multifunctional antigen-responsive T-cells.* Cancer Immunology Research, 2019. **7**(2 Supplement): p. B039-B039.
185. Bray, F., et al., *Global cancer statistics 2018: GLOBOCAN estimates of incidence and mortality worldwide for 36 cancers in 185 countries.* CA Cancer J Clin, 2018. **68**(6): p. 394-424.
186. Bedard, P.L., et al., *Tumour heterogeneity in the clinic.* Nature, 2013. **501**(7467): p. 355-364.
187. Hughes, C.S., L.M. Postovit, and G.A. Lajoie, *Matrigel: a complex protein mixture required for optimal growth of cell culture.* Proteomics, 2010. **10**(9): p. 1886-90.
188. Fang, Y. and R.M. Eglen, *Three-Dimensional Cell Cultures in Drug Discovery and Development.* SLAS discovery : advancing life sciences R & D, 2017. **22**(5): p. 456-472.
189. Xu, H., et al., *Organoid technology and applications in cancer research.* Journal of hematology & oncology, 2018. **11**(1): p. 116-116.
190. Dai, J., et al., *Up-regulation of E-cadherin by saRNA inhibits the migration and invasion of renal carcinoma cells.* INTERNATIONAL JOURNAL OF CLINICAL AND EXPERIMENTAL PATHOLOGY, 2018. **11**(12): p. 5792-5800.
191. Slipicevic, A., et al., *Isolation of melanoma cell subpopulations using negative selection.* Methods in molecular biology (Clifton, N.J.), 2014. **1102**: p. 501-512.
192. Justiz Vaillant AA, Q.A. *Interleukin*. 2020 Jan- Updated 2020 Aug 30 [cited 2021 2021-Feb-01]; Available from: https://www.ncbi.nlm.nih.gov/books/NBK499840/.
193. Erez, N., et al., *Cancer-Associated Fibroblasts Are Activated in Incipient Neoplasia to Orchestrate Tumor-Promoting Inflammation in an NF-kappaB-Dependent Manner.* Cancer Cell, 2010. **17**(2): p. 135-47.
194. Fukumura, D., et al., *Tumor induction of VEGF promoter activity in stromal cells.* Cell, 1998. **94**(6): p. 715-25.
195. Li, M., et al., *Targeting of cancer-associated fibroblasts enhances the efficacy of cancer chemotherapy by regulating the tumor microenvironment.* Mol Med Rep, 2016. **13**(3): p. 2476-84.
196. Liu, F., et al., *Targeting ERK, an Achilles' Heel of the MAPK pathway, in cancer therapy.* Acta Pharmaceutica Sinica B, 2018. **8**(4): p. 552-562.
197. Krishnamurthy, N. and R. Kurzrock, *Targeting the Wnt/beta-catenin pathway in cancer: Update on effectors and inhibitors.* Cancer Treat Rev, 2018. **62**: p. 50-60.
198. Hassan, M., et al., *Apoptosis and molecular targeting therapy in cancer.* Biomed Res Int, 2014. **2014**: p. 150845.
199. Gross-Goupil, M., et al., *Axitinib: a review of its safety and efficacy in the treatment of adults with advanced renal cell carcinoma.* Clin Med Insights Oncol, 2013. **7**: p. 269-77.
200. Niessner, H., et al., *PI3K Pathway Inhibition Achieves Potent Antitumor Activity in Melanoma Brain Metastases In Vitro and In Vivo.* Clin Cancer Res, 2016. **22**(23): p. 5818-5828.
201. Nguyen, H.H., et al., *Naïve CD8+ T cell derived tumor-specific cytotoxic effectors as a potential remedy for overcoming TGF-β immunosuppression in the tumor microenvironment.* Scientific Reports, 2016. **6**: p. 28208.
202. Alsaab, H.O., et al., *PD-1 and PD-L1 Checkpoint Signaling Inhibition for Cancer Immunotherapy: Mechanism, Combinations, and Clinical Outcome.* Front Pharmacol, 2017. **8**: p. 561.

203. Atkins, M.B., et al., *Axitinib in combination with pembrolizumab in patients with advanced renal cell cancer: a non-randomised, open-label, dose-finding, and dose-expansion phase 1b trial.* The Lancet Oncology, 2018. **19**(3): p. 405-415.
204. Di Nunno, V., M. Santoni, and F. Massari, *Re: Michael B. Atkins, Elizabeth R. Plimack, Igor Puzanov, et al. Axitinib in Combination with Pembrolizumab in Patients with Advanced Renal Cell Cancer: A Non-randomised, Open-label, Dose-finding, and Dose-expansion Phase 1b Trial. Lancet Oncol 2018;19:405-15.* Eur Urol, 2018. **74**(2): p. e50.
205. Aparicio, L.M.A., I.P. Fernandez, and J. Cassinello, *Tyrosine kinase inhibitors reprogramming immunity in renal cell carcinoma: rethinking cancer immunotherapy.* Clin Transl Oncol, 2017. **19**(10): p. 1175-1182.
206. Andersen, R.S., et al., *Dissection of T-cell antigen specificity in human melanoma.* Cancer Res, 2012. **72**(7): p. 1642-50.
207. Barnes, T.A. and E. Amir, *HYPE or HOPE: the prognostic value of infiltrating immune cells in cancer.* Br J Cancer, 2017. **117**(4): p. 451-460.
208. Grünwald, V., et al., *Axitinib plus immune checkpoint inhibitor: evidence- and expert-based consensus recommendation for treatment optimisation and management of related adverse events.* British Journal of Cancer, 2020. **123**(6): p. 898-904.
209. Dirkx, A.E., et al., *Anti-angiogenesis therapy can overcome endothelial cell anergy and promote leukocyte-endothelium interactions and infiltration in tumors.* FASEB J, 2006. **20**(6): p. 621-30.
210. Ahmadzadeh, M., et al., *Tumor antigen-specific CD8 T cells infiltrating the tumor express high levels of PD-1 and are functionally impaired.* Blood, 2009. **114**(8): p. 1537-1544.
211. Dijkstra, K.K., et al., *Generation of Tumor-Reactive T Cells by Co-culture of Peripheral Blood Lymphocytes and Tumor Organoids.* Cell, 2018. **174**(6): p. 1586-1598.e12.
212. Livak, K.J. and T.D. Schmittgen, *Analysis of relative gene expression data using real-time quantitative PCR and the 2(-Delta Delta C(T)) Method.* Methods, 2001. **25**(4): p. 402-8.
213. Bader, S., et al., *Evaluation of Protein Profiles From Treated Xenograft Tumor Models Identifies an Antibody Panel for Formalin-fixed and Paraffin-embedded (FFPE) Tissue Analysis by Reverse Phase Protein Arrays (RPPA).* Mol Cell Proteomics, 2015. **14**(10): p. 2775-85.
214. Willibald, M., et al., *Progesterone receptor membrane component 1 is phosphorylated upon progestin treatment in breast cancer cells.* Oncotarget, 2017. **8**(42): p. 72480-72493.

15. Appendix

15.1 SOC concentration used in SOC testing

Table 9: SOC concentration used in treatment of PDMs.

Tumor entities	SOC	Stock concentration	Plasma concentration	Concentrations tested
RCC	Axitinib	5 mM		5 µM, 3 µM, 1 µM 100 nM, 10 nM
	Torin-2	5 mM		10, 30, 50, 100, 500 nM
Melanoma	BKM	10 nM		1, 2, 3, 4, 10, 20 µM
	Trametinib	5 mM		10, 20, 30, 40, 80 nM

15.2 Heat map of the total protein analyzed using RPPA

Heat map of all proteins analyzed using RPPA. The signaling pathways look at in more detail are described in chapter 5.3.

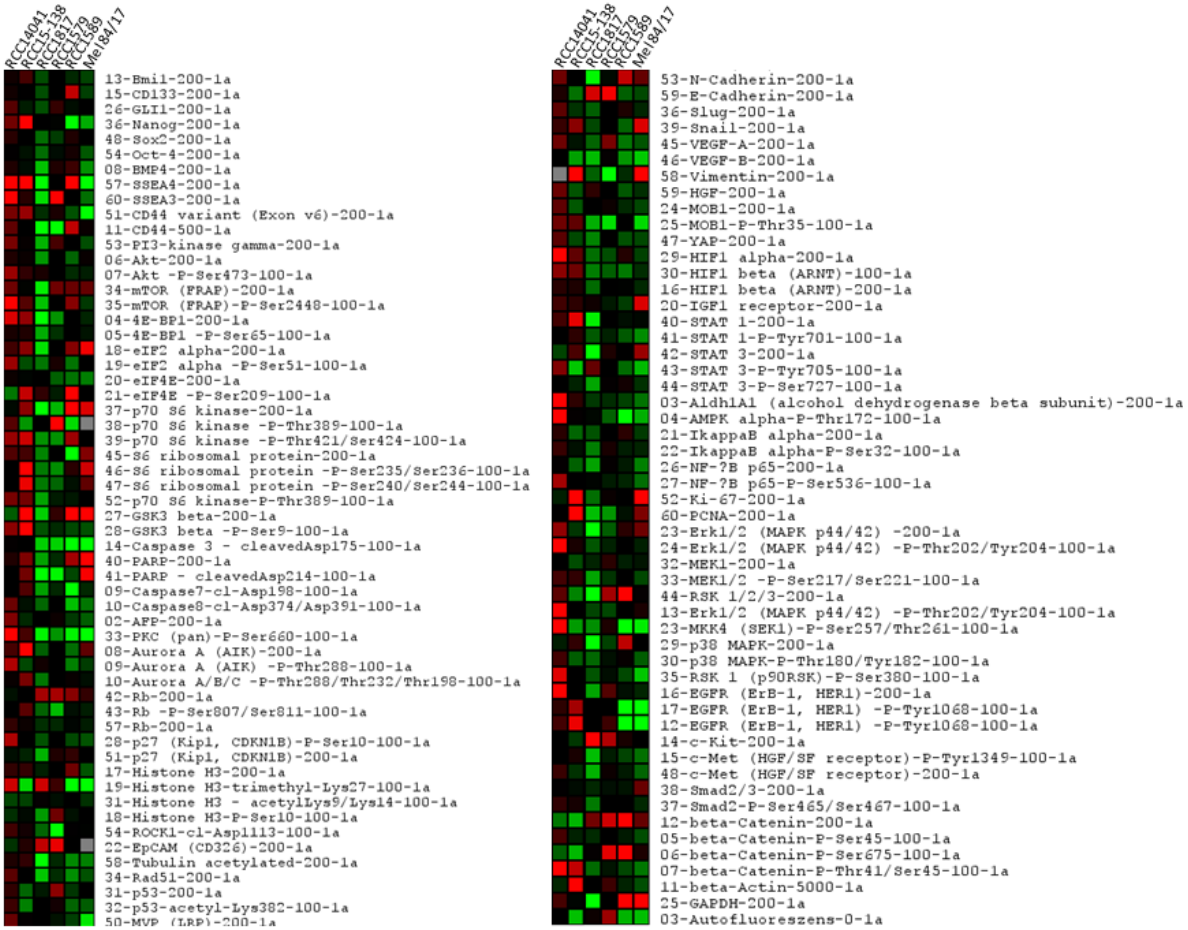

Figure 34: Heat map of all proteins analyzed using RPPA.

15.3 Figure legend

15.4 Table legend